

# NAVAL POSTGRADUATE SCHOOL

## Monterey, California

AD-A226 759



DTIC  
 ELECTE  
 SEP 27 1990  
 S B D

# THESIS

THE RESPONSE AND FAILURE MECHANISMS OF  
 CIRCULAR METAL AND COMPOSITE PLATES  
 SUBJECTED TO UNDERWATER SHOCK LOADING

by

ROBERT A. JONES

March 1990

Thesis Advisor:

Y. S. Shin

Approved for public release; distribution is unlimited.

90 09 21 045

REPORT DOCUMENTATION PAGE			
1a. REPORT SECURITY CLASSIFICATION UNCLASSIFIED		1b. RESTRICTIVE MARKINGS	
2a. SECURITY CLASSIFICATION AUTHORITY		3. DISTRIBUTION/AVAILABILITY OF REPORT Approved for public release; distribution is unlimited.	
2b. DECLASSIFICATION/DOWNGRADING SCHEDULE			
4. PERFORMING ORGANIZATION REPORT NUMBER(S)		5. MONITORING ORGANIZATION REPORT NUMBER(S)	
6a. NAME OF PERFORMING ORGANIZATION Naval Postgraduate School	6b. OFFICE SYMBOL (If applicable) 55	7a. NAME OF MONITORING ORGANIZATION Naval Postgraduate School	
6c. ADDRESS (City, State, and ZIP Code) Monterey, CA 93943-5000		7b. ADDRESS (City, State, and ZIP Code) Monterey, CA 93943-5000	
8a. NAME OF FUNDING/SPONSORING ORGANIZATION	8b. OFFICE SYMBOL (If applicable)	9. PROCUREMENT INSTRUMENT IDENTIFICATION NUMBER	
8c. ADDRESS (City, State, and ZIP Code)		10. SOURCE OF FUNDING NUMBERS	
		Program Element No.	Project No.
		Task No.	Work Unit Accession Number
11. TITLE (Include Security Classification) THE RESPONSE AND FAILURE MECHANISMS OF CIRCULAR METAL AND COMPOSITE PLATES SUBJECTED TO UNDERWATER SHOCK LOADING			
12. PERSONAL AUTHOR(S) Jones, R. A., LCDR, USN			
13a. TYPE OF REPORT Master's Thesis	13b. TIME COVERED From To	14. DATE OF REPORT (year, month, day) March 1990	15. PAGE COUNT 106
16. SUPPLEMENTARY NOTATION The views expressed in this thesis are those of the author and do not reflect the official policy or position of the Department of Defense or the U.S. Government.			
17. COSATI CODES		18. SUBJECT TERMS (continue on reverse if necessary and identify by block number)	
FIELD	GROUP	SUBGROUP	
		Underwater Shock, UNDEX, Fiber-reinforced Composite Material, Failure Response, Shock loading, Thin Circular Plates . (JS) ←	
19. ABSTRACT (continue on reverse if necessary and identify by block number) The response and failure mechanism of circular aluminum and S-2 glass fiber/polyester resin matrix composite panels in response to underwater shock loading were investigated. The response of the aluminum panels was compared to the characteristic response of thin circular metal plates subjected to shock loading with a good degree of correlation. The response of the aluminum panels was then used as a reference with which to compare the response of the composite panels. The response and failure mechanism of the composite panels were found to be highly dependent on the boundary conditions of the panel. For the conditions of this test series, in which the panel boundary was allowed limited motion in the radial direction, the response of the composite panel was determined to be generally similar to the response of the aluminum panels, mitigated by the high strength in tension of the glass fiber. The failure mechanism appeared to be localized matrix failure in compression due to the high circumferential stresses generated as a result of the panel being forced into the smaller diameter test fixture by the shock wave. The radial motion of the panel edge allowed by the boundary conditions appears to have exacerbated the circumferential stresses. )			
20. DISTRIBUTION/AVAILABILITY OF ABSTRACT <input checked="" type="checkbox"/> UNCLASSIFIED/UNLIMITED <input type="checkbox"/> SAME AS REPORT <input type="checkbox"/> DTIC USERS		21. ABSTRACT SECURITY CLASSIFICATION UNCLASSIFIED	
22a. NAME OF RESPONSIBLE INDIVIDUAL Dr. Y. S. Shin		22b. TELEPHONE (Include Area code) (408)646-2568	22c. OFFICE SYMBOL 69Sg

Approved for public release; distribution is unlimited.

The Response and Failure Mechanisms of  
Circular Metal and Composite Plates  
Subjected to Underwater Shock Loading

by

Robert A. Jones  
Lieutenant Commander, United States Navy  
B.S.M.E., Auburn University, 1977

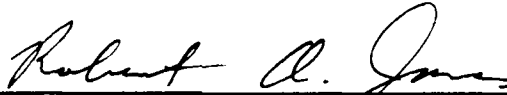
Submitted in partial fulfillment  
of the requirements for the degree of

MASTER OF SCIENCE IN MECHANICAL ENGINEERING  
and  
MECHANICAL ENGINEER

from the

NAVAL POSTGRADUATE SCHOOL  
March 1990

Author:

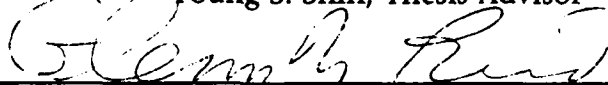


Robert A. Jones

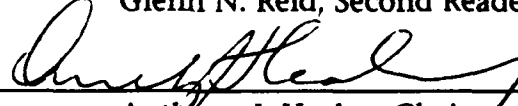
Approved by:



Young S. Shin, Thesis Advisor



Glenn N. Reid, Second Reader



Anthony J. Healey, Chairman  
Department of Mechanical Engineering



DEAN OF FACULTY  
AND GRADUATE STUDIES

## ABSTRACT

The response and failure mechanism of circular aluminum panels and S-2 glass fiber/polyester resin matrix composite panels in response to underwater shock loading were investigated. The response of the aluminum panels was compared to the characteristic response of thin circular metal plates subjected to shock loading with a good degree of correlation. The response of the aluminum panels was then used as a reference with which to compare the response of the composite panels.

The response and failure mechanism of the composite panels were found to be highly dependent on the boundary conditions of the panel. For the conditions of this test series, in which the panel boundary was allowed limited motion in the radial direction, the response of the composite panel was determined to be generally similar to the response of the aluminum panels, mitigated by the high strength in tension of the glass fiber. The failure mechanism appeared to be localized matrix failure in compression due to the high circumferential stresses generated as a result of the panel being forced into the smaller diameter test fixture by the shock wave. The radial motion of the panel edge allowed by the boundary conditions appears to have exacerbated the circumferential compressive stresses.

Accession For	
NTIS GRA&I	<input checked="" type="checkbox"/>
DTIC TAB	<input type="checkbox"/>
Unannounced	<input type="checkbox"/>
Justification	
By _____	
Distribution/	
Availability Codes	
Dist	Avail and/or Special
A-1	

## TABLE OF CONTENTS

I. INTRODUCTION .....	1
II. THEORETICAL BACKGROUND .....	3
A. THE UNDERWATER SHOCK WAVE .....	3
1. Empirical Relationships .....	5
2. Underwater Shock Wave Propagation .....	7
B. IMPULSE RESPONSE OF A FLAT CIRCULAR PLATE .....	10
1. Impulse Response of an Infinite Flat Plate .....	11
2. Impulse Response of a Flat Circular Plate .....	16
C. COMPOSITE MATERIAL BEHAVIOR .....	18
III. EXPERIMENTAL METHODS .....	21
A. TEST FIXTURE DESIGN .....	21
B. TEST ARRANGEMENT .....	24
1. Test Material Selection .....	24
2. Test Site Arrangement .....	27
3. Test Instrumentation .....	28
C. TEST PROCEDURE .....	31
D. PREDICTED RESPONSE .....	37

IV. RESULTS .....	43
A. PEAK PRESSURE AND PERFORMANCE OF THE EXPLOSIVE ...	44
B. OBSERVED EFFECTS ON THE TEST PANELS .....	46
1. Water Backed Plates .....	46
2. Air backed Plates .....	48
C. TRANSVERSE DISPLACEMENT OF THE TEST PANELS .....	51
1. Aluminum Panels .....	52
2. Composite Panels .....	55
D. TEST PANEL STRAIN HISTORIES .....	57
1. The Aluminum Test Panels .....	59
2. The Composite Test Panels .....	64
V. CONCLUSIONS AND RECOMMENDATIONS .....	72
A. WATER BACKED TESTS .....	72
B. AIR BACKED TESTS .....	73
C. RECOMMENDATIONS .....	75
APPENDIX A: MATERIAL PROPERTIES .....	77
APPENDIX B: PHOTOGRAPHS OF PANEL DAMAGE .....	78
LIST OF REFERENCES .....	88

INITIAL DISTRIBUTION LIST ..... 90

## LIST OF TABLES

Table I. Shock Wave Equation Parameters for TNT. . . . .	8
Table II. Preliminary Shock Wave Parameters. . . . .	38
Table III. Predicted Response of the Air Backed Test Panels. . . . .	39
Table IV. Measured Response of the Air Backed Panels From T1A, T2A, and T4A- 1. . . . .	71

## LIST OF FIGURES

Figure 1. Time / Distance Dependencies of the Shock Wave. . . . .	4
Figure 2. Time / Pressure History of a 300 Pound TNT Charge at 60 Feet [Ref. 3: p. 11]. . . . .	6
Figure 3. A Surface Cut Off Reaction. . . . .	9
Figure 4. Typical Pressure Profile From an Underwater Explosion. . . . .	9
Figure 5. Image Charge Geometry. . . . .	10
Figure 6. Response of an Infinite Plate to an Underwater Shock. . . . .	11
Figure 7. Propagation of the Plastic Bending Wave Through a Plate. . . . .	17
Figure 8. General Configuration of the Test Fixture. . . . .	23
Figure 9. Clamping Method For the Test Fixture. . . . .	24
Figure 10. Plot of Engineering Strain for Samples from the [ 0°/ 90°/ 0°/ 90°/ 0°] <sub>s</sub> Composite Panels. . . . .	26
Figure 11. Plot of Stress vs. Axial Strain for the Composite Tensile Test Specimens. . . . .	28
Figure 12. The General Test Arrangement. . . . .	29
Figure 13. Strain Gage Locations for Test 1. . . . .	33
Figure 14. Strain Gage Locations for Test 2 and Test 4. . . . .	34
Figure 15. Strain Gage Locations for Test 3. . . . .	35
Figure 16. Pressure Transducer Locations for Test 1. . . . .	36
Figure 17. Pressure Transducer Locations for Test 2. . . . .	37

Figure 18. Pressure Transducer Locations for Test 3. . . . .	39
Figure 19. Pressure Transducer Locations for Test 4. . . . .	40
Figure 20. Test Fixture Suspended Beneath the Test Barge. . . . .	41
Figure 21. Placing the Barge and Test Fixture in the Bay. . . . .	42
Figure 22. Comparison of the Peak Recorded Pressures with the Predicted Pressure Trace for the Five Pound TNT Charges. . . . .	45
Figure 23. Comparison of the Peak Recorded Pressures with the Predicted Pressure Trace for the Ten Pound TNT Charges. . . . .	47
Figure 24. The Aluminum Panel From Test T1W. . . . .	48
Figure 25. The $[0^\circ/90^\circ/0^\circ/90^\circ/0^\circ]_5$ Composite Panel From Test T2W. . . . .	49
Figure 26. The $[0^\circ/45^\circ/90^\circ/45^\circ/0^\circ]_5$ Composite Panel From Test T3W. . . . .	51
Figure 27. The Aluminum Panel From Test T1A. . . . .	52
Figure 28. The $[0^\circ/90^\circ/0^\circ/90^\circ/0^\circ]_5$ Composite Panel From Test T2A. . . . .	53
Figure 29. The $[0^\circ/90^\circ/45^\circ/90^\circ/0^\circ]_5$ Composite Panel From Test T4A- . . . . .	54
Figure 30. Edge View of a Matrix Failure. . . . .	55
Figure 31. View of the Test Panel From T4A-2 Immediately Following the Test. . .	56
Figure 32. Measuring Final Transverse Displacement with the Dial Depth Gage. . .	57
Figure 33. Final Transverse Displacement for the Aluminum Panel From Test T1W. . . . .	58
Figure 34. Final Transverse Displacement for the Aluminum Panel From Test T1A. .	59
Figure 35. Final Transverse Displacement for the $[0^\circ/90^\circ/0^\circ/90^\circ/0^\circ]_5$ Composite Panel From Test T2W. . . . .	60

Figure 36. Final Transverse Displacement for the $[0^\circ/45^\circ/90^\circ/45^\circ/0^\circ]_s$ Composite Panel From Test T3W. . . . .	61
Figure 37. Final Transverse Displacement for the $[0^\circ/90^\circ/0^\circ/90^\circ/0^\circ]_s$ Composite Panel From Test T2A. . . . .	62
Figure 38. Final Transverse Displacement for the $[0^\circ/90^\circ/45^\circ/90^\circ/0^\circ]_s$ Composite Panel From Test T4A-1. . . . .	63
Figure 39. Time of peak Transverse Extension for Test T1A. . . . .	65
Figure 40. Progress of the Plastic Bending Wave for Test T1A. . . . .	66
Figure 41. Progress of the Bending Wave for Test T2A. . . . .	69
Figure 42. Time of Peak Transverse Extension for Test T2A. . . . .	70
Figure 43. Side View of the Aluminum Panel From Test T1A. . . . .	78
Figure 44. Detail From the Upper Quarter of the Panel From T2A. . . . .	79
Figure 45. Detail From the Lower Left Quarter of the Panel From T2A. . . . .	79
Figure 46. Detail of the Lower Right Quarter of the Panel From T2A. . . . .	80
Figure 47. Detail of the Right Quarter of the Panel From T2A. . . . .	80
Figure 48. The Composite Panel From Test T3A. . . . .	81
Figure 49. Detail of the Left Quarter of the Panel From T3A. . . . .	82
Figure 50. Detail of the Lower Quarter of the Panel From T3A. . . . .	82
Figure 51. Detail of the Right Quarter of the Panel From T3A. . . . .	83
Figure 52. Detail of the Left Quarter of the Panel From T4A-1. . . . .	83
Figure 53. Detail of the Lower Quarter of the Panel From T4A-1. . . . .	84
Figure 54. Detail of the Right Quarter of the Panel From T4A-1. . . . .	84

Figure 55. The Composite Panel From Test T4A-2. . . . .	85
Figure 56. Detail of the Left Quarter of the Panel From T4A-2. . . . .	86
Figure 57. Detail of the Lower Right Quarter of the Panel From T4A-2. . . . .	86
Figure 58. Detail of the Upper Right Quarter of the Panel From T4A-2. . . . .	87

## ACKNOWLEDGEMENTS

A project of this magnitude cannot be accomplished without the assistance of many individuals. I would like to express my gratitude and appreciation to Dr. Y. S. Shin for his guidance and encouragement and to Dr. K. S. Kim and Mr. Glenn Reid for their assistance in conducting the testing program and for their thoughtful insight in interpreting the resulting data. Additionally, the support provided by the Mechanical Engineering Shop Facility and the Electronics and Instrumentation Support Facility by Mr. Tom Christian, Mr. Jim Selby, Mr. Jim Scholfield, Mr. Charles Crow, and Mr. Mardo Blanco, to name a few, were instrumental in performing the test program in a timely and professional manner. Many thanks to Dr. Tom Tsai and to DNA for their continued interest and support in underwater shock testing at NPS.

Finally, I would like to dedicate this work to my wife, Nancy, and my sons, Matthew, Jeffrey, and Jeremy. Their support and encouragement made it all possible.

## I. INTRODUCTION

Fiber-reinforced laminated composite materials, with their high strength to weight and stiffness to weight ratios, are rapidly finding uses in all aspects of mechanical design. The ability to control the mechanical properties of the material by altering the sequence of the lamina or the orientation of the fibers in each of the laminae in the material allows them to be engineered to meet many specific applications [Ref. 1: pp. 20,21]. The two characteristics that have attracted the attention of marine designers and have made them ideal for application to many types of underwater structures are the corrosion resistance and the non-magnetic properties of many composites.

Underwater shock loading is one of the least forgiving environments to which any material can be subjected. Significant research was conducted into the effects of underwater shock loading on metal structures as a result of World War II. Little, if any, research has been published on the effects of underwater shock loading on composite materials. This thesis, hopefully, will provide some information pertaining to the dynamic response and failure mechanisms of composite plates or panels that will be useful for the designer of marine structures that may experience shock loading.

In spite of the effort devoted to the development of composite material failure theories and to their correlation with test data, no single theory is available which can adequately predict the failure mechanism of fiber reinforced composite materials. Those theories that are easy to apply (primarily extensions of isotropic failure theory) are valid only for cases

of special orthotropy. Those theories not limited to special orthotropy must take into account the directional properties of the material, which are not always available. Thus they suffer from the need for elaborate testing required to determine the various interaction coefficients for the materials. [Ref. 2: p. 76]

The purpose of this research is to experimentally investigate the dynamic response and failure mechanisms of circular composite panels subjected to underwater shock loading. Initially, the response of circular aluminum panels will be measured and compared to typical response characteristics described in the historical studies. The response of the composite panels subjected to similar loading conditions will then be measured and compared to the aluminum panel response. The measured response of the composite panels will then be interpreted to determine the mode of failure of the panels. The information gained by this research will prove useful in determining when and how failure in composite materials will occur.

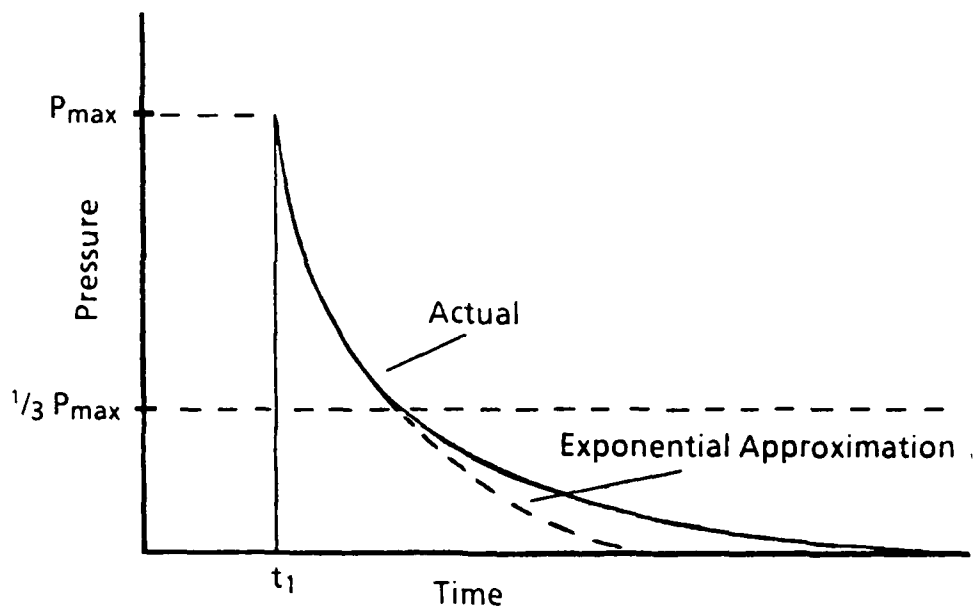
## II. THEORETICAL BACKGROUND

### A. THE UNDERWATER SHOCK WAVE

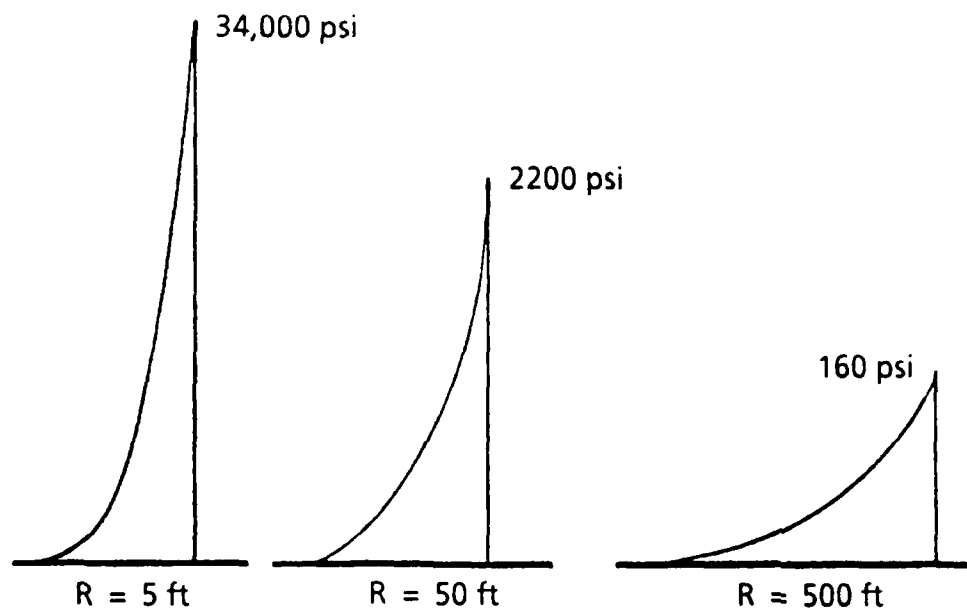
An underwater explosion produces an essentially discontinuous pressure wave or shock wave which, in the immediate vicinity of the explosive charge, can reach a peak pressure of  $2 \times 10^6$  psi and which propagates radially outward at a speed several times the speed of sound in water. The velocity of the shock wave decreases rapidly such that outside of about 10 times the explosive charge radius the disturbance is essentially traveling at sonic velocity. [Ref. 3: pp. 3-7]

In a working range of 10 to 100 times the charge radius, the peak pressure of the shock wave is found to decay as a logarithmic function of distance. At any given point in the working range the pressure profile sensed is essentially a step increase to the peak pressure followed by an exponential decay with time until the pressure has dropped to approximately one third of the peak pressure. After this point the pressure continues to decay, but at a slower rate. Outside of the working range the decay of peak pressure is proportional to the inverse of the distance [Ref. 3: pp. 124-126]. Additionally, as the shock wave radiates away from the explosion, it tends to gradually broaden in duration as it decreases in magnitude. Figure 1 illustrates the time and distance dependencies of the shock wave. [Ref. 3: pp. 3-7]

The kinetic energy contained in the gas bubble generated by the explosion causes it to expand until the internal pressure of the bubble balances the hydrostatic pressure and



a. Time - Pressure History of an Underwater Shock Wave at a Given Stand Off Range.



b. Pressure Distribution at Three Locations Following the Detonation of 300 lb of TNT. [Ref. 3, p. 6]

**Figure 1.** Time / Distance Dependencies of the Shock Wave.

surface tension forces acting on the bubble. Inertia forces cause an additional amount of expansion resulting in an internal pressure of the bubble much less than the hydrostatic pressure surrounding it. At this point the gas bubble begins to collapse in on itself. Depending on the depth and magnitude of the underwater explosion, secondary pressure pulses can be generated by the contraction and subsequent re-expansion of the bubble as shown in Figure 2. The expansion/contraction cycle of the bubble is repeated until all of the energy contained in the bubble is expended or the bubble reaches the surface and the remaining pressure vents to the atmosphere. Typically, only the first pulse, which may contain 10% to 20% of the energy of the initial shock wave, is of any importance as the peak pressure associated with these secondary pulses diminishes rapidly with each successive pulse. The secondary pressure pulses may be avoided if the explosion occurs at a shallow depth so that the bubble vents to the atmosphere during its initial expansion. [Ref. 3: pp. 10, 270-273]

### **1. Empirical Relationships**

Research and testing inspired by World War II resulted in a set of empirical equations that could be used to determine the pressures, decay constants and bubble parameters for underwater explosions generated by different explosives [Ref. 4: pp. 1087-1091]. The equations for peak pressure of the shock wave ( $P_{max}$ ) as a function of radial stand off distance, the shock wave decay constant ( $\theta$ ), pressure as a function of time ( $P(t)$ ), and the maximum radius of the initial gas bubble ( $r_{max}$ ) are shown below.

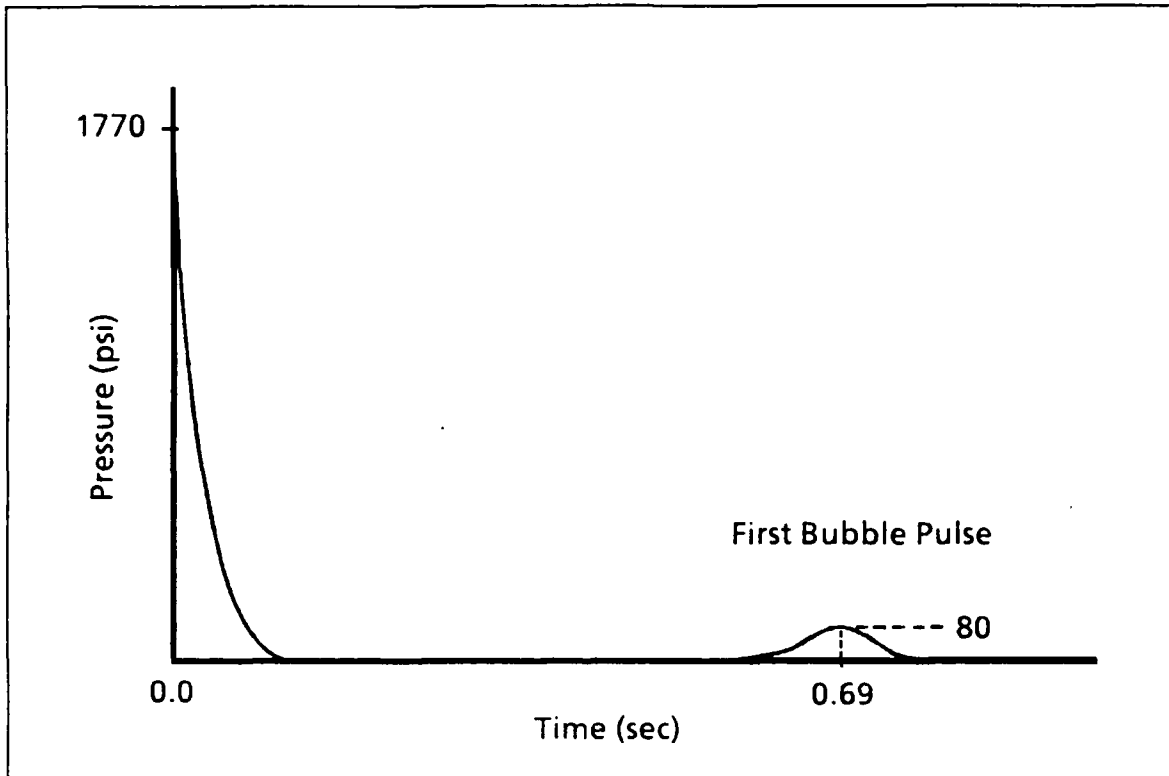


Figure 2. Time / Pressure History of a 300 Pound TNT Charge at 60 Feet [Ref. 3: p. 11].

$$P_{\max} = K_1 \left( \frac{W^{1/3}}{R} \right)^{A_1} \text{ psi.} \quad (1)$$

$$\theta = K_2 (W^{1/3}) \left( \frac{W^{1/3}}{R} \right)^{A_2} \text{ msec.} \quad (2)$$

$$P(t) = P_{\max} \exp\left( \frac{-(t-t_1)}{\theta} \right) \text{ psi.} \quad (3)$$

$$r_{\max} = K_3 \left( \frac{W}{D+33} \right)^{1/3} \text{ ft.} \quad (4)$$

Where:  $W$  = weight of the explosive in pounds.

$R$  = stand off distance in feet.

$t$  = elapsed time since explosion.

$t_1$  = arrival time of the shock wave.

$D$  = depth of the explosive in feet.

$K_1, K_2, K_3, A_1, A_2$  = constant parameters determined by the type of explosive.

Values of the constant parameters for trinitrotoluene (TNT) are shown in Table I [Ref. 5: p.46].

## 2. Underwater Shock Wave Propagation

One of the main differences between the propagation of underwater shock waves and the propagation of underwater acoustic waves lies in the manner in which pressure effects the density of the water. Water can no longer be considered an incompressible substance when large pressures are involved. One of the results of the effect of pressure on density is that the velocity of a shock wave is not constant, but is always greater than and asymptotically approaching the acoustic velocity of water. Some additional differences are noted when the shock wave interacts with a rigid interface, but these effects are negligible for peak pressures less than 14,000 psi [Ref. 3: pp. 55,56]. For the remainder of this analysis, the propagation of underwater shock waves will be treated in the same manner as the propagation of underwater acoustic waves.

Aside from the direct shock wave resulting from the explosion, an underwater target will also experience pressure pulses resulting from the interaction of the shock

**Table I. Shock Wave Equation Parameters for TNT.**

$K_1$	$A_1$	$K_2$	$A_2$	$K_3$
22,505	1.180	0.058	-0.185	12.67

wave with any fluid boundaries. Two boundary interactions that are always present are the surface interaction and the bottom interaction. The surface of the water can be modeled as a free surface and in most cases the bottom can be successfully be modeled as a rigid boundary.

A compressive pressure wave striking a free surface is reflected in accordance with Snell's Law as a rarefaction wave of the same magnitude [Ref. 6: p. 2.4-3]. As this rarefaction wave propagates into the water it travels through regions in the water some short time after the direct shock wave has passed through. The addition of the compressive direct shock wave and the surface reflected rarefaction wave results in a truncation of the direct shock wave pressure profile, termed the surface cut off, that is illustrated in Figure 3. It is possible for the resultant pressure following the surface cut off to approach the vapor pressure of the water, resulting in bulk cavitation. The shock wave can also be reflected from a rigid boundary before reaching the target. However, in this case only the propagation direction is altered with all other characteristics of the shock wave remaining unchanged. Figure 4 illustrates the potential pressure profile at a given location resulting from the direct shock wave, surface cut off, bottom bounce, and bubble pulse.

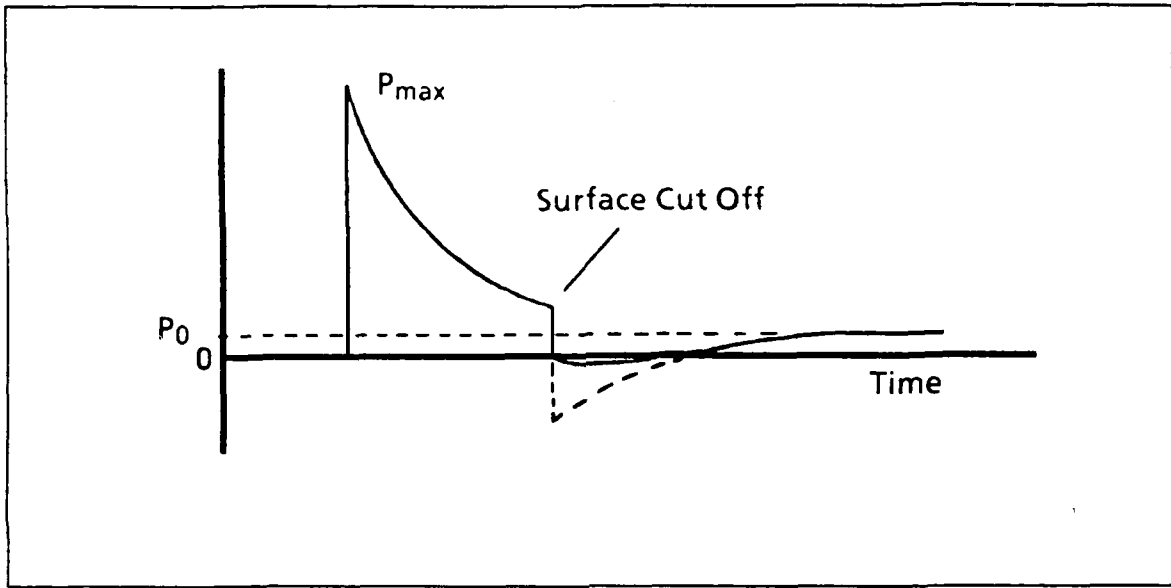


Figure 3. A Surface Cut Off Reaction.

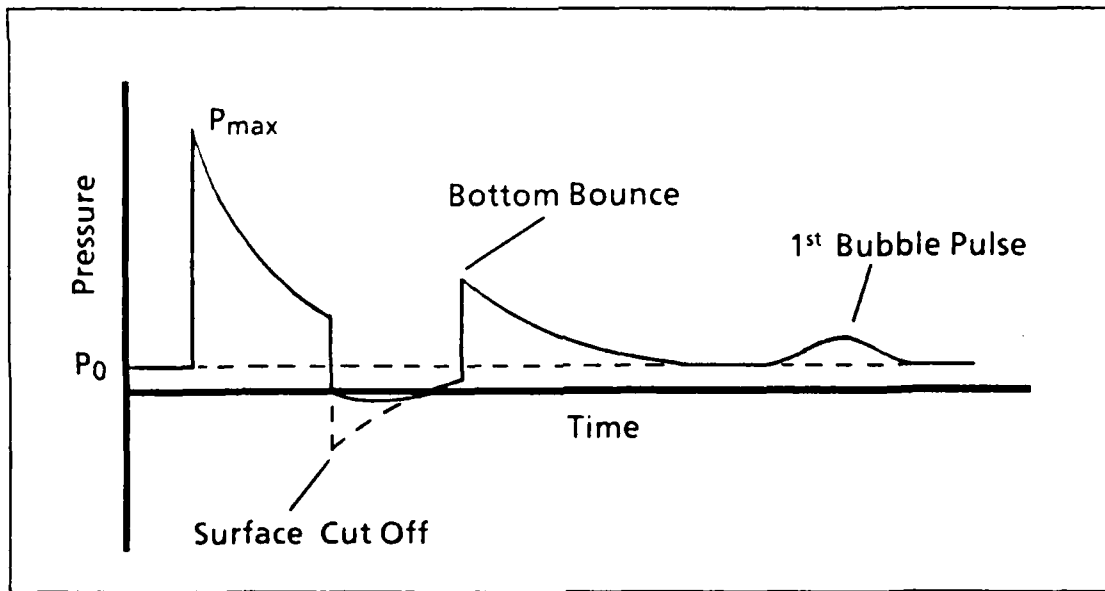


Figure 4. Typical Pressure Profile From an Underwater Explosion.

The arrival times of the various shock and pressure waves at the target location can be calculated by determining the ray path distance from the charge to the target for

each shock or pressure wave. The ray path distance is then divided by the speed of sound in water to obtain the propagation time. A convenient method for determining the ray path distance for reflected waves is to utilize image charges as shown in Figure 5.

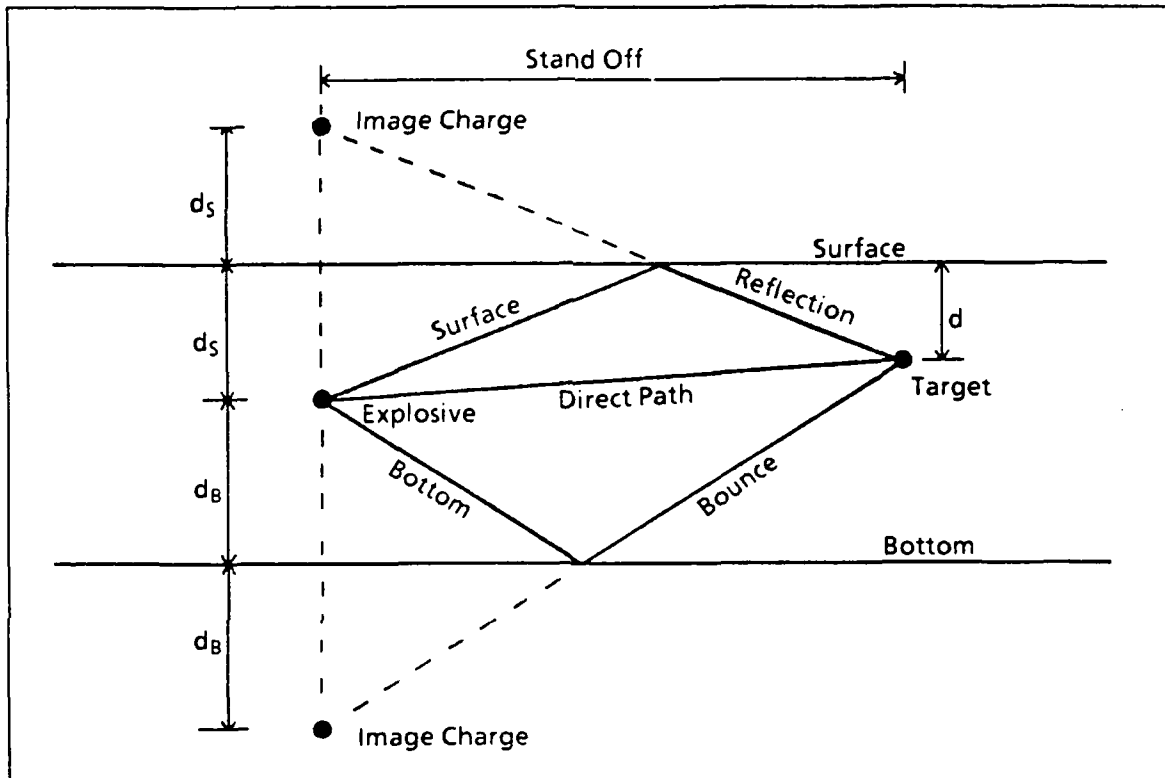


Figure 5. Image Charge Geometry.

## B. IMPULSE RESPONSE OF A FLAT CIRCULAR PLATE

The impulse response of flat circular plates is a complex function involving impulse magnitude, plate dimensions, material properties and the plate boundary conditions. Some understanding of the process can be achieved by analyzing the impulse response of an infinite flat plate, the Taylor plate model [Ref. 7: pp. 292-294], and then

examining the results of a series of underwater explosion effects tests conducted during and after World War II.

### 1. Impulse Response of an Infinite Flat Plate

Consider the situation depicted in Figure 6. A thin infinite plate with mass per unit area  $m$  is simultaneously subjected to the incident planar pressure wave  $P_1$  and the reflected planar pressure wave  $P_2$ . The incident pressure  $P_1$  is of the form

$$P_1 = P_{\max} \exp\left(-\frac{t}{\theta}\right) \quad (5)$$

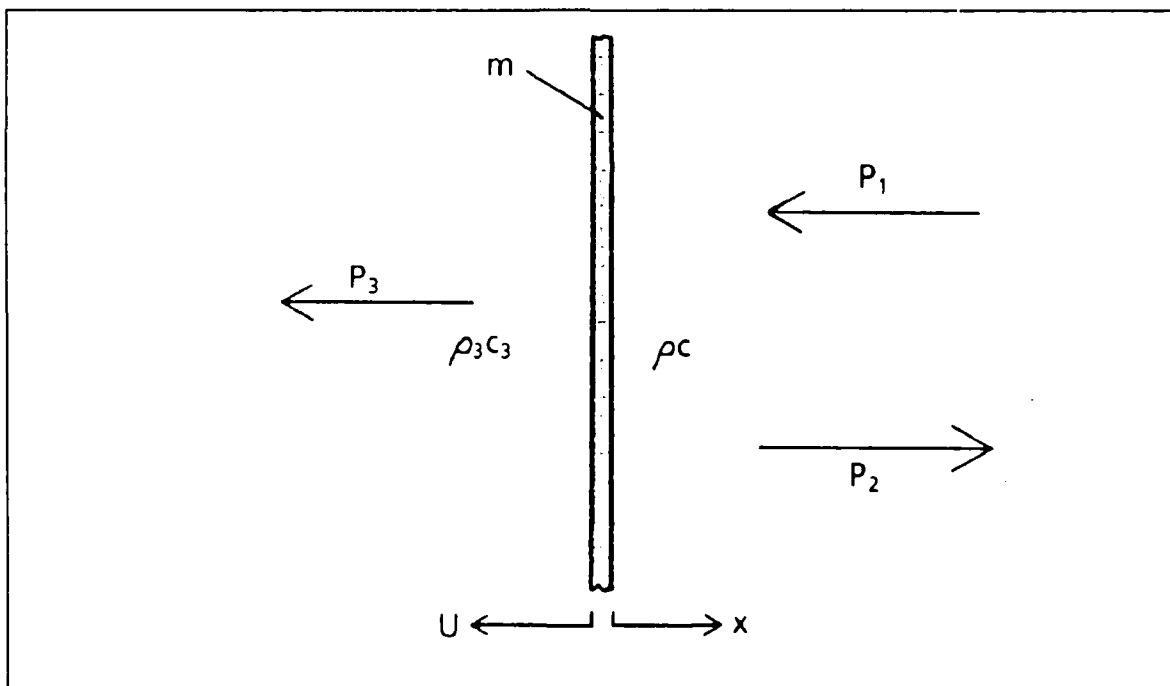


Figure 6. Response of an Infinite Plate to an Underwater Shock.

If the water is assumed to be incompressible, the incident and reflected pressures,  $P_1$  and  $P_2$ , can be related to the fluid particle velocity in the respective pressure waves by

$$P_1 = \frac{U_1}{\rho c} \quad (6)$$

and

$$P_2 = -\frac{U_2}{\rho c} \quad (7)$$

where  $\rho$  and  $c$  are the density and sonic velocity of the fluid. At the surface of the plate the plate velocity  $U$  can be expressed as

$$U = U_1 + U_2 \quad (8)$$

assuming no initial cavitation on the plate.

For an air backed plate, the effect of the air on the motion of the plate is negligible compared to the effect of the water acting on the face of the plate. The equation of motion for the infinite plate can be written as

$$m \frac{dU}{dt} = P_1 + P_2 \quad (9)$$

or substituting equations (7) and (8) for  $P_2$

$$m \frac{dU}{dt} = 2P_1 + U\rho c \quad (10)$$

Assuming that the plate is initially at rest,  $U$  is determined to be

$$U = \frac{2P_{\max}\theta}{m(1-\beta)} \left[ \exp\left(-\frac{\beta t}{\theta}\right) - \exp\left(-\frac{t}{\theta}\right) \right] \quad (11)$$

where

$$\beta = \frac{\rho c \theta}{m} \quad (12)$$

Substituting equation (11) back into equation (8), the reflected wave pressure  $P_2$  is determined to be

$$P_2 = \frac{P_{\max}}{(1-\beta)} \left[ (1+\beta) \exp\left(-\frac{t}{\theta}\right) - 2\beta \exp\left(-\frac{\beta t}{\theta}\right) \right] \quad (13)$$

The total pressure  $P_t$  on the face of the air backed plate is the sum of  $P_1$  and  $P_2$  can be determined by combining equations (5) and (13).

$$P_t = P_{\max} \left[ \exp\left(-\frac{t}{\theta}\right) + \frac{1+\beta}{1-\beta} \exp\left(-\frac{t}{\theta}\right) - \frac{2\beta}{1-\beta} \exp\left(-\frac{\beta t}{\theta}\right) \right] \quad (14)$$

Note that if the water cavitates or separates from the face of the plate the forces acting on the plate are reduced to zero and the plate has achieved its maximum velocity. Setting the total pressure  $P_t$  equal to zero, the cut off time  $\theta_c$  can be calculated as

$$\theta_c = \left( \frac{\theta}{\beta - 1} \right) \ln \beta \quad (15)$$

The maximum velocity of the plate can then be determined as

$$U_{\max} = \frac{2P_{\max}\theta}{m(1-\beta)} \left[ \exp\left(-\frac{\beta \ln \beta}{1-\beta}\right) - \exp\left(-\frac{\ln \beta}{1-\beta}\right) \right] \quad (16)$$

When analyzing the response of a water backed plate, the quantity  $\rho_3 c_3$  is equal to  $\rho c$  and  $P_3$  can no longer be neglected. The equation of motion for the water backed plate may be written as

$$m \frac{dU}{dt} = P_1 + P_2 - P_3 \quad (17)$$

Noting that

$$P_3 = \frac{U_3}{\rho_3 c_3} = \frac{U}{\rho c} \quad (18)$$

equation (17) may now be expressed as

$$m \frac{dU}{dt} = 2P_{\max} \exp\left(-\frac{t}{\theta}\right) - 2U\rho c \quad (19)$$

Solving equation (19) for the velocity of the plate, the following expression is obtained

$$U = \frac{2P_{\max}\theta}{m(1-2\beta)} \left[ \exp\left(-\frac{2\beta t}{\theta}\right) - \exp\left(-\frac{t}{\theta}\right) \right] \quad (20)$$

Substituting the expression for  $U$  back into equation (8), the reflected pressure  $P_2$  is determined to be

$$P_2 = P_{\max} \left[ \frac{1}{1-2\beta} \exp\left(-\frac{t}{\theta}\right) - \frac{2\beta}{1-2\beta} \exp\left(-\frac{2\beta t}{\theta}\right) \right] \quad (21)$$

Combining the previous expression with equation (14) allows the pressure on the face of the panel to be determined as

$$P_t = 2P_{\max} \left[ \frac{1-\beta}{1-2\beta} \exp\left(-\frac{t}{\theta}\right) - \frac{\beta}{1-2\beta} \exp\left(-\frac{2\beta t}{\theta}\right) \right] \quad (22)$$

Note that if  $\beta > 1.0$ , then  $P_t$  is always positive and cavitation cannot occur on the surface of the panel.

An attempt has been made to reconcile the plate response predicted by Taylor plate theory with the observed response of finite circular plates that will be discussed in more detail in the next section. The resulting expression for the maximum deflection of the center of the flat circular plate tries to account for the physical constraint at the boundary, the refraction of the shock wave around the plate and the additional loading of the plate due to after flow. This expression, which is applicable to the air backed plate only, is presented below without development.

For a circular air backed plate of radius  $a$ , thickness  $h$ , and yield strength  $\sigma_y$ , mounted in a finite rigid baffle, the maximum deflection of the center of the plate is determined by [Ref. 3: p. 420]

$$z_{\max} = \frac{P_{\max} a}{\rho c} \sqrt{\frac{2m}{\sigma_y h}} \beta^{\frac{1}{1-\beta}} \left(1 + \frac{\beta}{4}\right)^{\frac{1}{2}} \quad (23)$$

## 2. Impulse Response of a Flat Circular Plate

The response of rigidly mounted air backed circular metal plates to underwater shock loading has been of interest for diverse reasons. Circular plates were studied not only as a means of understanding the effects of underwater explosions on surface ships but also as a means of measuring the force of these explosions using the deflection of small metal diaphragms. In all cases the response of thin air backed metal plates to underwater shock loading followed a consistent pattern.

On impact of the shock wave, the plate attempts to move away from the source of the shock wave with a uniform rigid body motion. The portion of the plate adjacent to the rigid boundary is immediately restrained. The effect of the boundary restraint is communicated to the remainder of the plate as a radial elastic tension wave that proceeds from the plate boundary to its center, propagating at the sonic velocity in the material.

As the plate continues to move away from the source of the shock wave a plastic bending wave is generated in the material and propagates radially toward the center at a slower speed. During this time the central portion of the plate continues to move relatively unimpeded by the effect of the boundary. As shown in Figure 7, as the bending wave

propagates to the center of the plate, the plate achieves the characteristic shape of a nearly conical surface of revolution. Measurements of the tangential and radial strains along a radius show that the two strains tend to be nearly equal at each point.

The thickness of the plate shows a marked localized thinning and a subsequent tendency to shear at the plate boundary. Elsewhere, the thickness shows a gradual taper from full thickness near the boundary toward the center. At the center of the plate thinning again becomes prominent and results in a pronounced dimple. [Ref. 8: pp. 164-168]

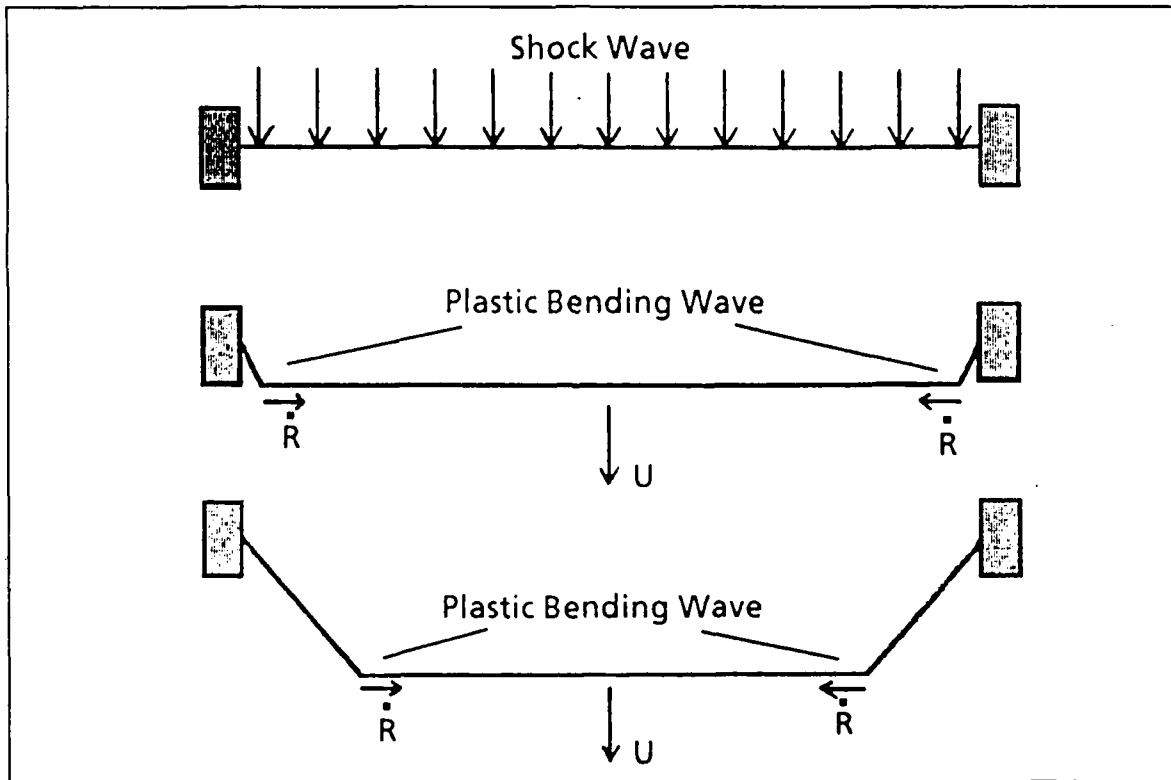


Figure 7. Propagation of the Plastic Bending Wave Through a Plate.

Differential equations describing the response of the plate to a distributed impulse load have been developed [Ref. 8: p. 168-182] but are extremely complex. By

assuming a material that does not work harden and by neglecting the reaction of the material in the central flat area of the plate, a simplified solution may be developed [Ref. 8: p. 183] in which the velocity of the plastic bending wave may be expressed as

$$\dot{R} = -\sqrt{\frac{\sigma_y}{\rho}} \quad (24)$$

where  $\sigma_y$  is the yield stress of the material. The displacement of the plate is described by

$$z = \frac{U}{c}(a-R) \quad (25)$$

where  $U$  is the velocity of the plate,  $R$  is the radial location,  $a$  is the radius of the plate and the quantity  $c$  is defined by

$$c^2 = \frac{\sigma_y}{\rho} \quad (26)$$

### C. COMPOSITE MATERIAL BEHAVIOR

The behavior of plates fabricated from orthotropic materials has been studied using classical plate theory [Ref. 9: pp. 242,243], which is limited in application to shock loading by the restrictions of small deflections compared to the plate thickness and neglecting out of plane stresses. Additionally, classical plate theory does not address a

fiber-reinforced composite by merely requiring orthotropic behavior. As such, little light can be shed on the failure mechanism of composite plates or panels.

An observed characteristic of failure in fiber-reinforced composites is that the components of the composite do not fail at the same time [Ref. 2: p. 33]. If the fiber is the first component to fail (high strength, stiff fiber and an elastic matrix), then the composite will undergo sudden and complete rupture. If the matrix fails first (high strength, elastic fiber and a brittle matrix), then the failure of the composite will initially show as cracks in the matrix material prior to complete failure of the structure.

In most composite materials, the strength of the reinforcing fiber is significantly greater than the strength of the matrix material. For this reason tension is a fiber dominated process. Specimens placed in uniaxial tension demonstrate a variety of failure mechanisms prior to the ultimate failure of the material. Matrix cracking and delamination are among the more detectable of these mechanisms. The loss of continuity in the material caused by matrix cracking or separation of a lamina results in a characteristic kink noted in the stress-strain curves for these types of composites. [Ref. 2: p. 33]

Under uniaxial compression, fiber-reinforced composites typically exhibit three modes of failure [Ref. 2: p. 230]

1. Buckling of the fibers (low stiffness matrices).
2. Transverse breakage due to Poisson's ratio differences of the material constituents and non-uniform transverse strain distributions along the specimen length (medium stiffness matrices).
3. Shearing of reinforcing fibers at an angle near  $45^\circ$  without local buckling (high stiffness matrices).

Combinations of the three modes are often seen and are accompanied by other phenomena such as lamina peeling, loss of stability, brooming, and splitting.

Behavior of the composite under the more complex stress states expected during an underwater shock test is not well understood. While some combination of the effects noted during uniaxial loading may be expected, the exact nature of the response of the material and the failure mechanism involved is not known.

### III. EXPERIMENTAL METHODS

#### A. TEST FIXTURE DESIGN

There were three major considerations that guided the design of the test fixture.

1. The fixture should be substantial enough to withstand several explosions without significant damage or warping.
2. The test fixture should allow for exposing a large area of the test panel surface to the explosion.
3. The test fixture size and weight should be within the limits of the handling and transportation equipment readily available to the Naval Postgraduate School.

Designing structures to be exposed to underwater explosions is at best an art, relying more often than not on the *prior experience* of the designer than on any generally accepted code or rule. Previous underwater shock testing conducted by NPS indicated that an adequately braced structure constructed from  $\frac{3}{4}$  inch thick structural grade steel plate would possess sufficient strength and stiffness to withstand multiple explosive tests. With the construction material chosen, the desired size and shape of the test panel and the limitations of the weight handling equipment at NPS became the controlling parameters governing test fixture design.

The desire to maximize the exposed surface area of the test panels while simultaneously limiting the overall weight of the test fixture to approximately 1000 pounds pointed toward using a circular section for the body of the fixture. As shown in

Figure 8, the final design consisted of a cylindrical shell body three feet in diameter and eight inches high, upper and lower clamp rings four feet in diameter and six inches wide, eight exterior rectangular gussets supporting the lower clamp ring, and a circular backing plate three feet in diameter to close off the back of the fixture. A second test fixture was designed identical to the first with the exception that the backing plate was not included. All components of the fixtures were fabricated from  $\frac{3}{4}$  inch thick structural steel plate except the gussets, which were  $\frac{1}{2}$  inch steel plate. Both fixtures were coated with red primer for corrosion control.

The test plate was positioned in the test fixture by the upper and lower clamp rings. Shallow recesses were machined into the clamp rings to assist in positioning the test plate. The lower clamp ring was welded to the upper end of the cylindrical body. The upper clamp ring was attached to the lower clamp ring by 64  $\frac{3}{4}$  inch SAE Grade 7 bolts arranged in two concentric circles along the outer edge of the clamp rings. The fixture could accommodate circular test panels 40 inches in diameter and provided an exposed target area three feet in diameter.

Two methods were considered for securing the panel in the test fixture. Bolting through the panel would have provided the best approximation of a fixed boundary condition. This method was rejected because of the increased costs that machining the bolt holes in the test panel would have generated and because of concern that the holes might have caused premature failure in the boundary region of the panel. As shown in Figure 9, the method chosen was to clamp the panel between the upper and lower clamp rings. This method of securing the panel would allow some motion in the radial

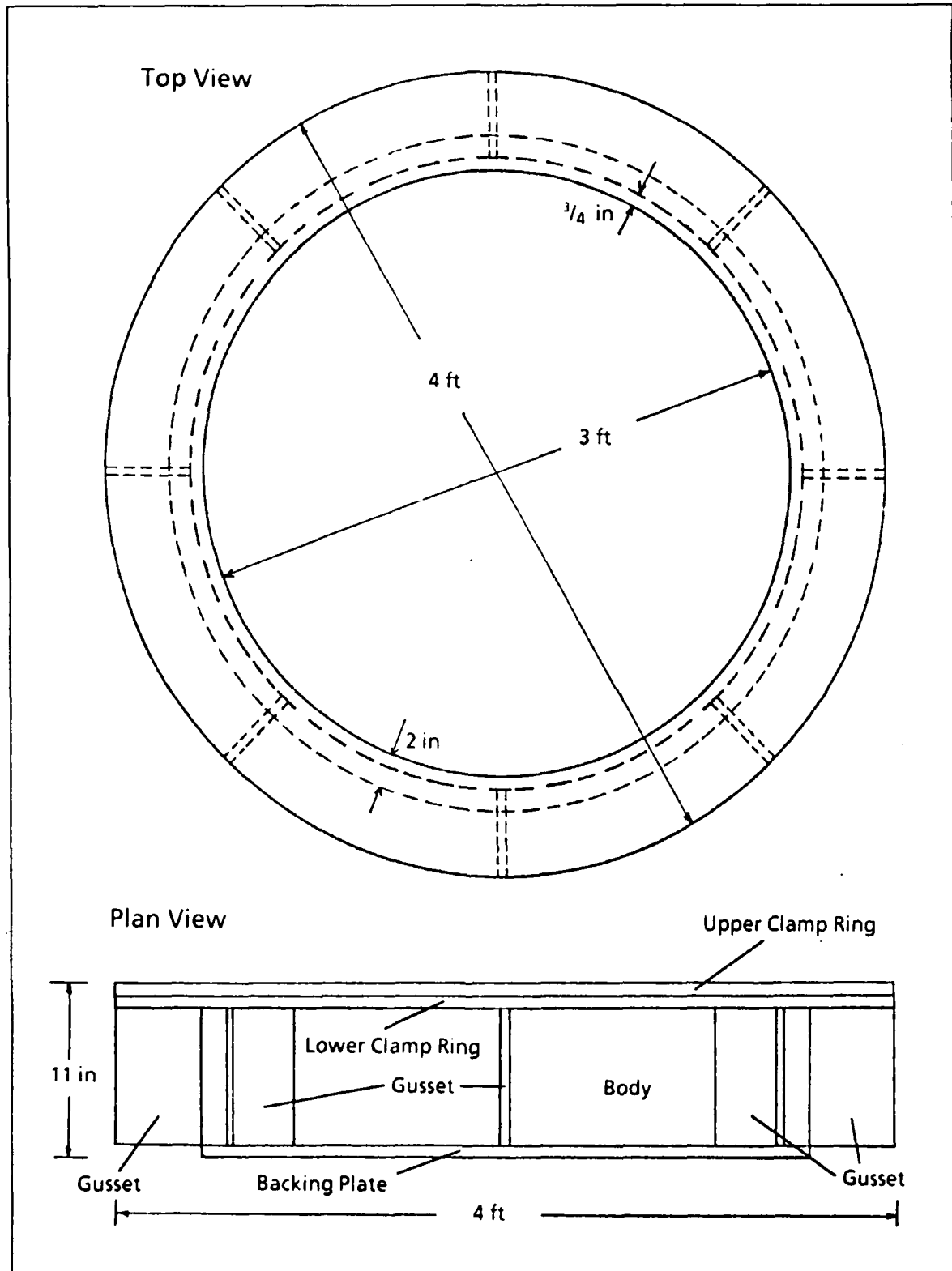


Figure 8. General Configuration of the Test Fixture.

direction, but the trade-off was considered to be an acceptable means of keeping the panel intact.

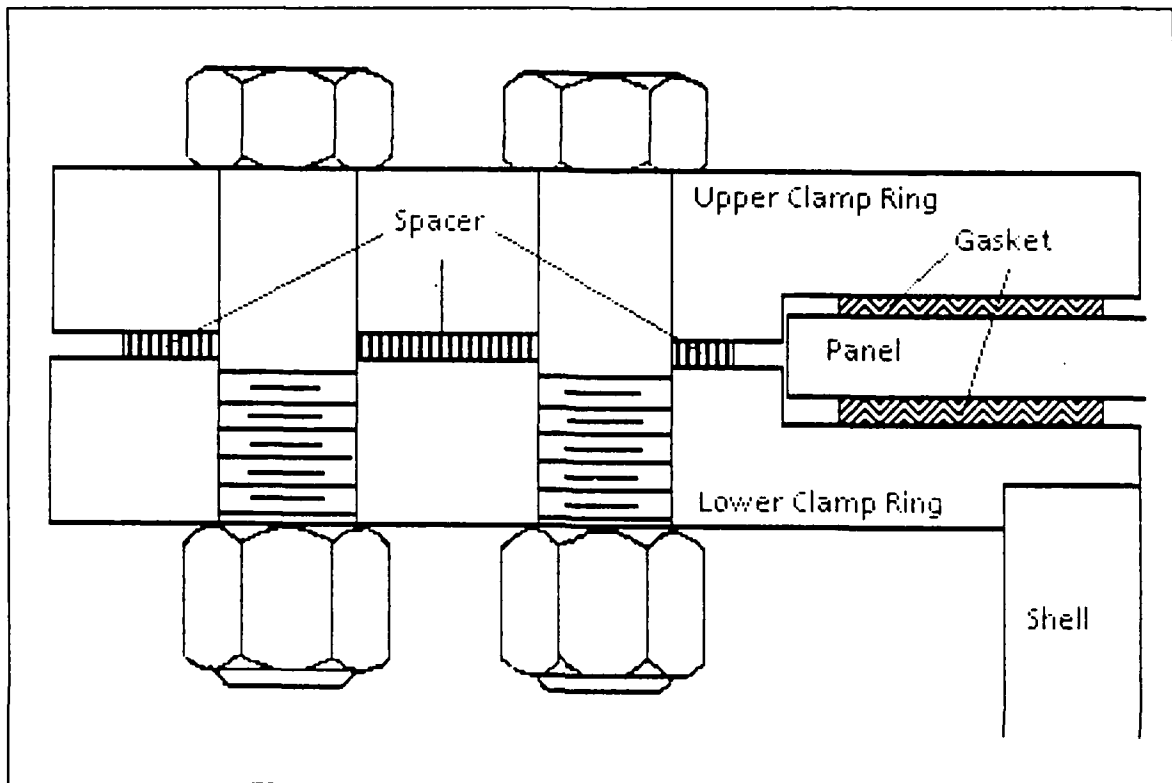


Figure 9. Clamping Method For the Test Fixture.

## B. TEST ARRANGEMENT

### 1. Test Material Selection

Six circular composite plates , 40 inches in diameter and  $\frac{1}{4}$  inch thick, were obtained for this research. The composite panels were fabricated from a plain weave S-2 glass fabric having equal numbers of fiber rovings running in the warp and fill directions and a polyester resin matrix. The balanced weave of the S-2 glass fabric provides equivalent material properties in the two principle directions. Each panel was composed

of 10 layers of the glass/polyester pre-impregnated mats and was vacuum bag cured. The panels were produced using three symmetric stacking sequences:

1.  $[0^\circ/90^\circ/0^\circ/90^\circ/0^\circ]_s$
2.  $[0^\circ/90^\circ/45^\circ/90^\circ/0^\circ]_s$
3.  $[0^\circ/45^\circ/90^\circ/45^\circ/0^\circ]_s$

Two panels were produced using each stacking sequence. Because of the balanced weave of the glass fabric the  $0^\circ$  and  $90^\circ$  laminae are structurally equivalent and the  $\pm 45^\circ$  laminae are structurally equivalent.

Additionally, two alloy 6061-T6 aluminum panels with the same dimensions as the composite test panels were procured. The aluminum panels were used for the initial two explosive tests. This allowed the test arrangement and data acquisition systems to be tested against a material with well known properties.

The physical properties of the composite and the aluminum test materials are summarized in Appendix A. A small number of samples of the  $[0^\circ/90^\circ/0^\circ/90^\circ/0^\circ]_s$  composite test panels were tested in accordance with ASTM Standard D 3039-74 for tensile tests of composite materials [Ref. 10]. The results of these tests were used as a gage for how well the properties of this particular composite lay up matched the nominal properties for the material.

Figure 10 illustrates the performance of the composite in terms of engineering strain for specimens cut parallel to the warp direction ( $0^\circ$ ), perpendicular to the warp direction ( $90^\circ$ ), and at a  $45^\circ$  angle to the warp direction. The  $0^\circ$  and  $90^\circ$  specimens

showed essentially identical responses. The discontinuity appearing at approximately 37,000 psi on both plots represents first ply failure for the samples. The ultimate tensile strength for these samples could not be determined. The testing of each sample had to be secured when the adhesive joint joining the specimen to the end tabs failed. The behavior of the 45° samples was radically different. Since no fibers ran continuously through the sample, the response is dominated by the matrix characteristics. Evidence of matrix cracking began appearing at less than 10,000 psi stress. The sample retained some load bearing ability until the applied stress reached approximately 16,000 psi. The large strains in this region resulted as the glass fibers were pulled free of the matrix.

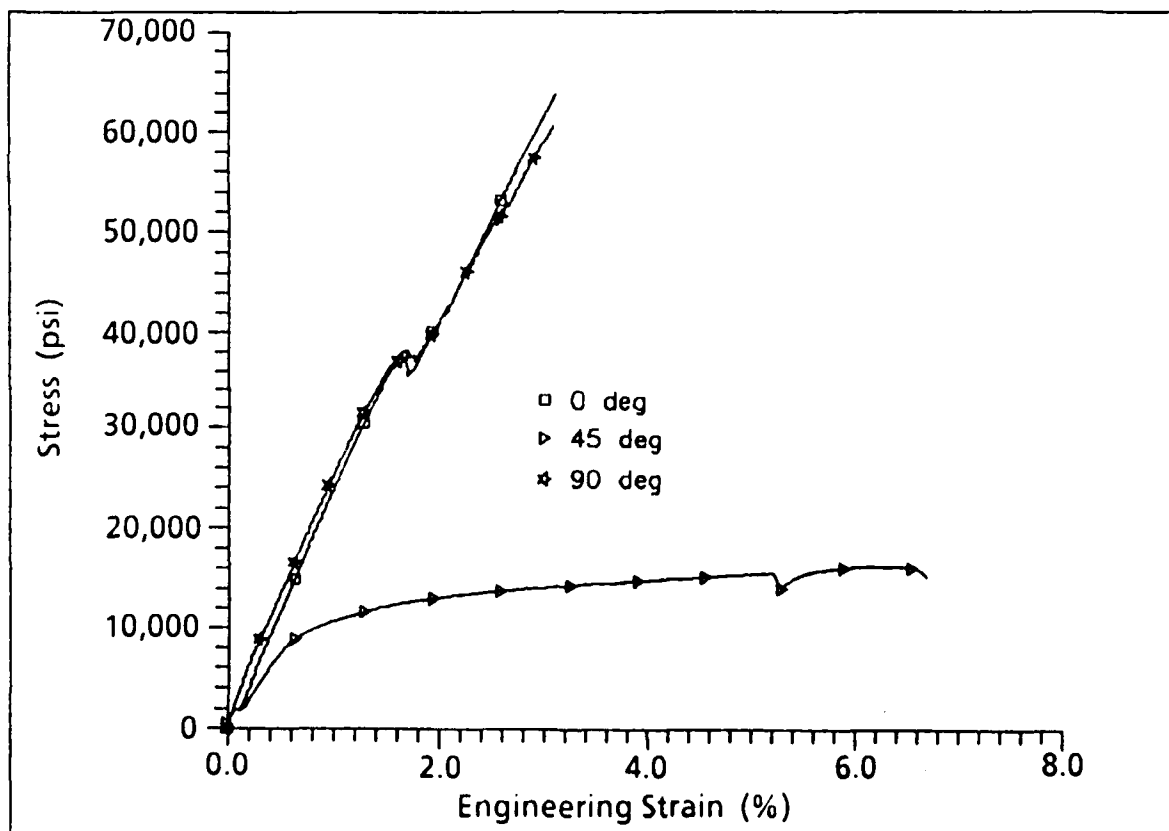


Figure 10. Plot of Engineering Stress for Samples from the  $[0^\circ/90^\circ/0^\circ/90^\circ/0^\circ]_s$  Composite Panels.

The strain values recorded from a strain gage mounted axially on the surface of the test specimens are shown in Figure 11. These results are generally identical to the engineering strain values discussed previously. The strain gages on all of the samples failed at approximately 1.7% strain. The 0° and 90° specimens exhibited a discontinuity representing first ply failure at 37,000 psi. The values of  $E_x$  and  $E_y$  determined from the 0° and 90° specimens were  $2.83 \times 10^6$  psi. This compares very favorably with the published value of  $2.7 \times 10^6$  psi from Appendix A.

## 2. Test Site Arrangement

The overall testing arrangement was coordinated with the West Coast Test Facility (WCSF) located at Hunter's Point Naval Shipyard, San Francisco, CA. WCSF provided a pontoon test barge capable of positioning the test fixture and the explosive charge. The test barge also located the junction box connecting the leads from the instrumentation mounted on the fixture and the test panel to the shielded cable leading back to the data recorders.

Because of the relatively shallow water depth at WCSF, a vertical arrangement of the test fixture and explosive charge was not possible. A three point suspension system was devised that held the test fixture beneath the barge at a depth of approximately 11 feet with the normal vector of the test panel aligned 30° from horizontal. An A-frame support projecting from the front of the barge positioned the explosive charge approximately 12 feet horizontally from the test panel and at a depth of approximately four feet. The location of the explosive charge was adjustable to maintain a 14 foot stand off normal to the center of the test panel. A three piece brace fabricated

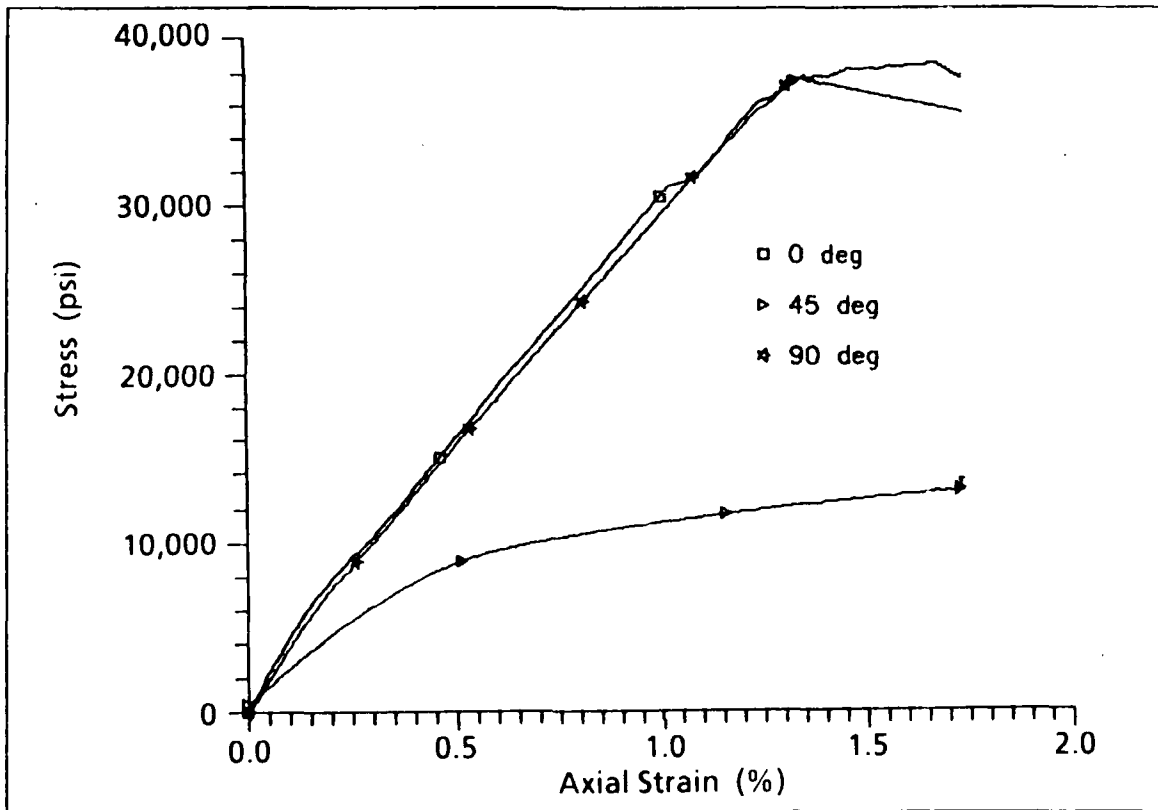


Figure 11. Plot of Stress vs. Axial Strain for the Composite Tensile Test Specimens.

from one inch steel angle beams was used to hold the fixture at the correct angle and as an additional attachment point for the suspension cables. Figure 12 provides a representation of the test arrangement.

### 3. Test Instrumentation

Measurements were desired of several parameters from each of the shock tests.

These included:

1. Surface strains on the test panel.
2. Shock wave pressure, both free field and at the test panel.
3. Acceleration of the panel center and the test fixture.

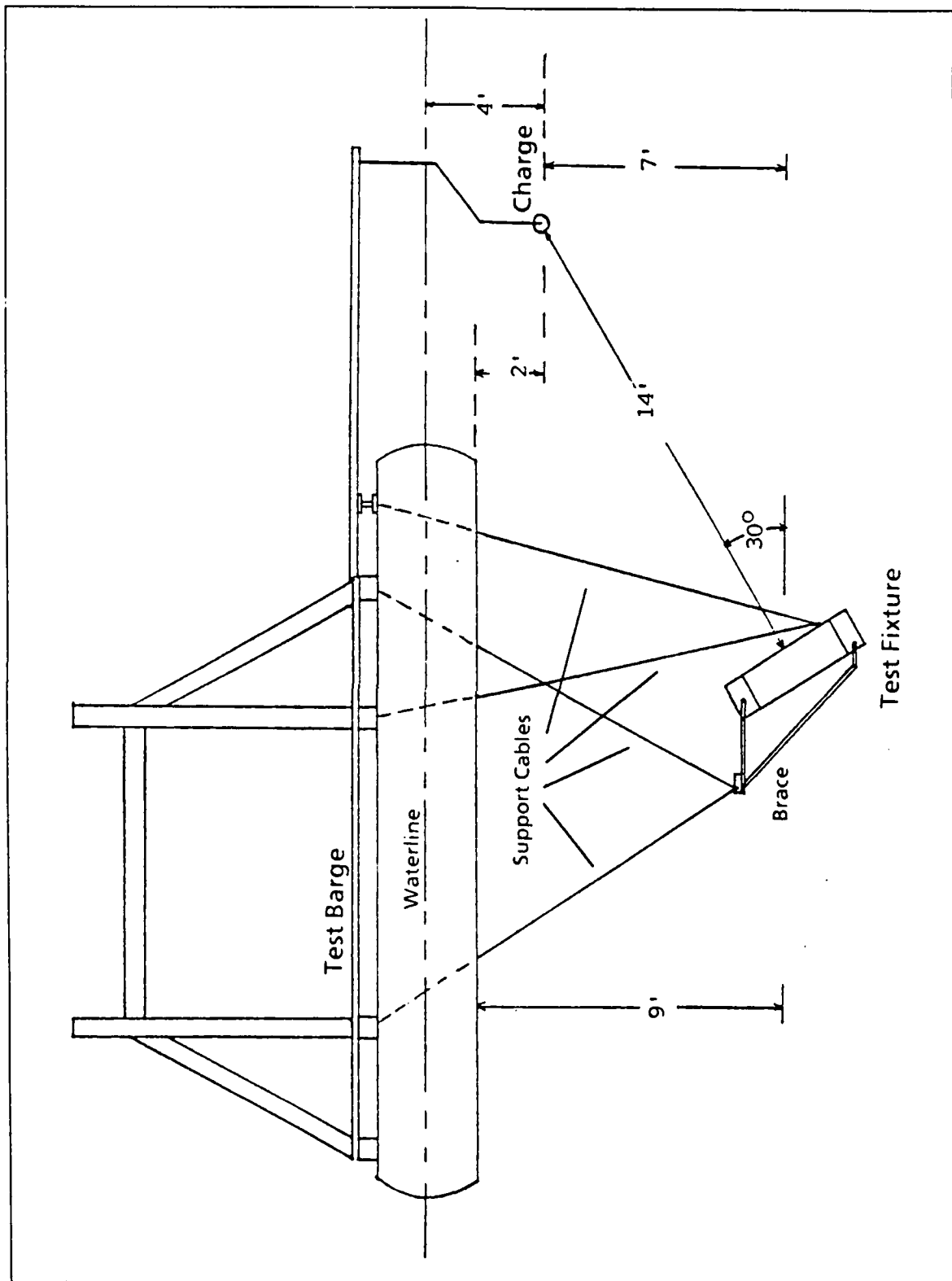


Figure 12. The General Test Arrangement.

Micro-Measurements CAE-13-250UN-350 strain gages were chosen for the aluminum panels. These gages have a gage length of 0.125 inches and a width of 0.120 inches. The relatively small size of these gages made them a good choice for measuring the localized strains in an isotropic material. These gages were rated for 5% strain.

Because of the heterogeneity of the composite panels, larger area strain gages were required to provide a measure of the average strain at a particular area. BLH Electronics strain gages FAE-50-35-S13-EL, with a gage length of 0.500 inches and a width of 0.250 inches were chosen for this application. These gages are also rated at 5% strain.

The pressure transducers and accelerometers selected for these shock tests were produced by PCB Piezotronics, Inc. Blast pressure transducers model 138A50 were chosen to measure the shock wave pressure. These tourmaline crystal element transducers have a range of 50,000 psi and a rise time of 1.5 microsecond. The accelerometers chosen were High-Shock Accelerometers model 350A. These accelerometers are lightweight (4.5 grams) and have a range of 100,000g.

Two data recorders were available for recording the output of the strain gages, pressure transducers, and accelerometers. A Raycal Storehorse, 14 channel, magnetic tape Instrumentation Recorder was used to record the output of the strain gages. Output from the pressure transducers and the accelerometers was recorded on a Honeywell Model 101 magnetic tape recorder. Digitization of the recorded test data was accomplished using a Hewlett-Packard 9000/300 desk top computer running HPVista Signal Analysis software.

### C. TEST PROCEDURE

Two basic types of tests were conducted during this series of experiments: water backed tests, in which the test panel was exposed to seawater on both the front and back, and air backed tests, in which the front of the test panel is exposed to seawater and the back is exposed to an air space. The water backed tests were designed to investigate the elastic response of the various test panels, while the air backed tests were designed to investigate the plastic response and failure mode of the test panels.

A test plan was developed consisting of eight explosions to be conducted in groups of two shock tests on a given test day. One test each day would be an air backed shock test and the other would be a water backed shock test. This test plan was modified during the testing such that both of the last two tests were air backed tests. A temporary backing plate was welded to the back of the water backed test fixture in order that this test plan modification might be accomplished.

A brief description of each test and its desired results is listed below.

1. Test No. 1: Test 1 used the aluminum panels as targets for the shock tests. The purpose of Test 1 was to verify the test arrangement and the data acquisition system and to gather test data from panels with fairly predictable response. Five pound charges of TNT were used for this test.
2. Test No. 2: Test 2 used the  $[0^\circ/90^\circ/0^\circ/90^\circ/0^\circ]_s$  set of the composite panels as targets. The purpose of Test 2 was to investigate the dynamic response and failure mechanism of a highly orthotropic composite panel. Five pound charges of TNT were used for this test.
3. Test No. 3: Test 3 used the  $[0^\circ/45^\circ/90^\circ/45^\circ/0^\circ]_s$  set of the composite panels as targets. The purpose of Test 3 was to examine the response and failure mechanism of a "quasi-isotropic" composite panels. Ten pound charges of TNT were used for this test.

4. Test No. 4: Test 4 was designed to utilize the remaining set of  $[0^\circ/90^\circ/45^\circ/90^\circ/0^\circ]_s$  composite panels as targets and to provide additional data describing the response and failure mode of the composite material. One five pound TNT charge and one ten pound TNT charge were used for this test.

Each individual shock test was assigned a test identifier consisting of a 'T' followed by the general test number and either an 'A' or a 'W' to differentiate between the air backed and water backed tests. For instance, T1W refers to the water backed test conducted on the first test day while T3A refers to the air backed test conducted on the third test day. This nomenclature was utilized when referring to each individual test and the data it provided.

Each test panel was instrumented with 12 strain gages mounted such that radial and circumferential strains could be recorded at various locations on the front and back surfaces of the panel. For Test 1 the strain gages were mounted along three radials spaced  $120^\circ$  apart as shown in Figure 13. Because of the orthotropic nature of the composite panels, the strain gage mounting pattern was altered to that shown in Figure 14 and Figure 15 for Tests 2 through 4. A slightly different numbering sequence from that used in Tests 2 and 4 was inadvertently used for the strain gages of Test 3.

Initially, five blast pressure transducers were used for each test. However, considerable attrition was suffered among the transducers mounted closest to the explosive charge. By the last test, only three pressure transducers remained operational. Since the primary uses of the pressure transducers were to verify proper detonation of the explosive charges and to provide a positive indication of the time of impact of the shock wave with

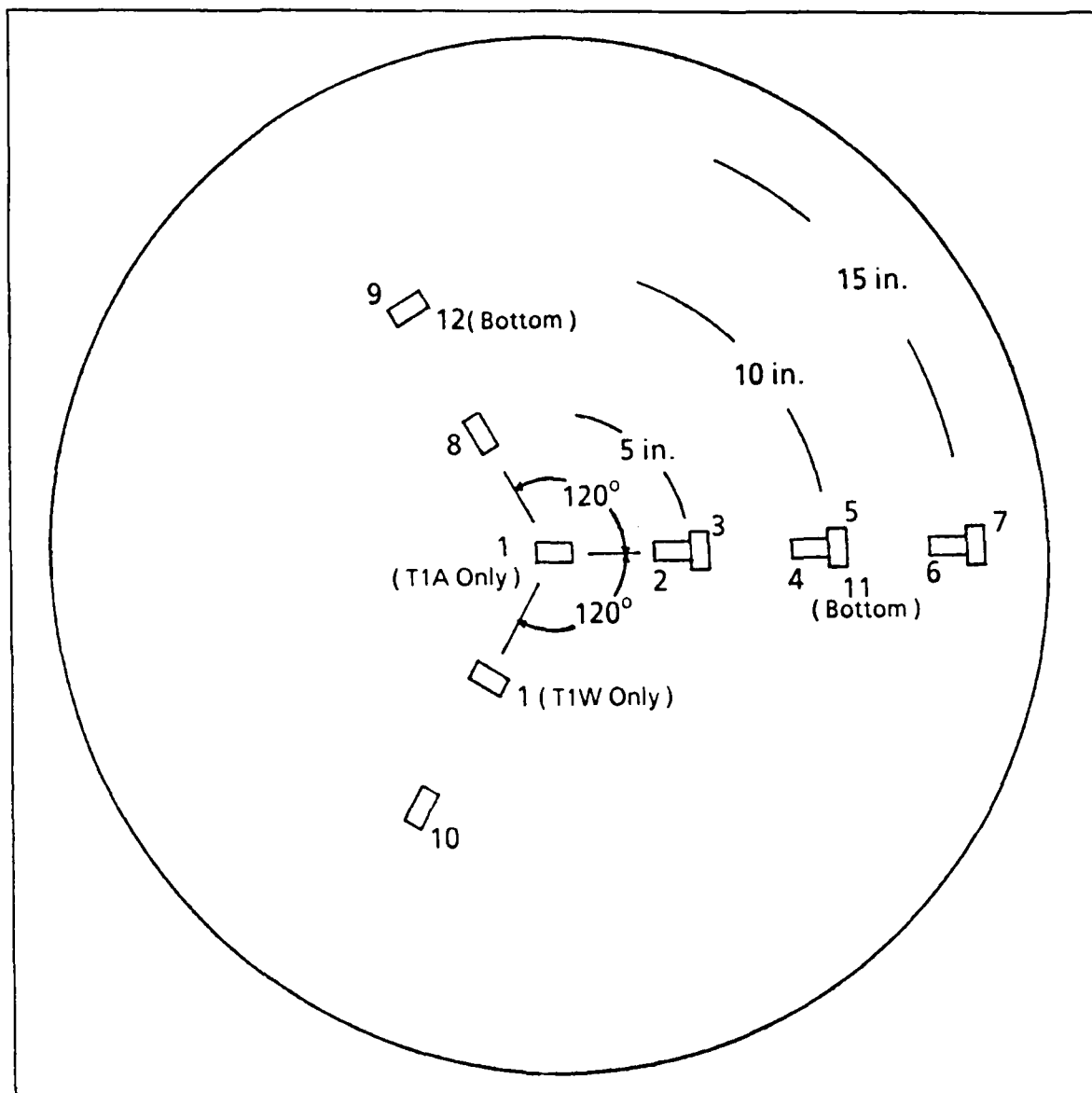


Figure 13. Strain Gage Locations for Test 1.

the test panel, the reduction in the number of transducers did not significantly affect the testing. The blast pressure transducer locations for Tests 1 through 4 are shown in Figure 16 through Figure 19 respectively.

Accelerometers were mounted on the underside center of the test panel for T1W and on the underside of the lower clamp ring for T1A, T2W, and T2A. Since mounting the

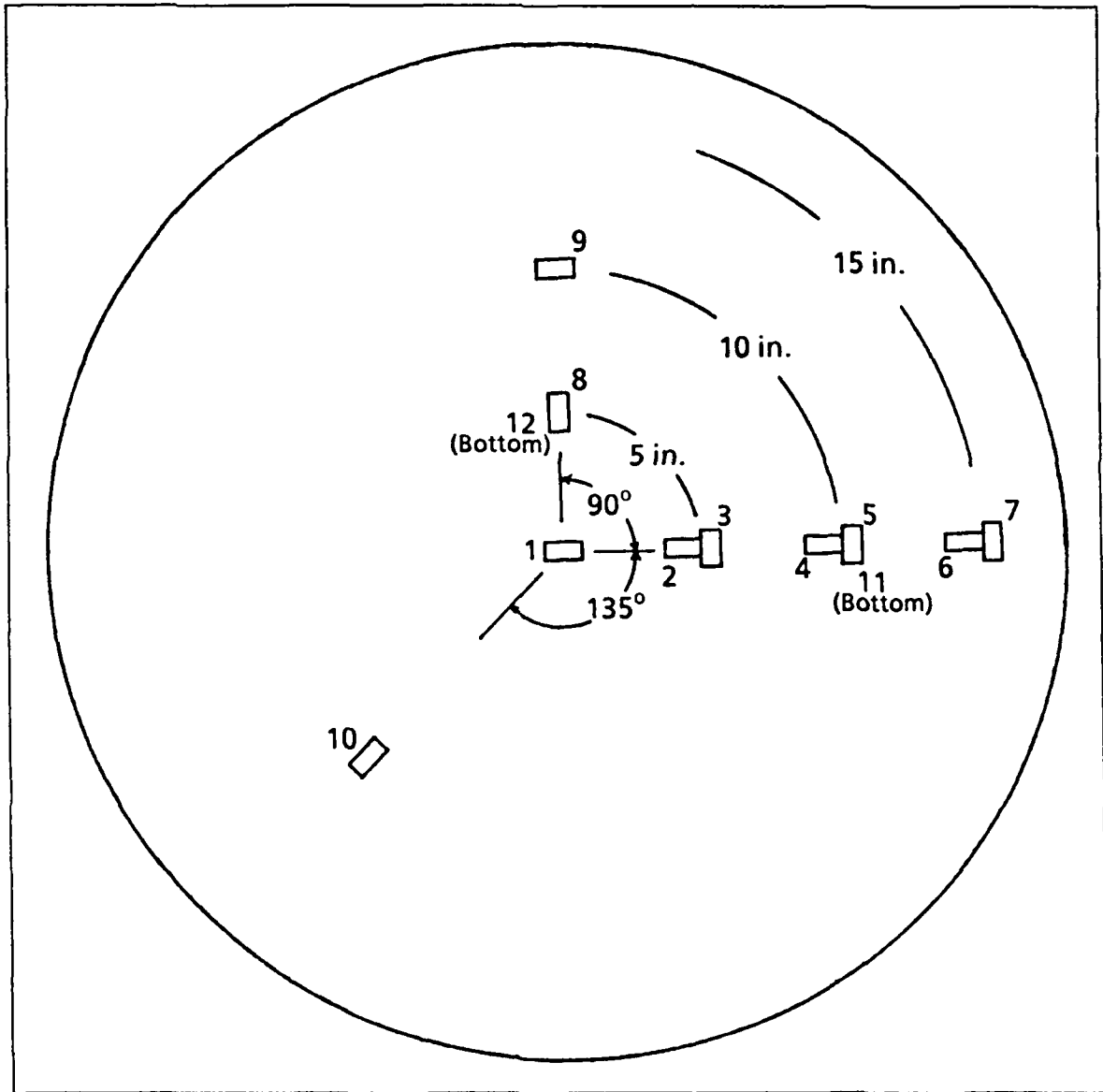


Figure 14. Strain Gage Locations for Test 2 and Test 4.

accelerometer on the panel required tapping a hole approximately half way through the panel, test panel accelerometers were not used for air backed tests because of the large deflections expected or for the composite panels because of the unknown effect such a hole might have on the failure mechanism. Use of the accelerometers was discontinued entirely after Test 2 because of the difficulty in recording valid data.

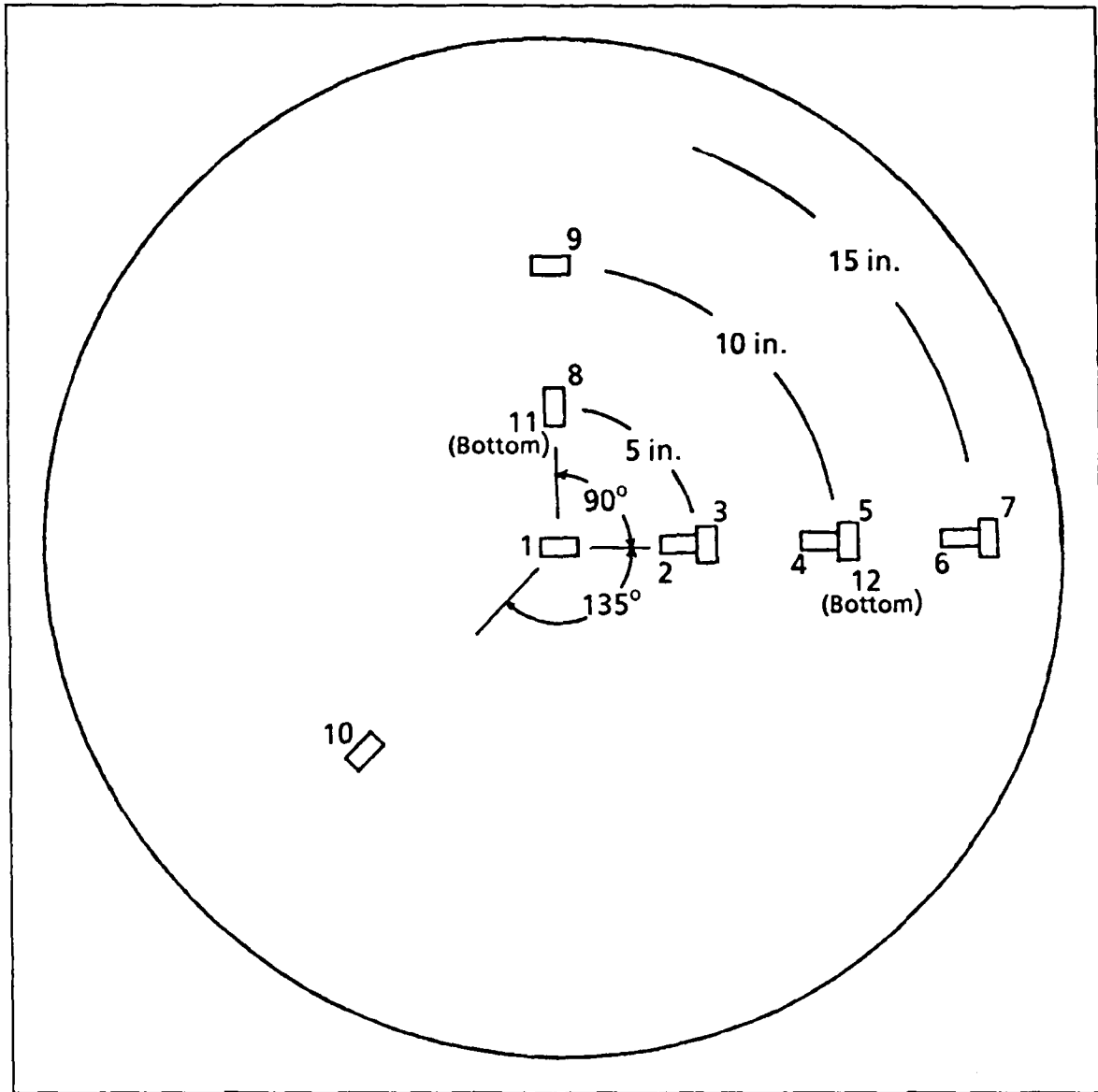


Figure 15. Strain Gage Locations for Test 3.

All instrumentation was applied to the test panels and the test panels were mounted in the test fixtures at NPS. Silicon sealing compound was applied to the strain gages for protection and to provide additional waterproofing. In order to prevent excessive motion during the test, all exposed instrumentation leads were secured to the test plate with the silicon sealing compound.

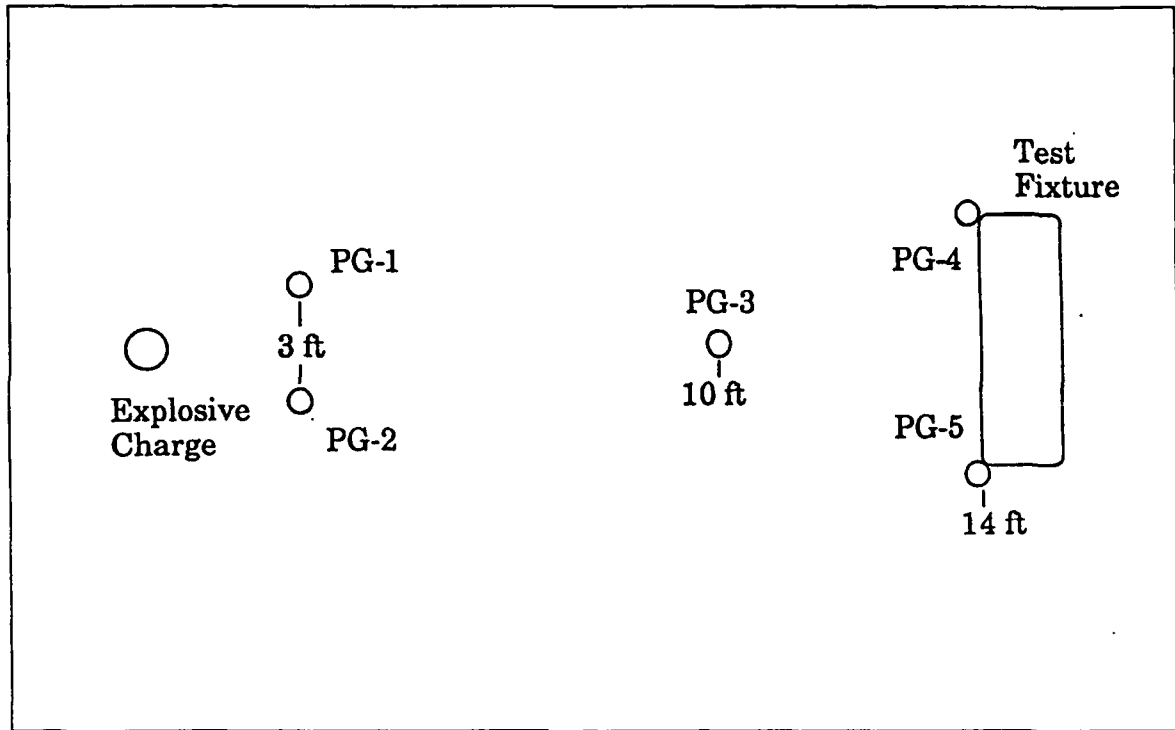


Figure 16. Pressure Transducer Locations for Test 1.

The test fixtures were transported to WCSF and suspended beneath the test barge as shown in Figure 20. Figure 21 shows the barge and test fixture being lifted by crane and lowered into the bay. The barge was positioned away from the pier by winches. Once in position, the explosive charge was attached to the barge and armed by WCSF staff. Detonation of the charge was initiated from the pier. The two data recorders were started approximately 20 seconds prior to detonation to allow the tape speed to stabilize. Following the tests, the data recorders and tapes were returned to NPS where the transverse displacement of the test panels was measured and the recorded test data was digitized and displayed.

#### D. PREDICTED RESPONSE

Two types of response were predicted for the panels tested. The water backed panels were not anticipated to demonstrate any permanent deformation due to the shock waves. The inclusion of the water backed tests was primarily to provide data on the elastic response of the various test panels. It was anticipated that the air backed panels would react significantly to the shock wave and would provide the most useful data for reconstructing the response and failure mechanisms of the panels.

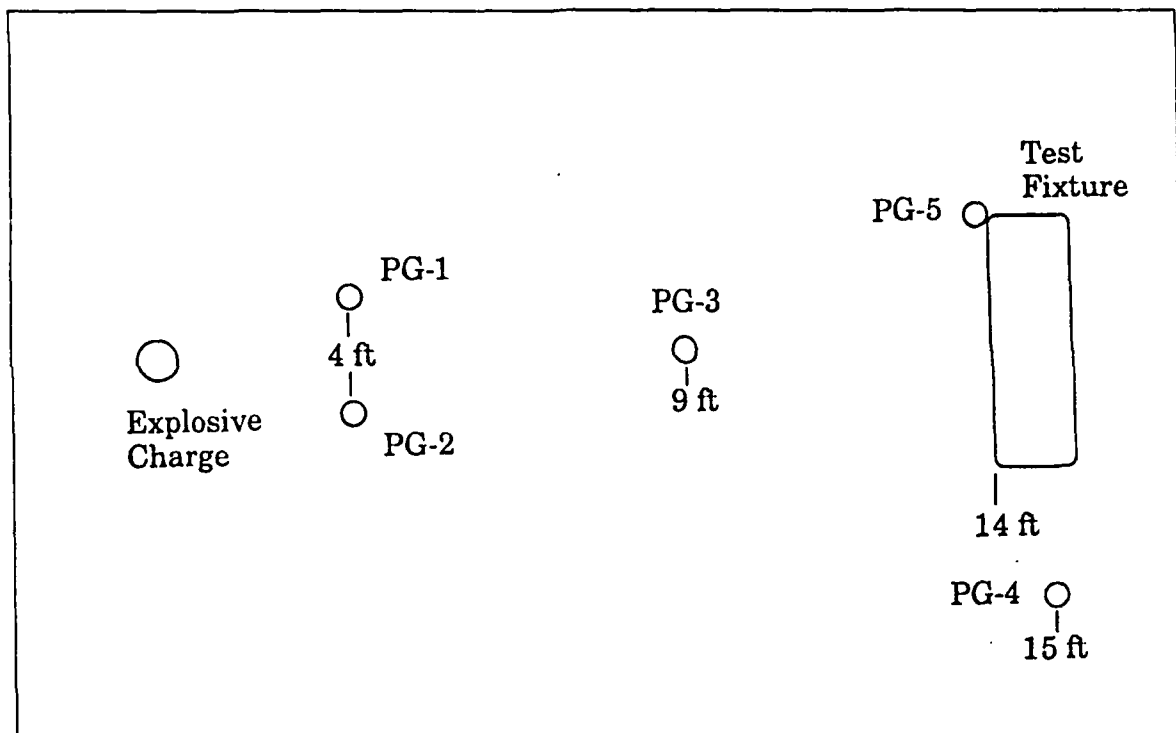


Figure 17. Pressure Transducer Locations for Test 2.

The predicted response of the air backed panels was determined using the infinite plate and finite plate models discussed in Chapter II. Using an assumed value of the density of seawater of 1.996 slugs per cubic foot and an assumed velocity of sound in water of 4900 feet per second, the predicted maximum plate velocity, maximum plate

deflection, and velocity of the plastic bending wave across the plate were determined. Table II provides the results of preliminary calculations using equations (1), (2), and (12). The response of the air backed panels was determined from equations (15), (16), (23), (24), and (25). Since yield strength data is not readily defined for the composite material, the value of stress at first ply failure determined from Figure 11 was utilized when the bending wave velocity and the transverse deflection of the center of the panel were calculated.

**Table II. Preliminary Shock Wave Parameters.**

Material	Explosive Weight lbf	Density $\frac{\text{lbf sec}^2}{\text{in}^4}$	m $\frac{\text{lbf sec}^2}{\text{in}^3}$	$P_{\text{max}}$ psi	$\theta$ msec	$\beta$
Aluminum	5	$2.54 \times 10^{-4}$	$6.35 \times 10^{-5}$	1883	0.146	13.02
Composite	5	$1.80 \times 10^{-4}$	$4.50 \times 10^{-5}$	1883	0.146	18.37
	10	$1.80 \times 10^{-4}$	$4.50 \times 10^{-5}$	2473	0.177	22.27

**Table III. Predicted Response of the Air Backed Test Panels.**

Material	Explosive Weight lbf	Infinite Plate Model			Finite Plate Model	
		$\theta_c$ msec	$U_{max}$ in/sec	$Z_{max}$ in	Bending Wave Velocity in/sec	$Z_{max}$ in
Aluminum	5	0.0312	-10719	-1.127	-12549	-15.38
Composite	5	0.0245	-14448	-0.632	-14337	-18.14
	10	0.0258	-22510	-0.918	-14337	-28.26

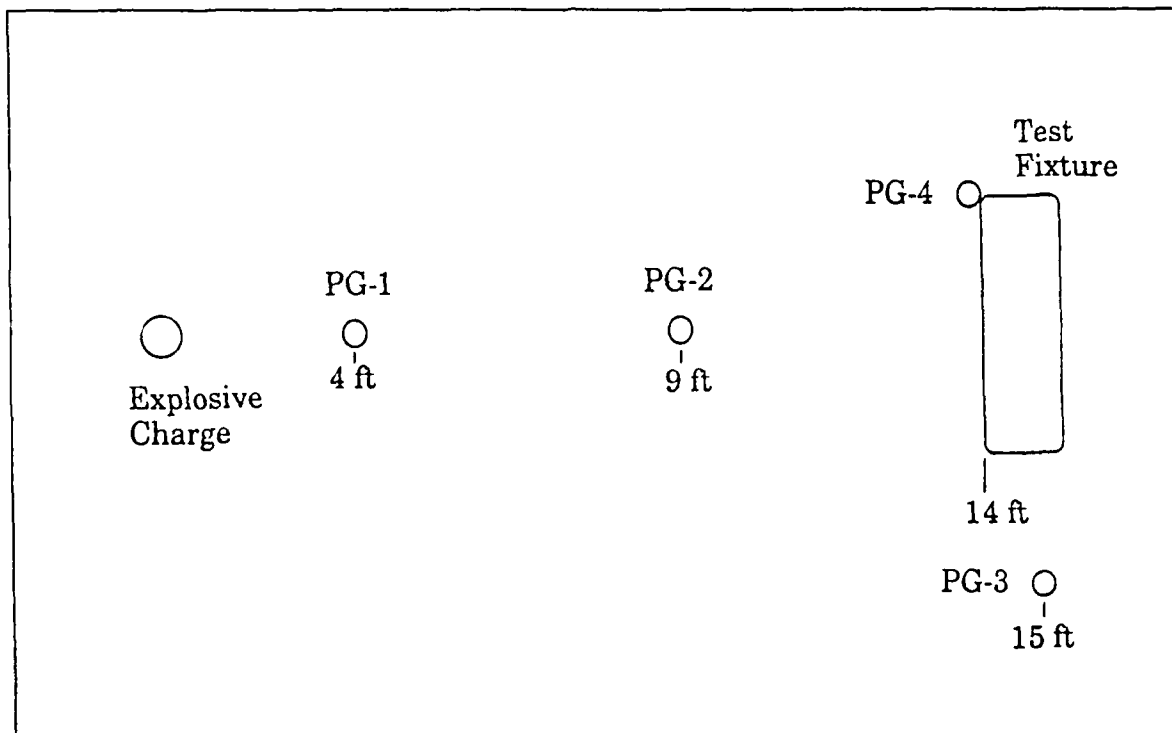


**Figure 18. Pressure Transducer Locations for Test 3.**

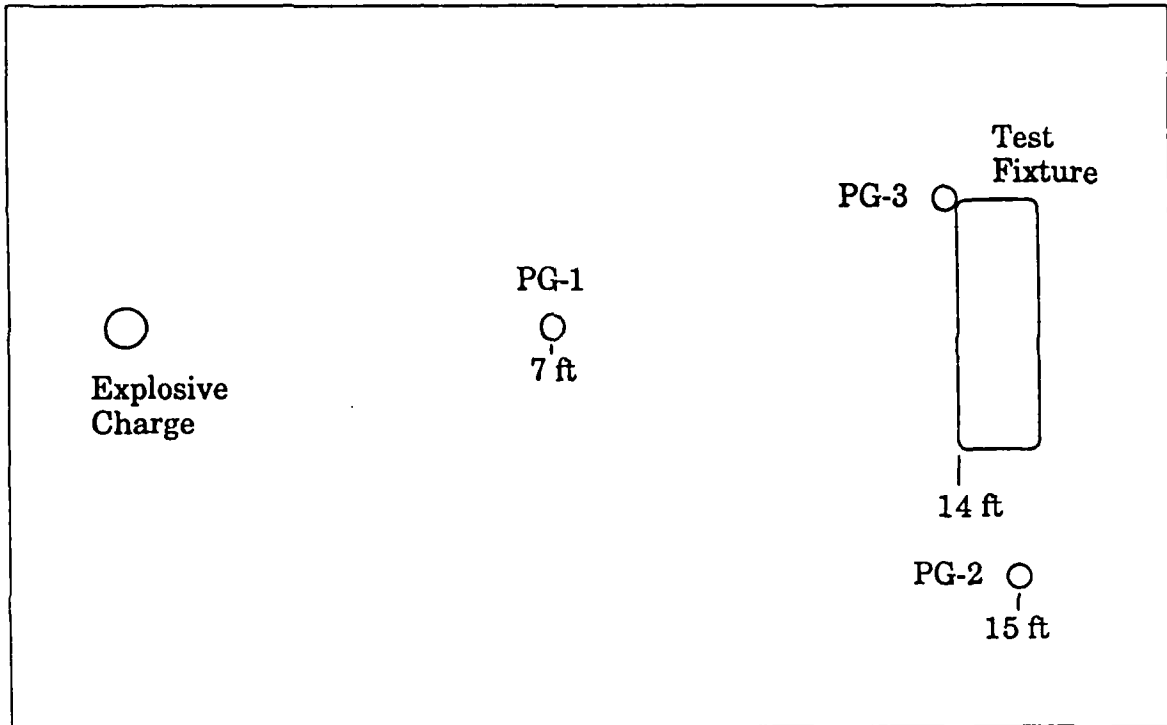
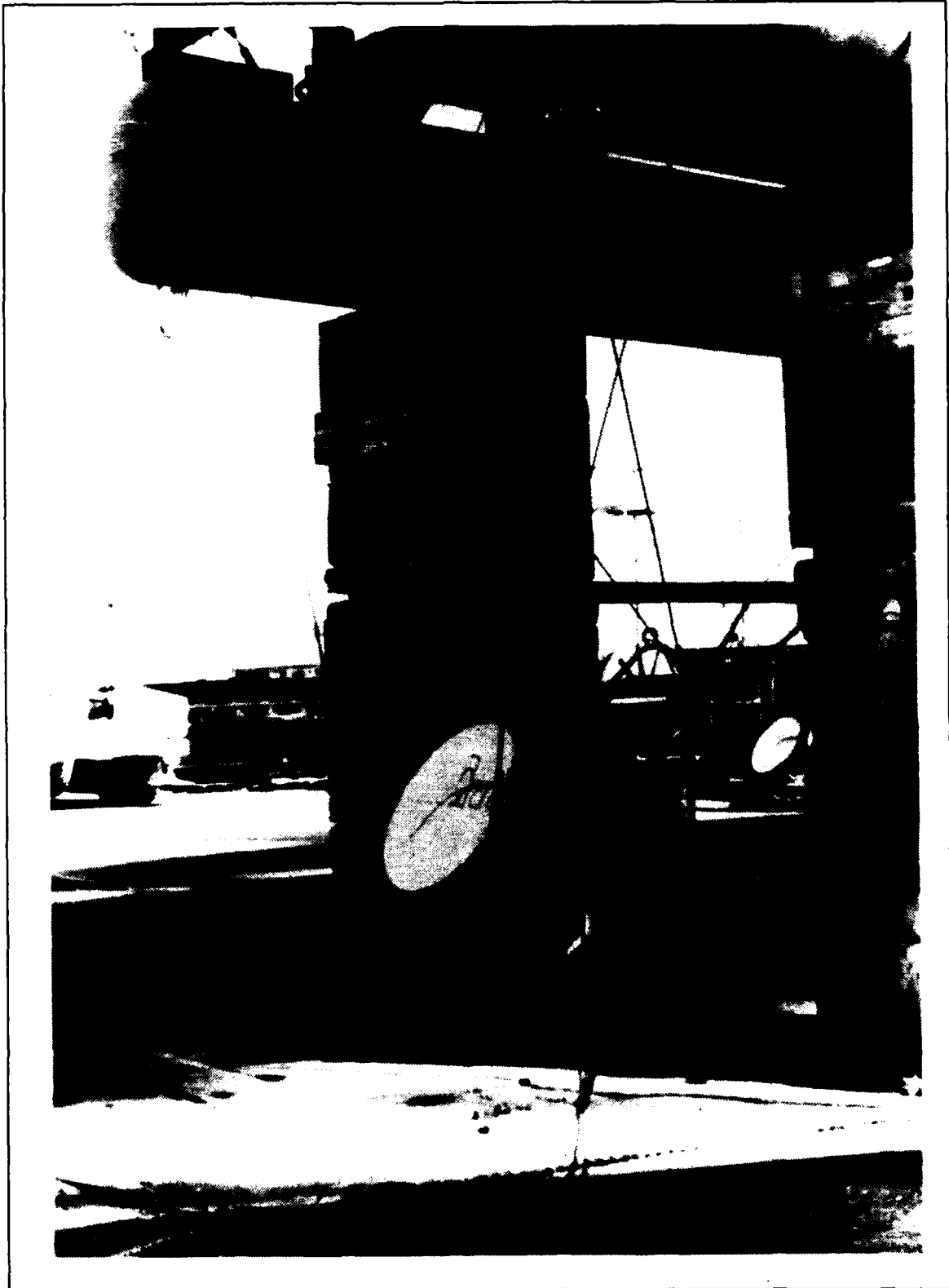


Figure 19. Pressure Transducer Locations for Test 4.



**Figure 20. Test Fixture Suspended Beneath the Test Barge.**

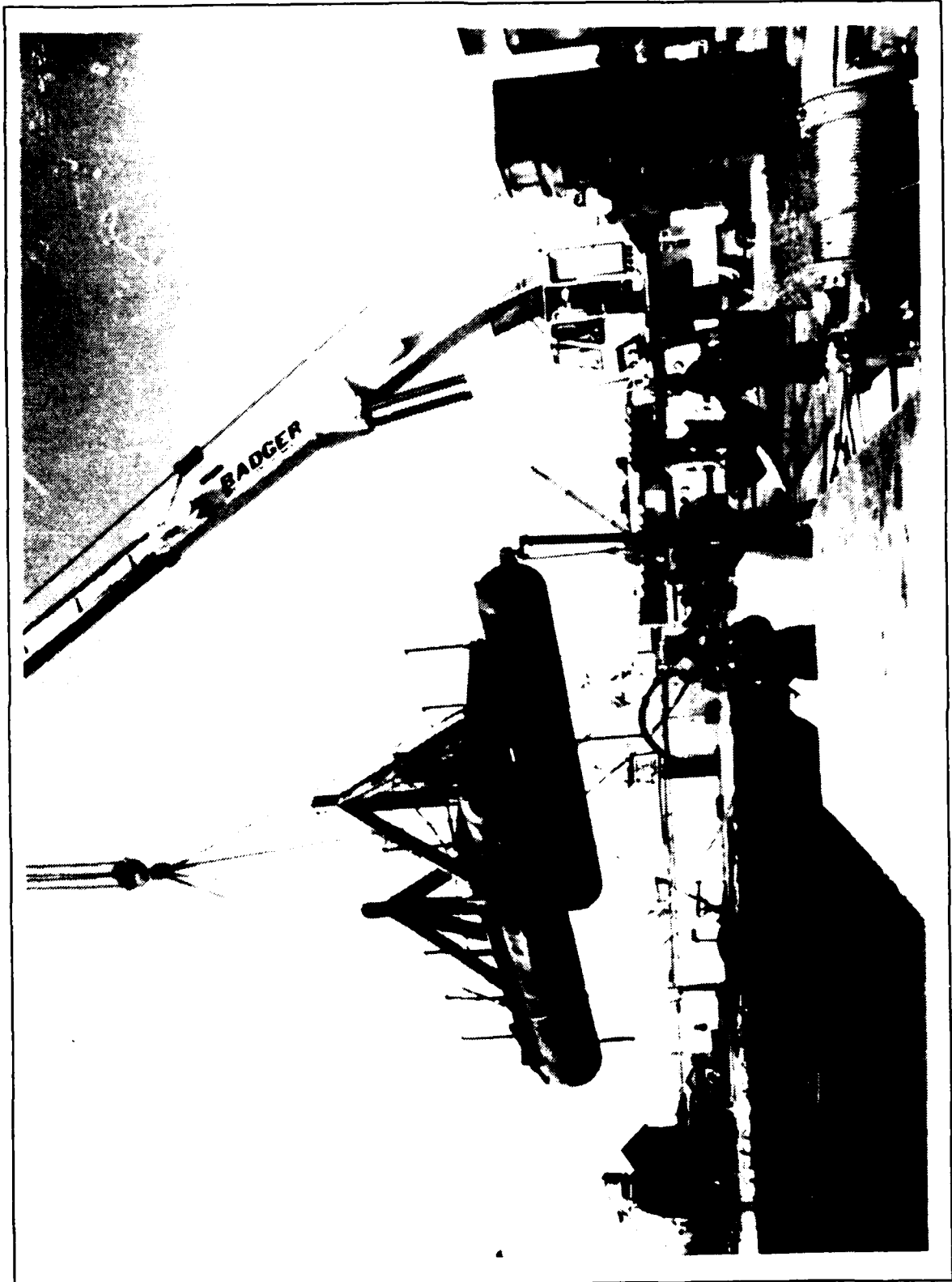


Figure 21. Placing the Barge and Test Fixture in the Bay.

#### IV. RESULTS

The eight shock tests of this test series were conducted as planned. A complete set of the resulting data may be found in Appendix C of Reference 11. Individual data records will be reproduced in the text as required to illustrate the results.

During digitization, all of the strain gage data was filtered to a band of 0 - 12,800 Hz with the exception of strain gage data from T1A, which was filtered to a band of 0 - 25,600 Hz. The filtering is automatically accomplished by the HPVista software and is a function of the session length and data block length selected. These parameters were adjusted to remove the high frequency and noise components of the signal without significantly effecting the magnitude or the form of the signal and to provide a record length long enough to capture the plate response. The trigger signal for T1A was lost seconds prior to the detonation of the explosive. Fortunately, the high voltage used to set off the detonator produced an electromagnetic pulse that was recorded on the data channels. This firing pulse was used instead of the trigger signal to initiate downloading and digitization of the data from T1A. The firing pulse was present when the data was reduced using the 0 - 25,600 Hz band but was invisible to the HPVista software when the data was reduced using the 0 - 12,800 Hz band. This necessitated the use of the different frequency band for T1A. All of the pressure data was digitized using a frequency band of 0 - 51,200 Hz. The higher frequency band was necessary in order to capture the near vertical rise of the pressure signal so that the time of arrival could be accurately determined.

The firing pulse that proved so useful in reducing the strain data caused problems in the pressure and acceleration data. The effect of the pulse had not decayed away by the time the shock wave reached the pressure transducers closest to the explosive charge and the pressure signal is imposed on the transient from the firing pulse. By the time the shock wave reached the test fixture the firing pulse had decayed away and the data recorded from these transducers was unaffected. The firing pulse transient had a more significant effect on the accelerometers. Here the transient totally masked the signal from the accelerometers. Several test equipment and test procedure modifications were made over the course of the test program to eliminate the firing pulse transient. Some improvement was noted in the pressure data, but the accelerometers remained sensitive to the transient. For this reason the use of the accelerometers was discontinued after Test 2.

The following sections summarize and discuss the data collected.

#### **A. PEAK PRESSURE AND PERFORMANCE OF THE EXPLOSIVE**

The performance of the explosive charges was determined by comparing the predicted maximum shock wave pressure calculated using equation (1) with the peak pressure values measured by the blast pressure transducers. Some variance between the predicted and measured peak pressures was expected due to slight differences in charge density and due to aging effects on the explosive. Additionally, equation (1) was developed based on the detonations of spherical charges. The explosive charges used in this test series were cylindrical charges fabricated with the diameter of the cylinder approximately equal to the length of the cylinder so as to approximate the size of a similar spherical charge as close as possible.

As shown in Figure 22 and Figure 23 the measured maximum pressures at each pressure transducer were in good agreement with the predicted pressures of equation (1) with the exception of the peak pressures recorded by transducer number three for Test 1. The indicated stand off distance for this transducer is ten feet. A review of the pressure history plot for this transducer indicated that approximately 1.6 msec elapsed before the arrival of the shock wave. Using a nominal value of 4900 feet per second for the speed of sound in water, the calculated stand off distance for this transducer was determined to be 7.84 feet. The large discrepancy between the calculated and measured peak pressure for transducer number three in Test 1 was most likely due to an error in positioning the transducer.

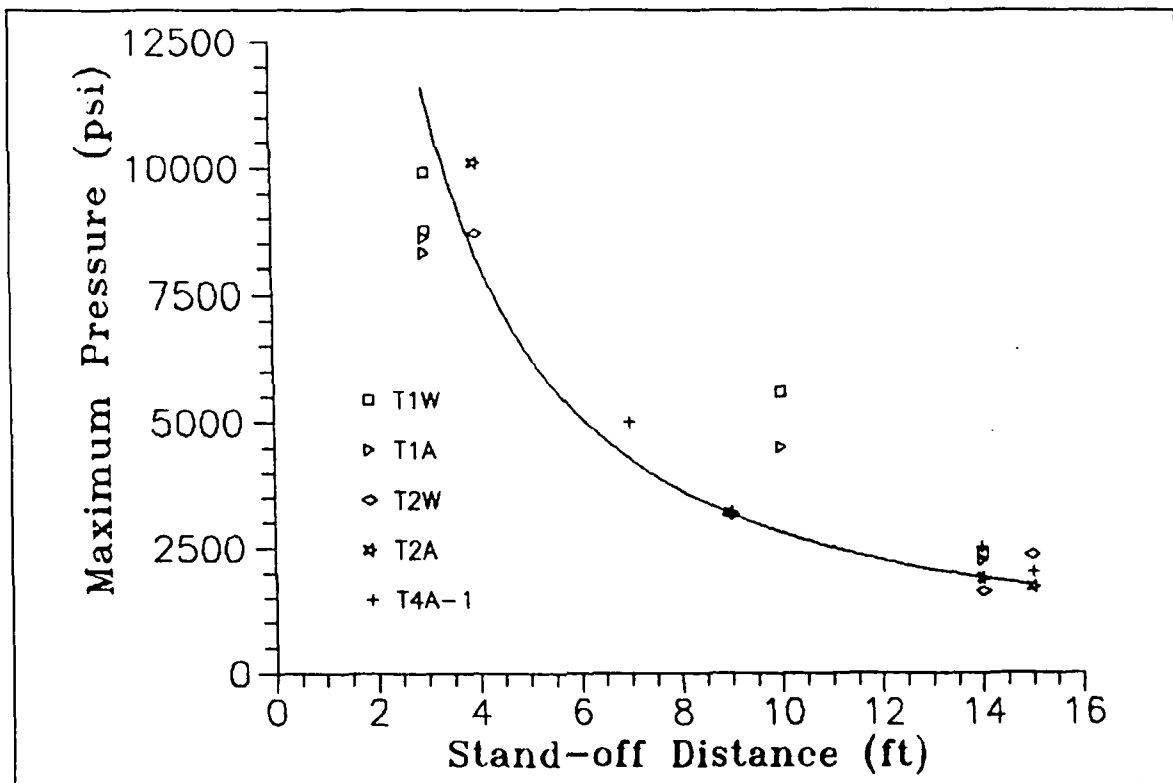


Figure 22. Comparison of the Peak Recorded Pressures with the Predicted Pressure Trace for the Five Pound TNT Charges.

During Tests 2 and 3, some problems were noted due to the rapid deterioration of the connectors that attached the pressure transducers to the data collection system. Repeated exposure to the shock from underwater explosions caused the connectors to loosen slightly. Use of the transducer during subsequent tests resulted in the generation of high magnitude electrical noise as the instrumentation wiring was buffeted about in the wake of the shock wave. Since the noise is only evident after the shock wave has passed the transducer, it does not interfere with determining the time of arrival of the shock wave or with determining the peak pressure of the shock wave at the transducer. This problem was finally overcome for Test 4 by totally replacing the pressure transducers and refurbishing the connectors.

## **B. OBSERVED EFFECTS ON THE TEST PANELS**

Following each shock test a visual inspection of each test panel was conducted while it was still mounted in the test fixture. Items that were checked included the status of all accessible panel mounted instrumentation and any evidence of plate failure such as plastic deformation or plate rupture. Additionally, the composite panels were checked for signs of delamination, glass fiber breakage or matrix failure.

### **1. Water Backed Plates**

The water backed test panels showed little or no damage from the underwater explosions regardless of the charge weight used. As shown by Figure 24 the aluminum plate of test T1W was unaffected by the shock wave produced by five pounds of TNT. No noticeable deformation was noted in the composite plates subjected to the shock from five pounds of TNT in test T2W and to the shock from ten pounds of TNT in test T3W. The

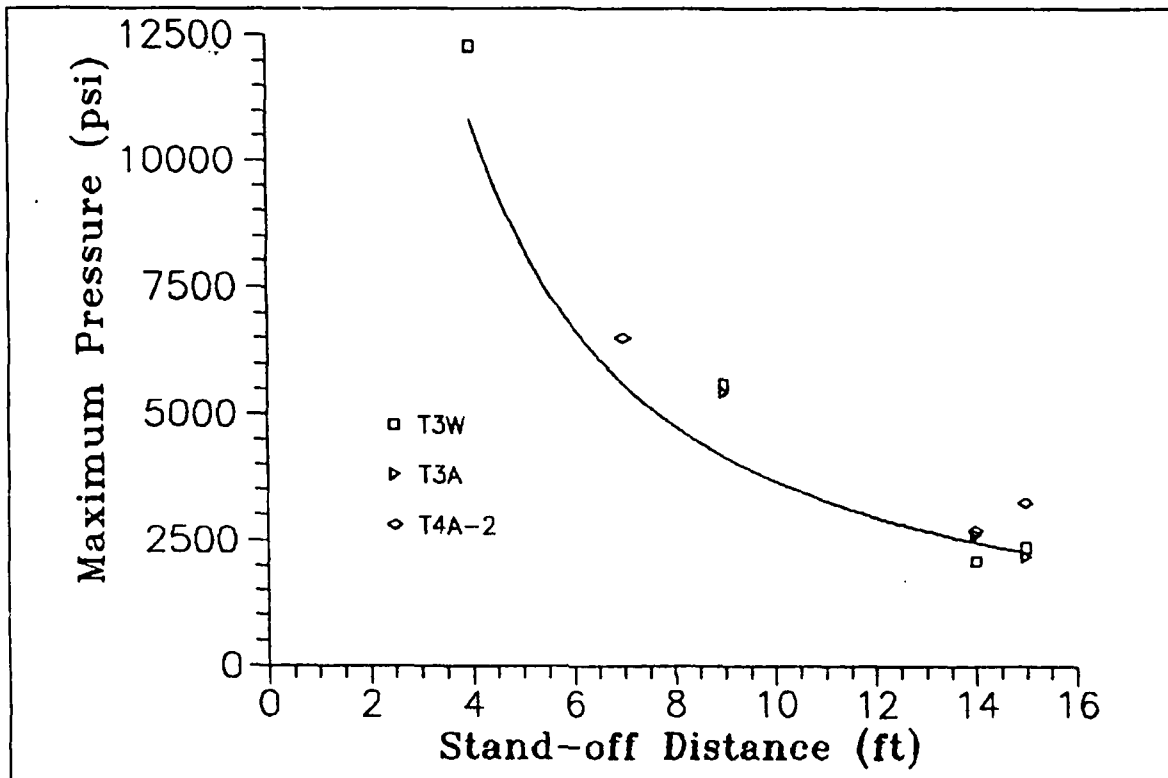


Figure 23. Comparison of the Peak Recorded Pressures with the Predicted pressure Trace for the Ten Pound TNT Charges.

most significant effect on the water backed panels was noted in the composite panel from test T2W. A crescent shaped internal delamination located at the top of the panel was visible when the panel was back lighted. From the shape and location of the delamination, it appeared to have been caused by a trapped air bubble behind the panel that allowed that section of the panel to flex more than the water supported sections surrounding it. The water backed test fixture vents that were supposed to allow air to escape from behind the test panel were carefully inspected and verified clear prior to test T3W. No delaminations were found in the composite panel following that test even though a ten pound charge was detonated. The composite panels used in test T2W and T3W are shown in Figure 25 and Figure 26.



**Figure 24. The Aluminum Panel From Test T1W.**

## **2. Air backed Plates**

As anticipated, the effect of the underwater explosions was much more pronounced on the air backed panels than on the water backed panels. The aluminum test panel of test T1A, shown in Figure 27, exhibited a conical shape following the shock wave from the five pound charge of TNT. All of the composite panels used in the air backed

tests T2A, T3A, T4A-1, and T4A-2 showed significant permanent transverse deformation and localized rupture of the matrix material.

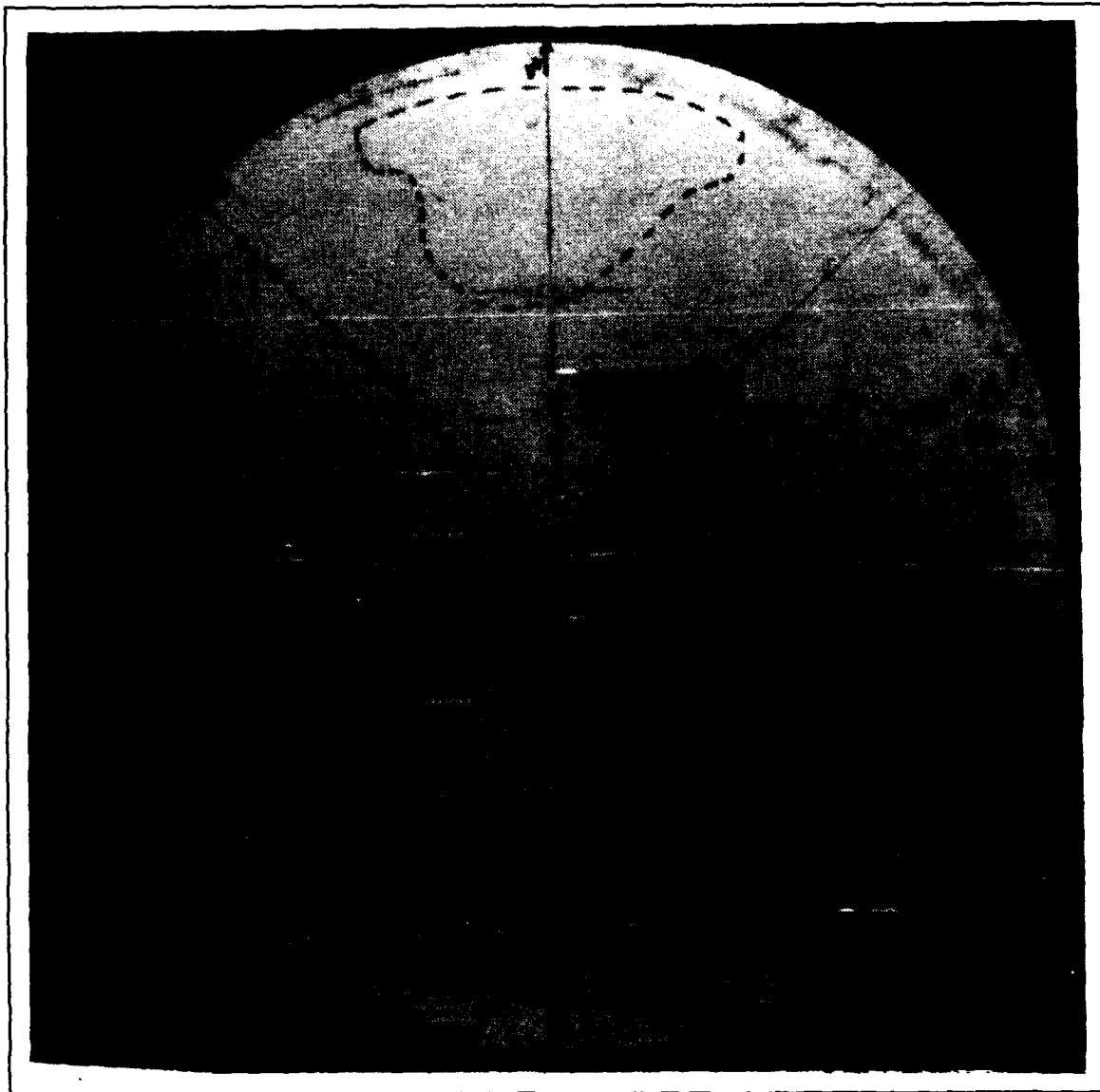


Figure 25. The  $[0^\circ/90^\circ/0^\circ/90^\circ/0^\circ]_5$  Composite Panel From Test T2W.

The composite panels of the five pound charge tests, T2A and T4A-1, exhibited an appearance similar to the aluminum panel of T1A but were not as obviously conical shaped. As shown in Figure 28 and Figure 29, each of the panels had, in general, radially

oriented narrow strips of localized matrix rupture that appeared to initiate at the outer edge of the panel and to propagate toward the center of the panel. The fiber rovings in these regions of matrix failure appeared to have buckled away from the central layers of the panel. An edge on view of each of the failure regions showed that the matrix failure occurred at an angle to the thickness of the panel as illustrated by Figure 30. The visual evidence suggests that the brittle matrix material failed due to compressive stress imposed in the circumferential direction.

The composite panels subjected to the shock wave from the ten pound charges used in tests T3A and T4A-2 deflected to such an extent that one edge of the panel was pulled free of the clamp rings. When this occurred the panels were forced into the bottom of the test fixture. Figure 31 shows the test panel from T4A-2 while still in the test fixture. One mode of failure for these panels was still the radially oriented strips of localized matrix rupture apparently due to compressive stresses in the circumferential direction. Superposed on this failure mode was a second mode consisting of generalized delamination of the panel due to the severe bending and folding of the panel when it was forced into the bottom of the fixture.

As shown in the detailed photographs found in Appendix B of the damaged areas, glass fiber breakage in all of the composite panels was minimal. The primary locations for fiber breakage were on the panels from T3A and T4A-2 where the composite panels were constrained from bending by the portion of the panel that stayed within the clamp rings. A small amount of breakage was also found at the outer end of the radial matrix failures on the panels used for the five pound charge air backed tests.

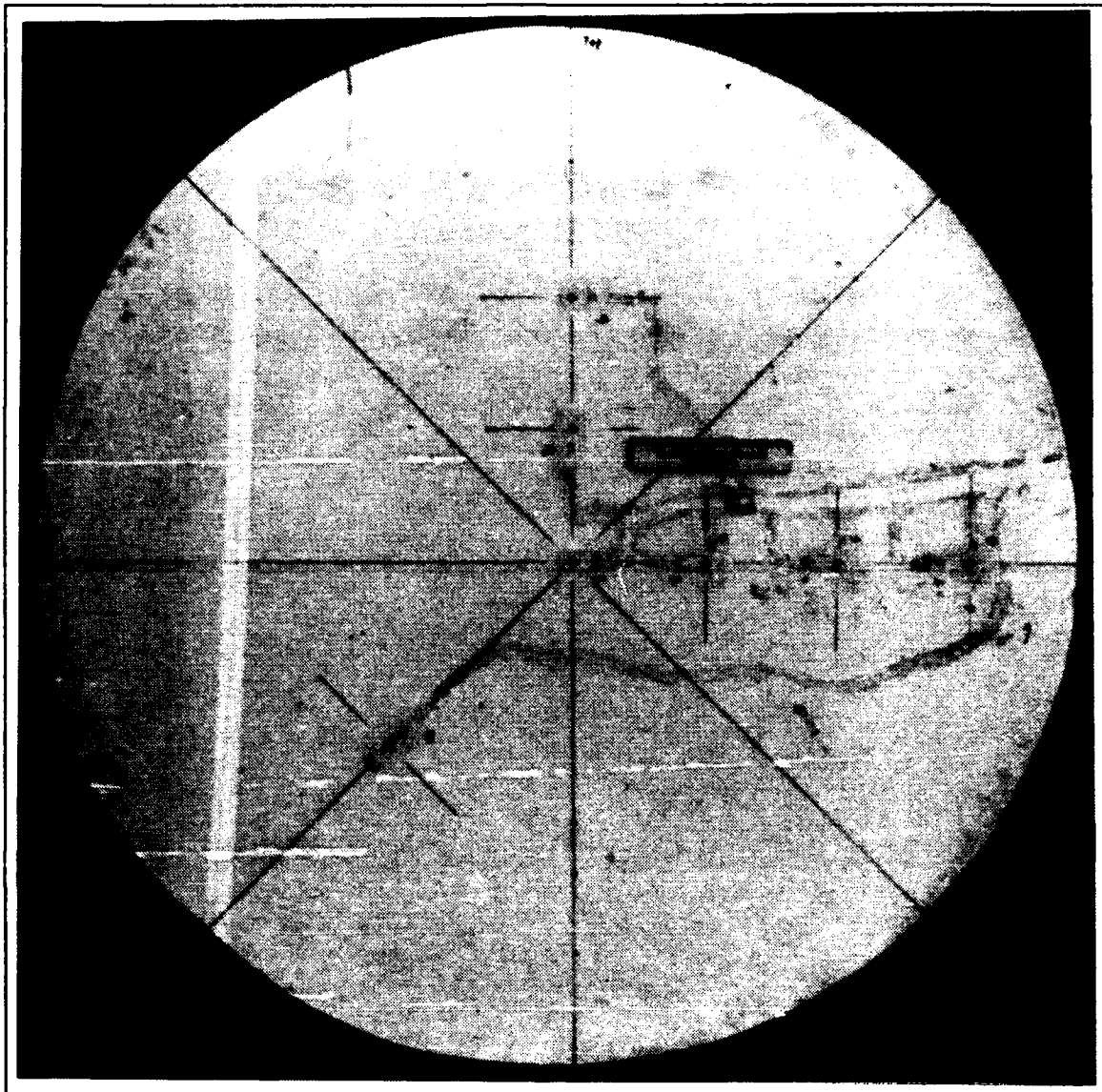
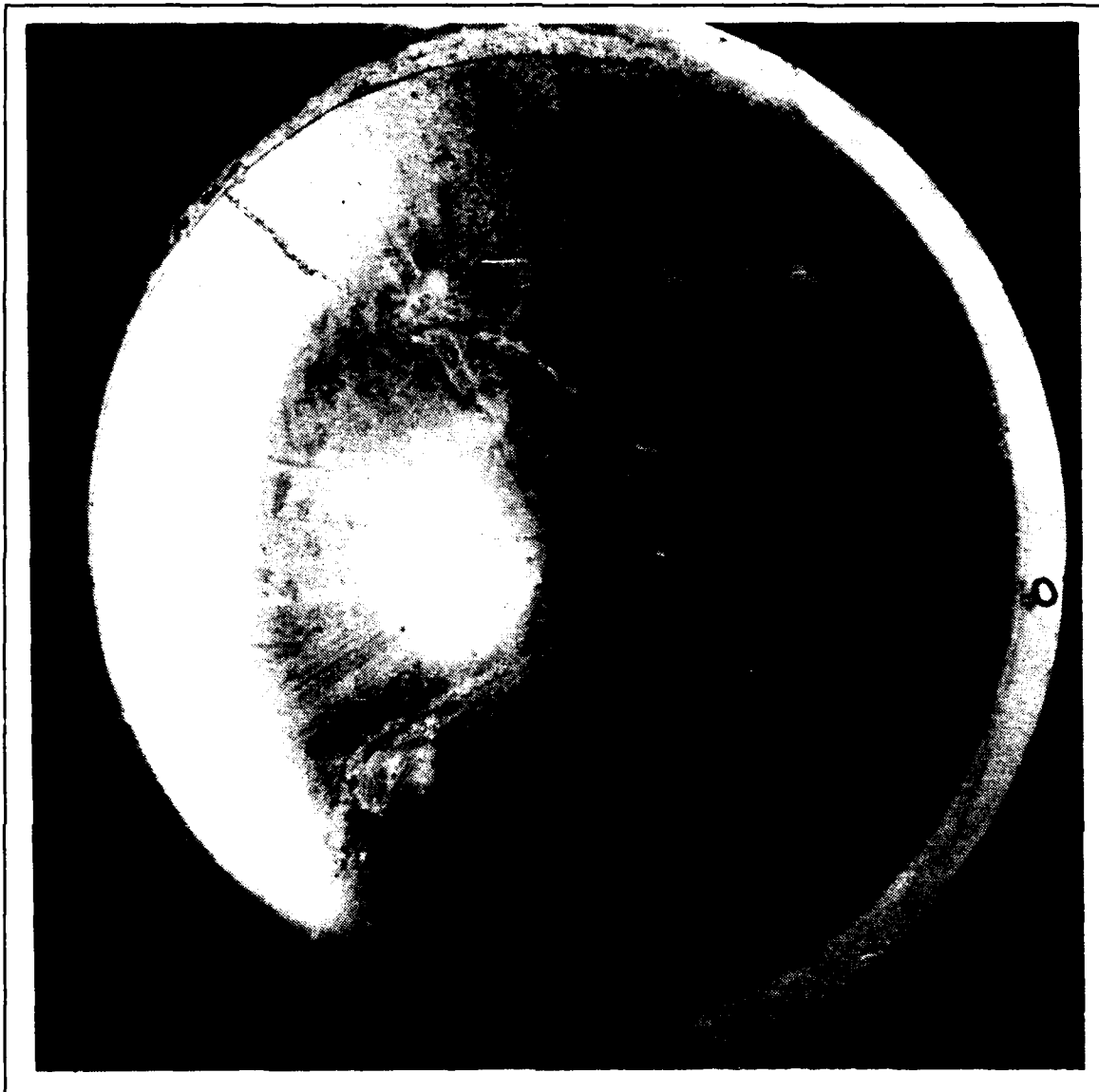


Figure 26. The  $[0^\circ/45^\circ/90^\circ/45^\circ/0^\circ]_s$  Composite Panel From Test T3W.

### C. TRANSVERSE DISPLACEMENT OF THE TEST PANELS

Following each shock test the final transverse displacement of each test panel was measured relative to the panel center prior to removing the panel from the test fixture. A dial depth gage and rigid track, pictured in Figure 32, were used to take the measurements.



**Figure 27. The Aluminum Panel From Test T1A.**

Each panel was traversed several times along different diameters to give a more complete picture of the pattern of displacement.

### **1. Aluminum Panels**

The final transverse displacement of the aluminum panels used in tests T1W and T1A are shown in Figure 33 and Figure 34. The displacement pattern for both cases is

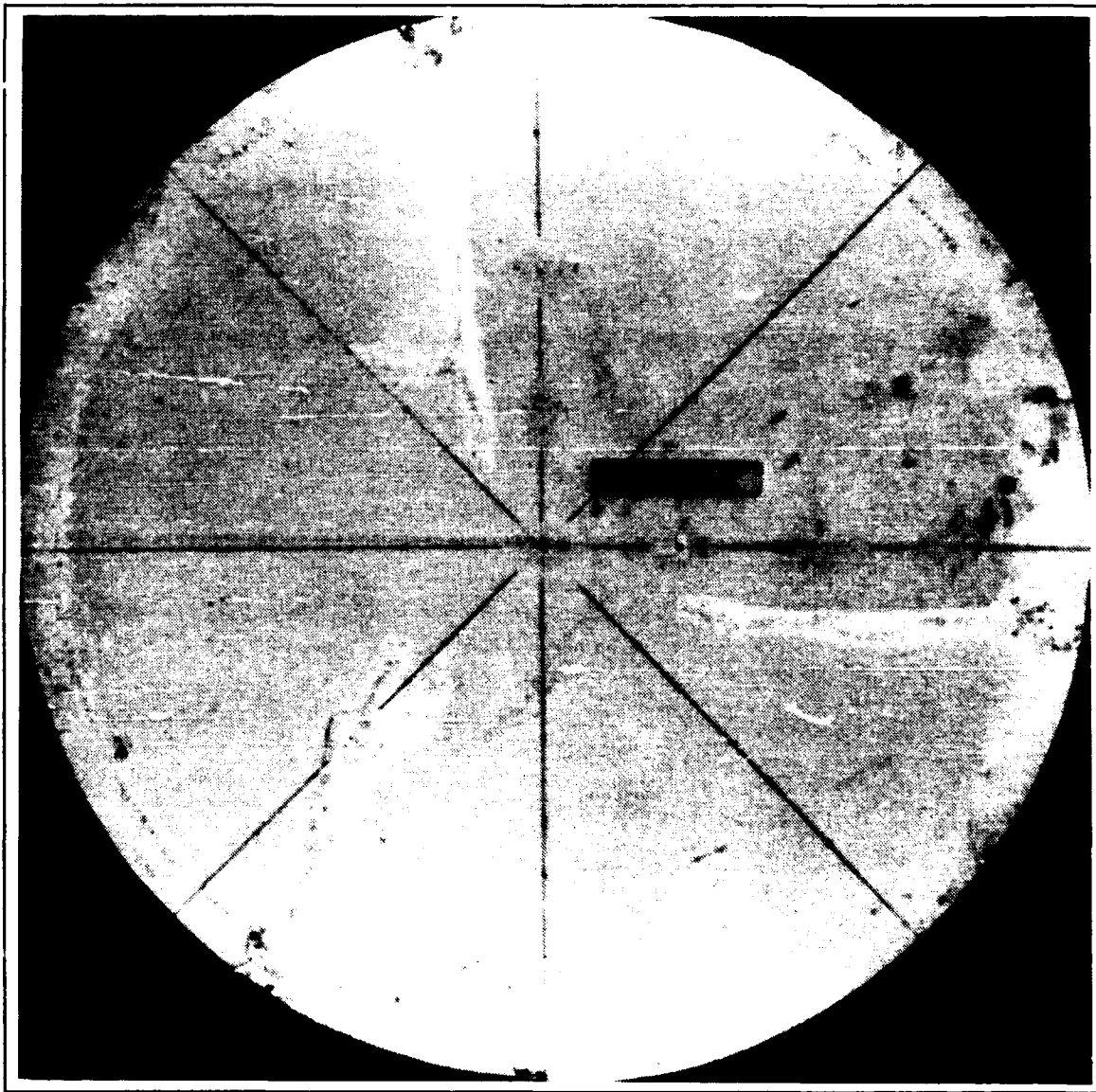


Figure 28. The  $[0^\circ/90^\circ/0^\circ/90^\circ/0^\circ]_5$  Composite Panel From Test T2A.

symmetric about the center of the panel. The water backed panel of T1W was essentially undeformed by the explosion. It was unclear whether the 0.2 inch deflection measured along the  $120^\circ$  traverse at the center of the panel represented a permanent distortion of the panel or was caused by hysteresis in the radial motion of the panel edge due to friction from the gasket material.

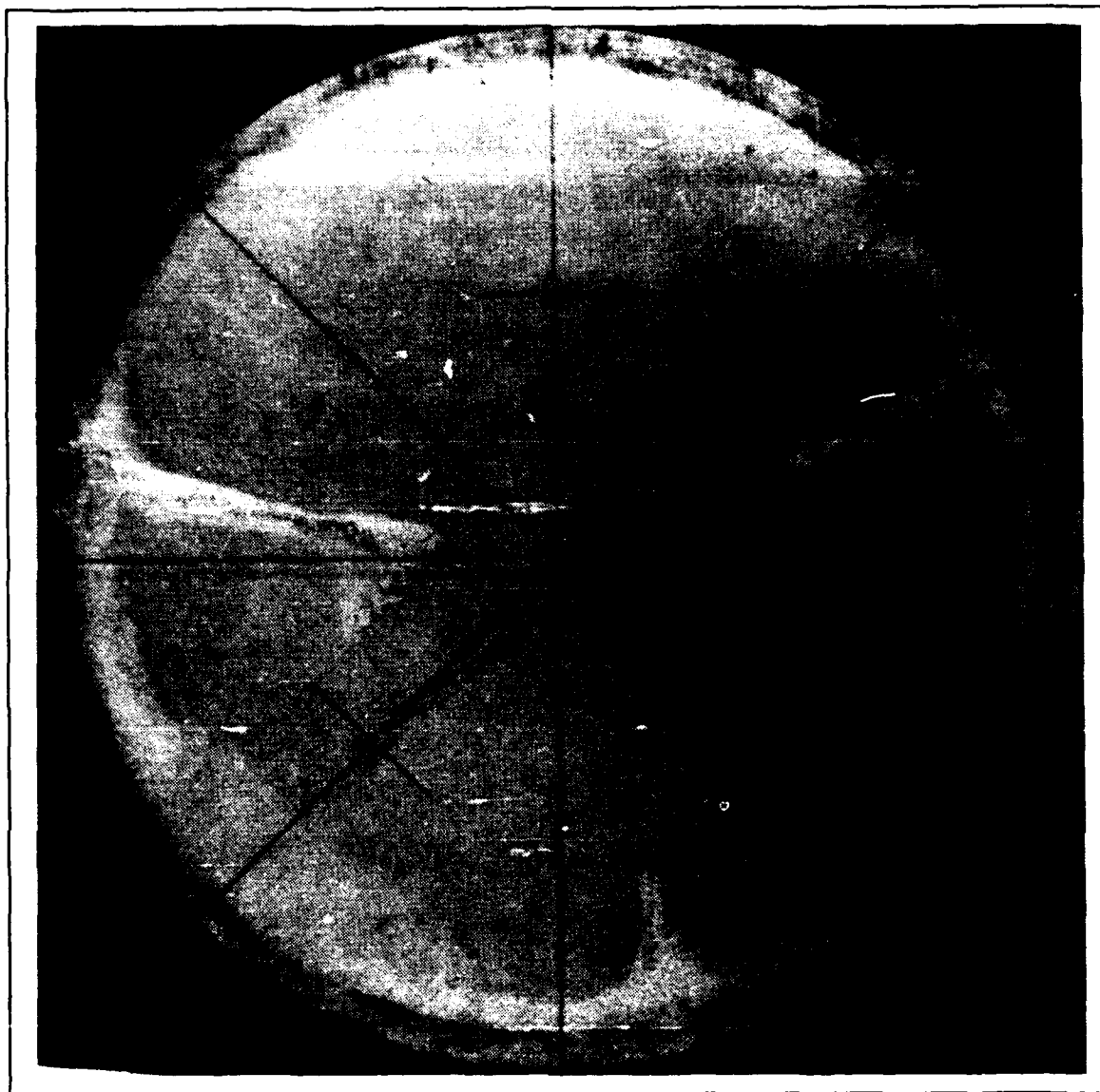


Figure 29. The  $[0^\circ/90^\circ/45^\circ/90^\circ/0^\circ]$ , Composite Panel From Test T4A-1.

The measurements of the final transverse displacement of the air backed panel from T1A were more definitive. The center of the test panel was displaced approximately 2.4 inches by the explosion. The resulting shape of the panel closely approximates the conical surface of revolution typical of the response of air backed metal panels to underwater explosions.



Figure 30. Edge View of a Matrix Failure.

## 2. Composite Panels

The final transverse displacements of the test panels from tests T2W and T3W are shown in Figure 35 and Figure 36. Measurements indicated that the panel from T2W had a maximum permanent deflection of 0.12 inch at the panel center. This panel had suffered an internal delamination in the upper portion of the panel due to the effects of an air bubble trapped behind the plate. The small transverse displacement of this plate was judged to be a result of the internal delamination. The panel from T3W which was exposed to the shock produced by the detonation of ten pounds of TNT had negligible permanent transverse displacements.



**Figure 31. View of the Test Panel From T4A-2 Immediately Following the Test.**

No transverse deflection measurements could be taken from the test panels used for the ten pound charge tests T3A and T4A-2. The final transverse displacement of the panels from T2A and T4A-1 are shown in Figure 37 and Figure 38. The peak deflection measured at the center of the panel from test T2A was 0.75 inches . The deflected shape of the panel was generally symmetric about the center of the panel. It approximated a

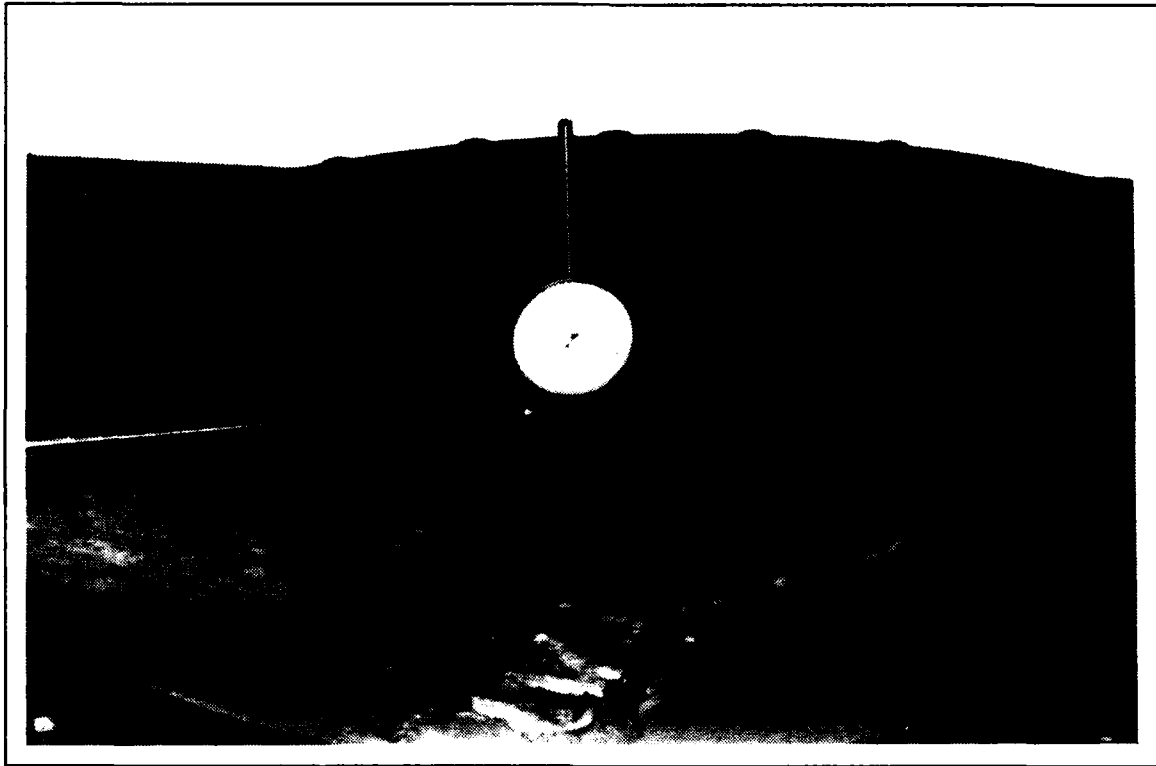


**Figure 32. Measuring Final Transverse Displacement with the Dial Depth Gage.**

surface of revolution, but appeared to be more parabolic than conical in shape due to the lack of extensive yielding in the material. The maximum permanent deflection of the panel from T4A-1 was 1.26 inches. The deflected shape was skewed to one side so that the maximum deflection occurred at a point three inches to the left of the center of the panel on the  $0^\circ$  traverse.

#### **D. TEST PANEL STRAIN HISTORIES**

Two presentations were made of the strain history data from each strain gage. The first was a long time strain history running for 250 msec. This presentation was useful for determining if any permanent deformation of a panel had occurred and for illustrating the long term reaction of the panel. The second presentation represented 15 msec of

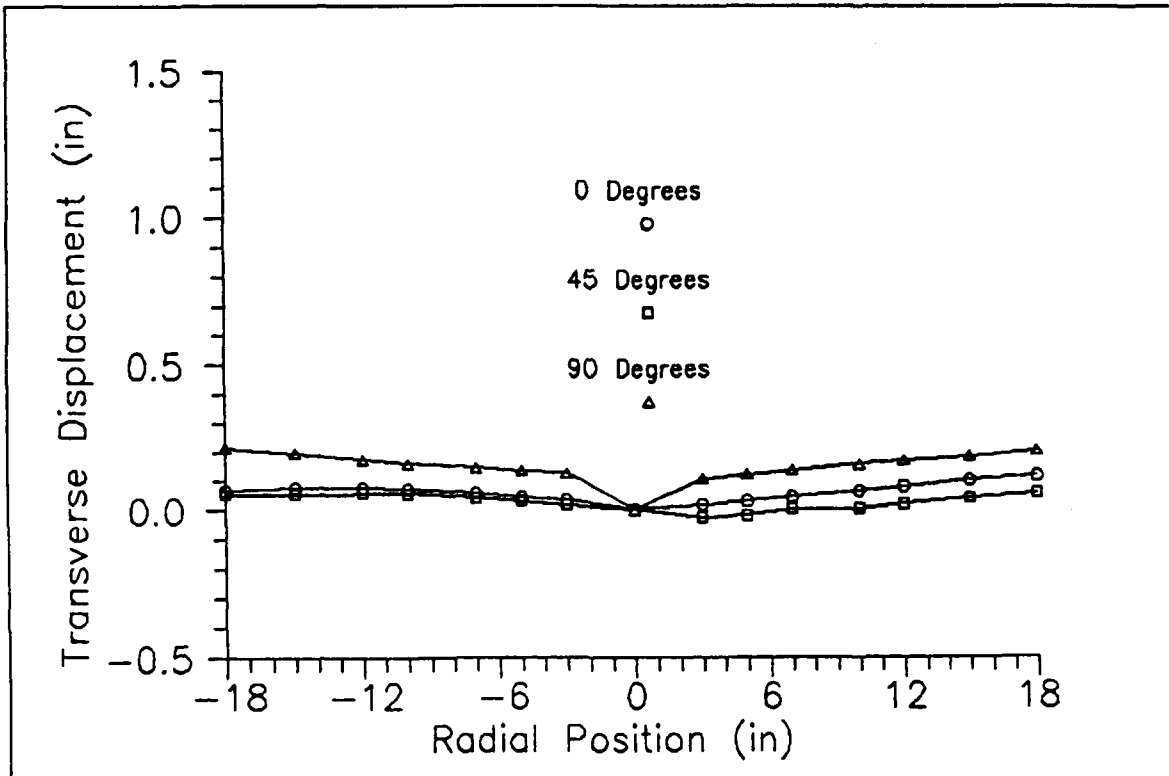


Figure 33. Final Transverse Displacement for the Aluminum Panel From Test T1W.

information and was useful for determining the response of the panel immediately after the impact of the underwater shock wave. The strain gages mounted on the test panels were wired such that a concentrated static load applied inward at the center of the panel resulted in a positive deflection in the output of all strain gages. Under this loading condition and for the mounting locations used in this test series the strain gages on the upper surface of the panel were in compression while the strain gages on the lower surface of the panel were in tension. For this reason a positive deflection in the strain histories for strain gages 1 through 10 represented compression while a positive deflection in the strain histories for strain gages 11 and 12 represented tension.

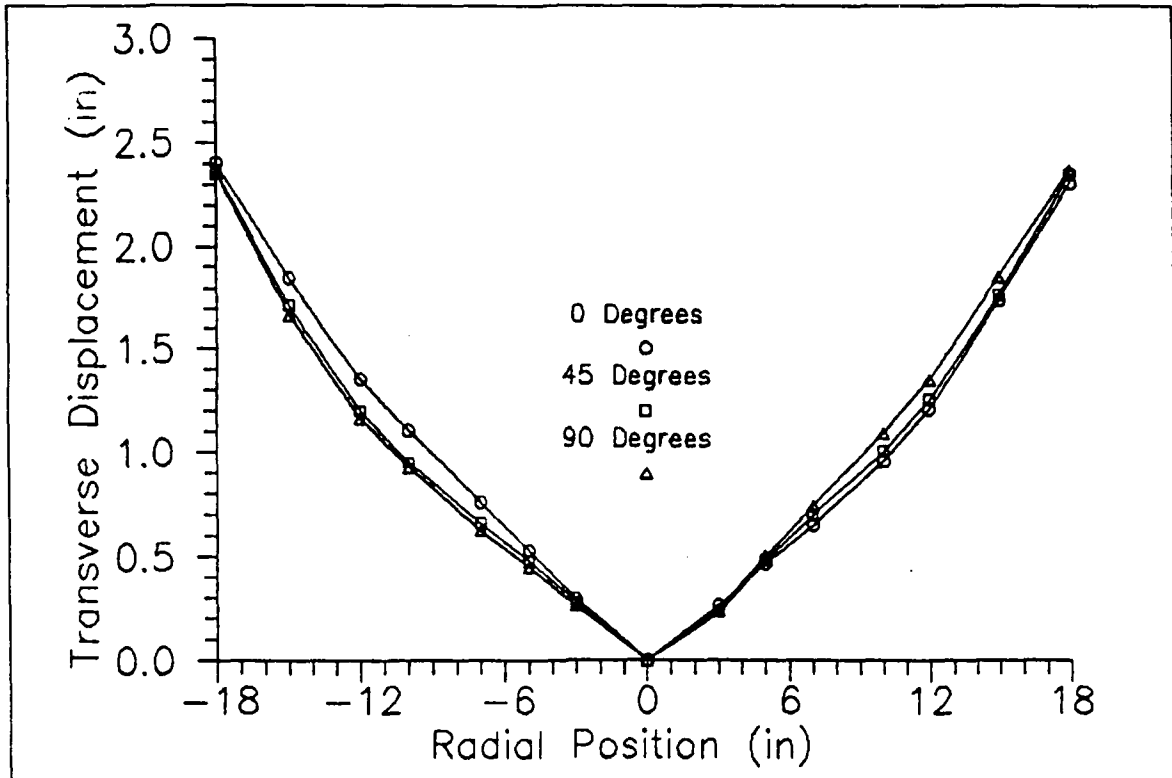


Figure 34. Final Transverse Displacement for the Aluminum Panel From Test T1A.

### 1. The Aluminum Test Panels

An examination of the long time strain gage data from the water backed aluminum panel of test T1W revealed that the peak recorded strains were much less than the  $\pm 0.8\%$  strain band allowed for in the data recorders. The peak transient strain recorded was 0.25% compression at strain gage 12. Most of the strain gages exhibited negligible strain with the exception of strain gage 8 which recorded a residual strain of 0.06% compression and strain gage 10 which indicated a 0.02% compressive residual strain. These residual strains are small, but appear to agree with the small transverse deflections noted for the center of the panel. In general, The radial strains measured appeared to be twice the circumferential strain at the same location.

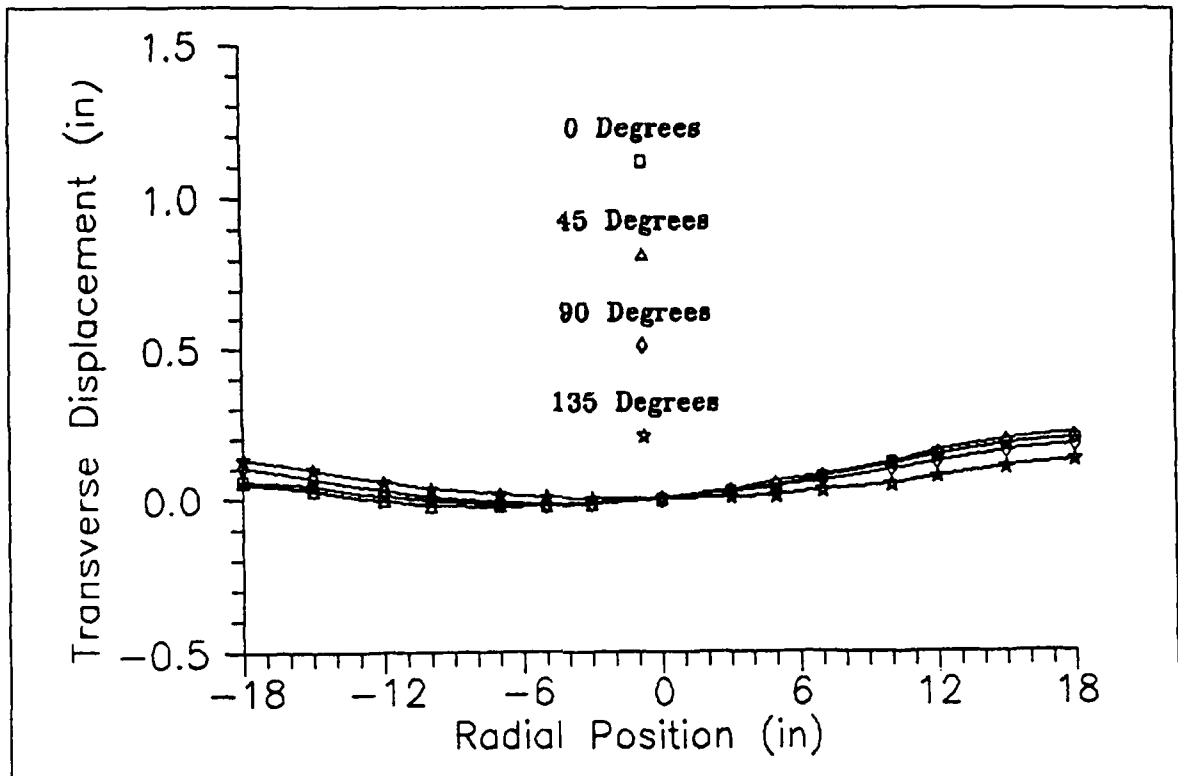


Figure 35. Final Transverse Displacement for the  $[0^\circ/90^\circ/0^\circ/90^\circ/0^\circ]$  Composite Panel From Test T2W.

From examination of the pressure history for this test, the time of impact was 3.07 msec after detonation. The most violent response of the plate was completed by 25 msec and after 50 msec since detonation had passed the plate appeared to be oscillating about its new rest position. The frequency of these oscillations, determined from the strain histories, varied between 11.69 Hz and 13.1 Hz.

Analysis of the short time strain data provided little additional information. System noise levels were only slightly less than the signal for some of the strain gages, making interpretation of the data difficult. Additionally there was an anomalous signal, which appeared to be an artifact of the firing pulse, that appeared at 0.07 msec. From shock wave impact at 3.1 msec until approximately 10.5 msec, the short time strain data attested

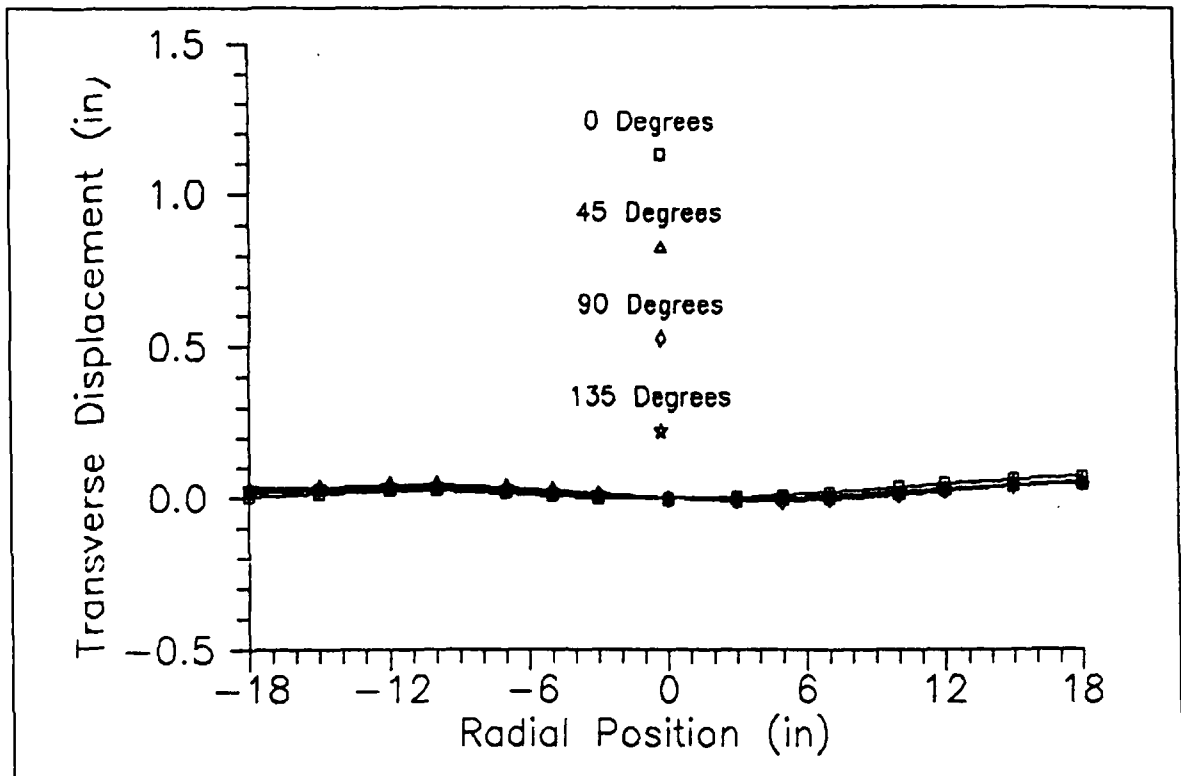


Figure 36. Final Transverse Displacement for the  $[0^\circ/45^\circ/90^\circ/45^\circ/0^\circ]_s$  Composite Panel From Test T3W.

to the elastic nature of the strain. At 10.5 msec most of the strain gages recorded a period of relatively constant strain that appeared to approximate the final residual strain observed in the long time strain presentation. The response of the panel from test T1W can best be characterized as primarily elastic with possible small amounts of plastic deformation in the central region of the panel.

The air backed aluminum panel of T1A provided more useful data for analysis. Reviewing the long time strain history data showed that strain gage 1, located at the center of the panel, over ranged almost immediately after impact of the shock wave. At some point during the test, strain gage 1 was ripped from the surface of the panel and torn free from its wiring. As the bare wires were buffeted about during the test large magnitude

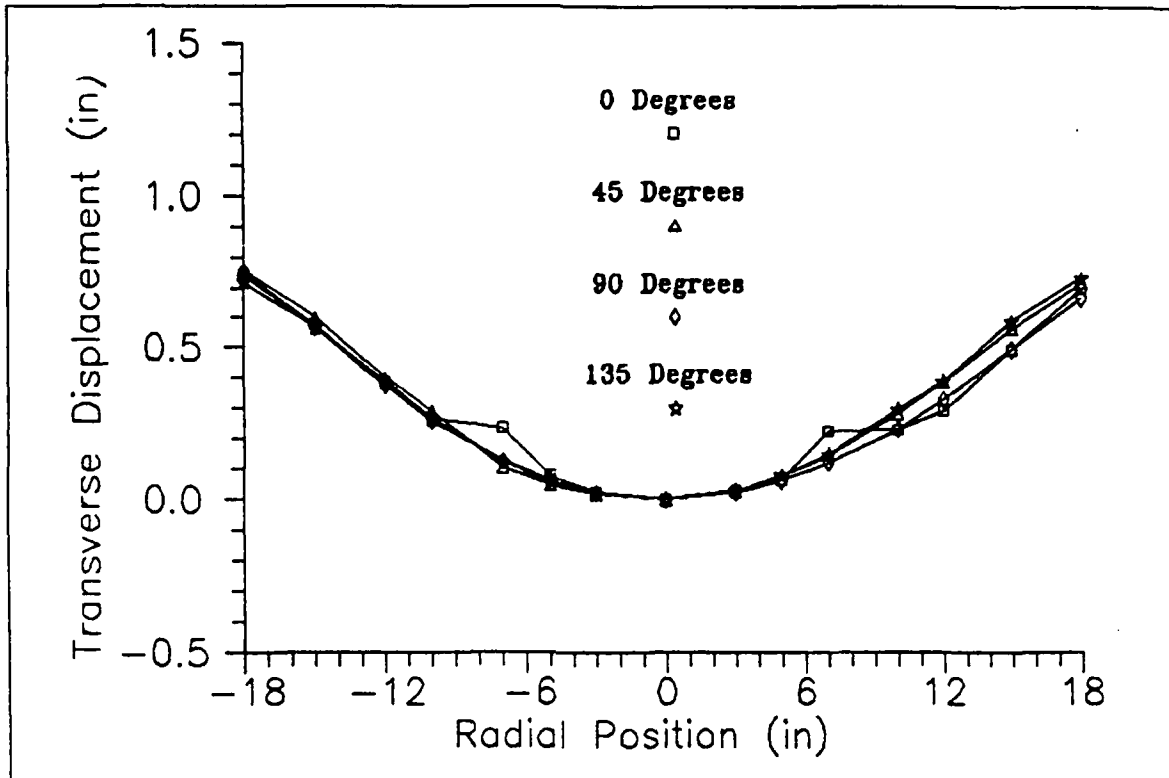


Figure 37. Final Transverse Displacement for the  $[0^\circ/90^\circ/0^\circ/90^\circ/0^\circ]_5$  Composite Panel From Test T2A.

fluctuations in the recorded signal were produced. These fluctuations were carried over into the signals recorded for other strain gages as large magnitude spikes. Strain gages 4 and 8 failed later in the test and also caused spikes to appear on some of the other strain channels. Comparison of the good strain channels with the traces from strain gages 1,4, and 8 allowed these spurious spikes to be discounted when reviewing the data. The maximum recorded permanent strain for T1A was 0.46% tension at strain gage 2. Strain gage 7 followed closely with 0.35% strain compression. The permanent strain in the radial direction appeared to be largest toward the center of the panel while the largest magnitude of the circumferential strain occurred at the boundary. In general, the circumferentially

oriented strain gages recorded permanent strains that were compressive and the radially mounted strain gages recorded permanent strains that were tensile in nature.

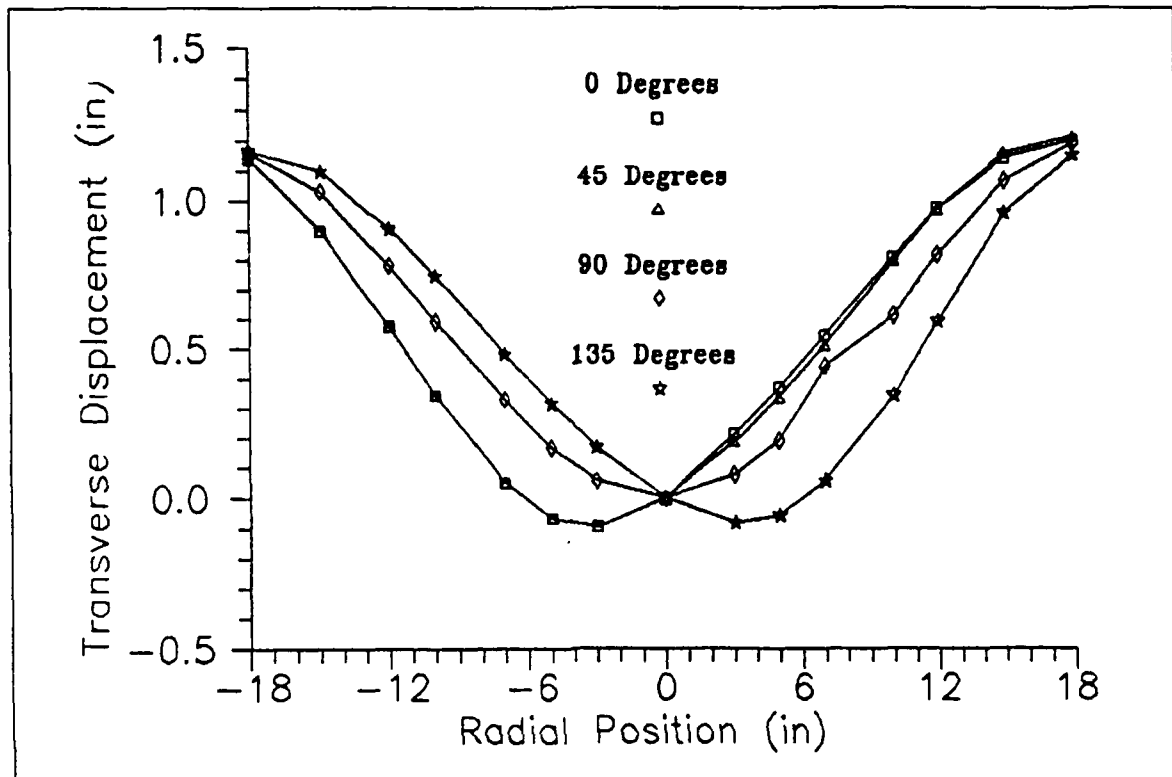


Figure 38. Final Transverse Displacement for the  $[0^\circ/90^\circ/45^\circ/90^\circ/0^\circ]_s$  Composite Panel From Test T4A-1.

Examination of the short time strain histories from T1A provided clues to the behavior of the panel during the period immediately following the impact of the shock wave. Shock wave impact was distinct enough to allow determination of the time of impact directly from the short time strain histories. As in T1W, the shock wave arrived at 3.1 msec. Initially, all of the radially mounted strain gages, numbers 1, 2, 4, 6, 8, 10 and 12, recorded a tensile strain caused by the initial interaction of the boundary with the panel. As shown in Figure 39, strain gage 7, the outer mos. circumferentially mounted strain gage, registered a compressive strain simultaneously with the shock wave impact. This

compressive strain increased almost linearly with time to a maximum of 0.62% compressive strain at approximately 8.3 msec. From this peak the strain decreased to the vicinity of 0.35% strain where it oscillated for about 50 msec before stabilizing at this value of residual strain. The output of the strain gages 5 and 9, located at 10 inches from the center of the panel, also exhibited a peak compressive strain at approximately the same time. The strain peaks at 8.3 msec were interpreted to mark the point of maximum transverse extension of the panel.

Examination of the radially mounted strain gages provided information on the passage of the plastic bending wave through the panel. As shown in Figure 40, evidence of the plastic bending wave first appears on strain gage 6. The tensile strain produced at shock wave impact at 3.1 msec is abruptly reversed at approximately 3.2 msec. The strain reversal was due to the relatively short radius of curvature of the bending wave. This placed the upper surface of the panel in radial compression. As the bending wave passed strain gage 6 the compressive strain was relieved as the radius of curvature increased. The bending wave arrived at strain gages 4 and 10, located ten inches from the panel center, at 3.5 msec and arrived at strain gages 2 and 8, located five inches from the panel center at 3.9 msec. Permanent radial strain was maximum near the center of the panel, probably as a result of the slight thinning of the material in the central region of the panel characteristic of metal panels deformed by underwater shock.

## **2. The Composite Test Panels**

Comparison of the strain histories from the water backed composite panels of tests T2W and T3W with the response of the aluminum panel from T1W showed many

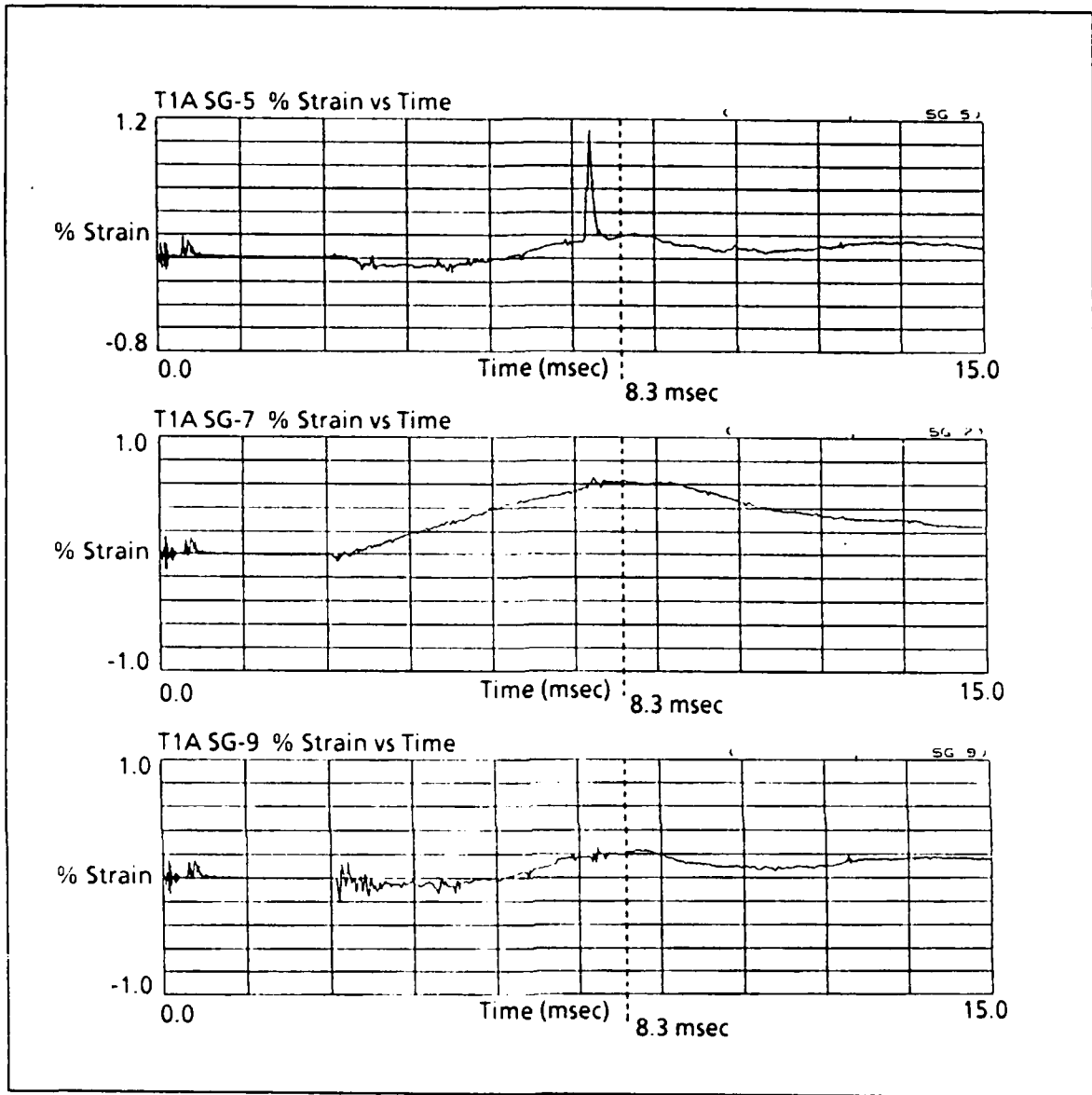


Figure 39. Time of peak Transverse Extension for Test T1A.

similarities. As with T1W, the most vigorous response of the panels to the shock wave occurred in the period from impact to 50 msec. After 75 msec had elapsed, most of the high frequency components of the response were gone and the panels were exhibiting a decaying low frequency oscillation. The best estimates of the frequency of this oscillation

that could be determined from the strain histories were between 12.67 Hz and 14.3 Hz for T2W and between 10.0 Hz and 10.9 Hz for T3W.

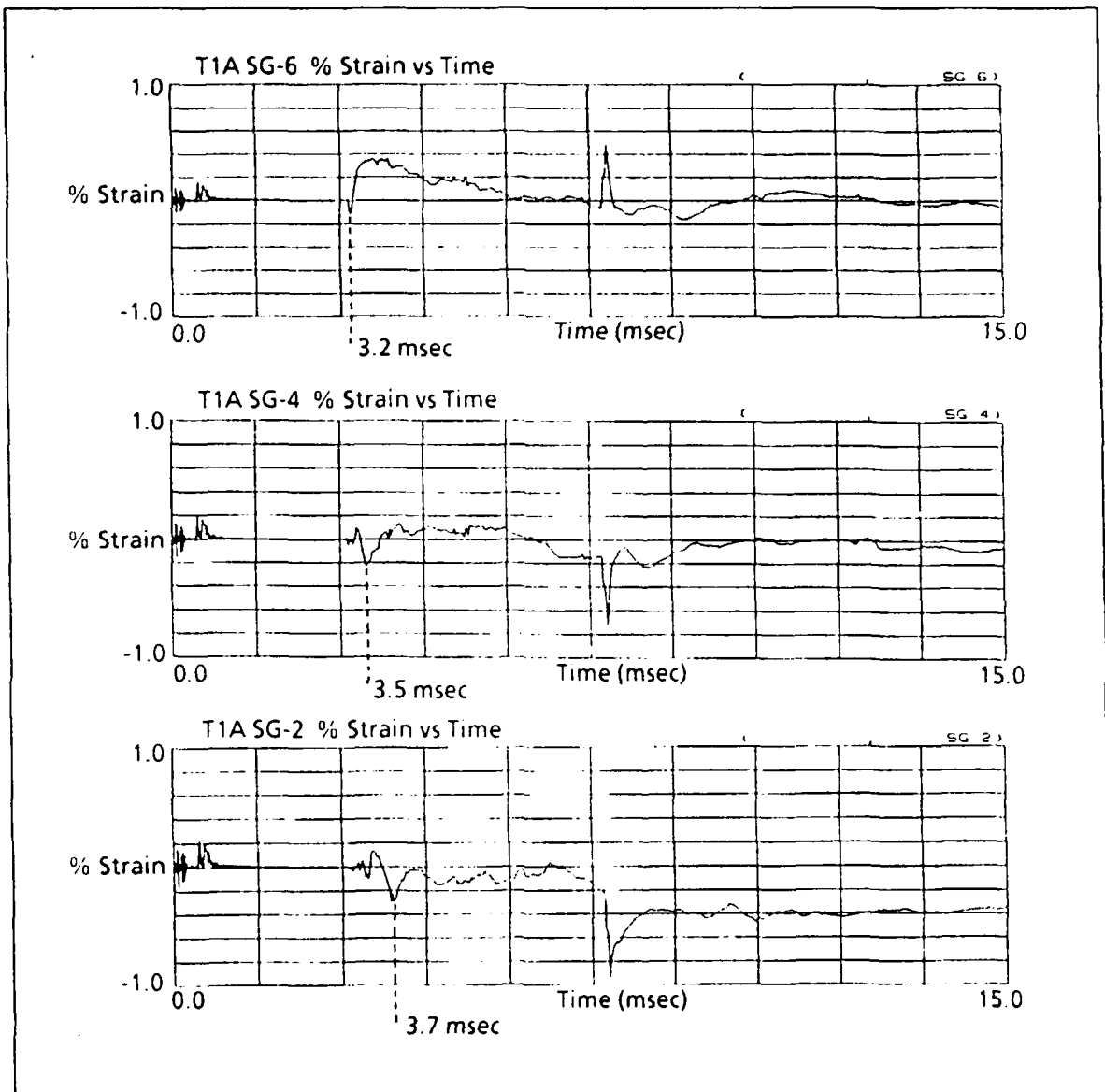


Figure 40. Progress of the Plastic Bending Wave for Test T1A.

The permanent deformation of the panel from T2W that was noted in the transverse deflection of the panel could not be verified from the strain history data. Strain gage 8, which was ideally placed to measure the strain associated with the transverse

deflection, failed when the test fixture was lowered into the water. The strain history for strain gage 9 are still oscillating at the end of 250 msec, but appear to be tending toward zero strain. The long time strain histories for the composite panel from T3W indicated no residual strain and verified the finding of no permanent transverse deflection.

Contrasting the behavior of the two composite panels revealed little difference between the panel from T2W (five pound TNT charge,  $[0^\circ/90^\circ/0^\circ/90^\circ/0^\circ]_5$  lay up) and the panel from T3W (ten pound TNT charge,  $[0^\circ/45^\circ/90^\circ/45^\circ/0^\circ]_5$  lay up) other than in the magnitude of the strains measured. Surprisingly, the overall strain levels for T2W, which used a five pound TNT charge, are greater than the overall strain levels for T3W, which used a ten pound TNT charge. Reviewing the pressure histories for these two tests, the peak pressure at the test panel was 1900 psi for T2W and was 2100 psi for T3W. Given that the peak pressures for the two tests were relatively close, the presence of an air bubble behind part of the panel from test T2W (as discussed in section IV.B) might have allowed larger deflections of the panel that would have resulted in larger strain measurements. Additionally, the quasi-isotropic nature of the panel from T3W may have allowed a better distribution of the strain across the panel than the orthotropic panel from T2W and resulted in lower recorded strain levels.

Review of the long time strain data from the air backed tests T2A and T4A-1 showed an initial response to the shock wave that was similar to that demonstrated by the aluminum panel from T1A. In T2A, most of the High frequency components of the strain history were attenuated in the time between impact and 75 msec. The remaining low frequency response exhibited a very long period of between 106 msec and 135 msec as

measured on the strain histories. This corresponded to a frequency between 7.4 Hz and 9.4 Hz. The response of T4A-1 was more chaotic. The high frequency components of the strain history are not attenuated until after a total elapsed time of 100 msec. The long term response of the strain gages after 100 msec did not exhibit a recognizable cyclic pattern as did the strain histories for T1A and T2A.

The residual strain for the panel from T4A-1 was greater than the residual strain for the panel from T2A as was expected after comparing their relative transverse deflections. There appeared to be little correlation between the magnitude of the strains and the location of the strain gage for either test. Even strain gages mounted at the same location but on opposite sides of the panel did not corroborate each other in all cases.

The short time strain histories from T2A were compared to the corresponding strain histories from T1A. An attempt to overlay the pattern of failure noted in T1A met with limited success. As shown in Figure 41, what appeared to be the corresponding phenomena in the composite material of the plastic bending wave in the aluminum can be seen arriving at strain gage 6 at a total elapsed time of 2.8 msec, strain gages 4 and 10 at 3.24 msec, and strain gages 2, 8 and 12 at 3.95 msec. Next, the circumferentially mounted strain gages were examined to determine the time to peak transverse extension. As shown in Figure 42, strain gage 7 exhibited a peak at 5.05 msec that appeared to represent maximum transverse extension. Unlike T1A, none of the other circumferentially mounted strain gages corroborated this time.

The short time strain histories of T4A-1 told much the same story as those from T2A. The path of the bending wave from boundary to panel center could be tracked as it

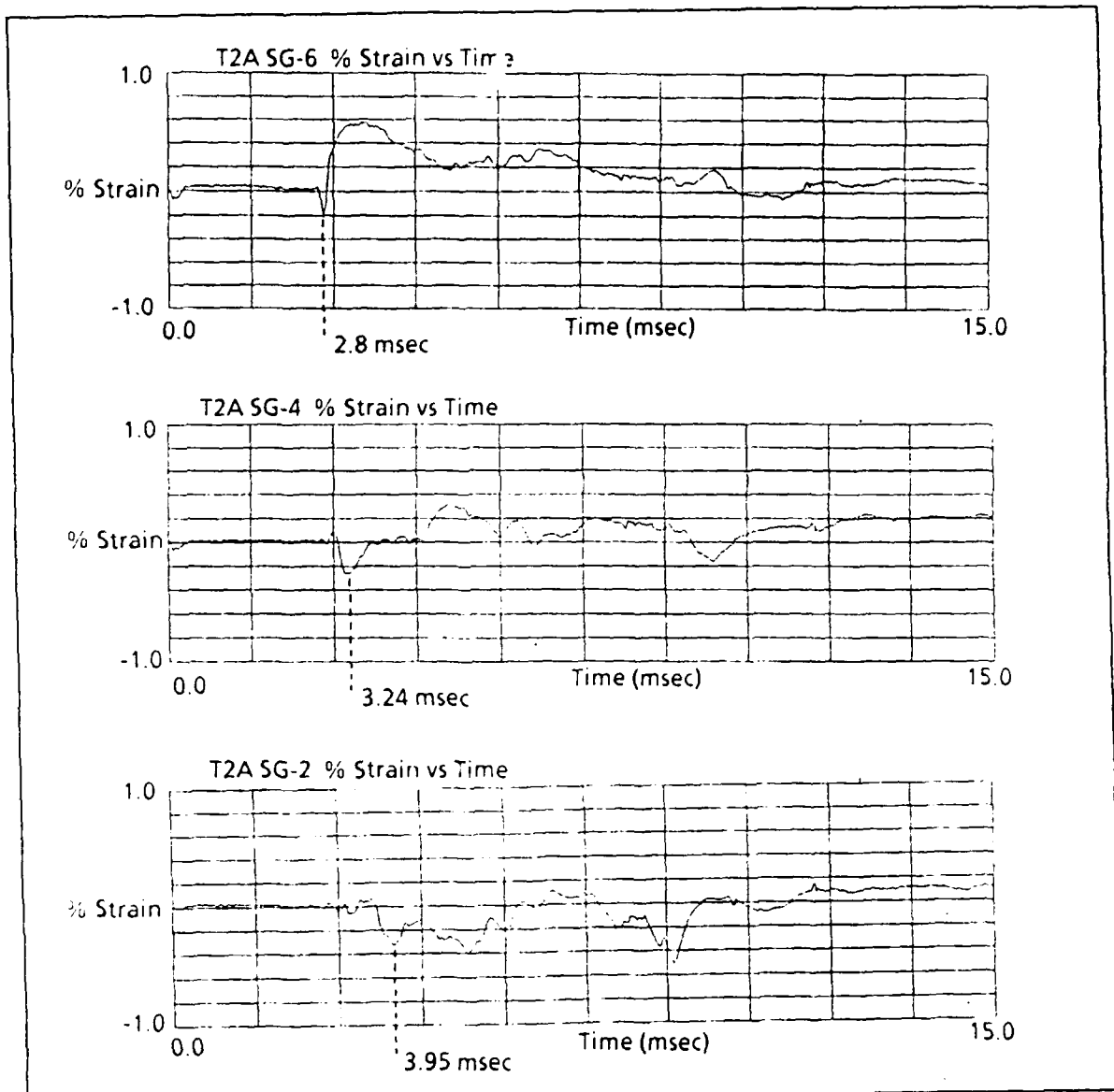


Figure 41. Progress of the Bending Wave for Test T2A.

arrived at strain gages 4 and 10 at a total elapsed time of 3.69 msec and at strain gages 2 and 8 at 4.38 msec. Strain gage 6 had failed prior to the test. When the output of the circumferential strain gages was reviewed no clear indication of the time of maximum transverse extension was evident.

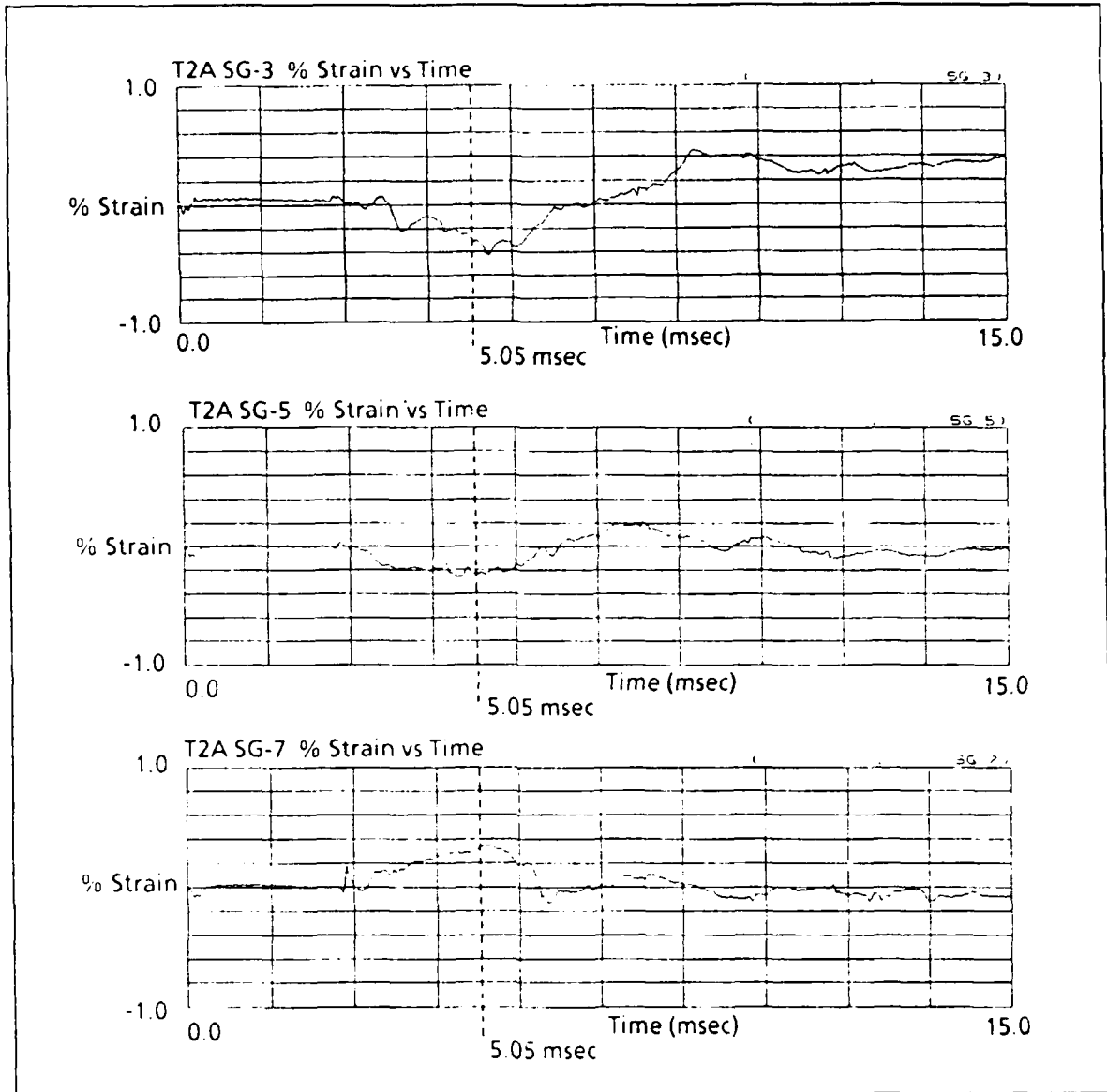


Figure 42. Time of Peak Transverse Extension for Test T2A.

The data discussed in this section, along with the measured transverse deflection of the air backed panels, was used to calculate values for the average panel velocity,  $U_{avg}$ , and the nominal speed of the plastic bending wave. The results of these calculations follow in Table IV.

**Table IV. Measured Response of the Air Backed Panels From T1A, T2A, and T4A-1.**

Test	Material	Explosive Weight lbf	$Z_{center}$ in	$U_{avg}$ in/sec	Bending Wave Velocity in/sec
T1A	Aluminum	5	2.4	-461.5	-14286
T2A	Composite	5	0.75	-327.5	-8,696
T4A-1	Composite	5	1.26	-	-7246

## V. CONCLUSIONS AND RECOMMENDATIONS

### A. WATER BACKED TESTS

Within the limits of the charge weights used, neither the aluminum panel nor the composite panels used in the water backed tests exhibited a great deal of sensitivity to the size of the explosive charge. With the exception of test T2W, all of the panels behaved in a primarily elastic manner and exhibited no indications of impending failure.

The composite panel used in test T2W was determined to be a special case. Although the presence of an air bubble behind the panel at the time of the test could not be proven, the evidence certainly suggested this possibility. The only other reasonable explanation for the localized interior delamination noted in this panel was a preexisting flaw in the panel that was exacerbated by the underwater shock. Steps were taken in the follow on water backed test to ensure that the test fixture vents were clear and the gasket material was sectioned at the top edge of the panels to provide additional vent paths. Additionally, all of the panels used in the remaining tests were inspected for possible internal flaws by shining a bright light behind the panel and then searching for shadows in the translucent composite material. In either case, the phenomena was not repeated in the follow on water backed tests even though a larger explosive charge was used.

The two extremes of the composite panels were tested during the water backed test sequence. The panel from T2W represented the most orthotropic lay up of the panels tested. The panel from T3W represented the most isotropic of the composite lay ups tested.

Even though subjected to the more severe shock, the panel of T3W appeared to distribute the resulting strain more evenly than the panel from T2W.

## **B. AIR BACKED TESTS**

The air backed tests provided the most useful information from this investigation. The residual transverse deflection of the aluminum panel from T1A gave evidence that the aluminum panel was responding in much the same manner as the steel panels had during the postwar experiments. The strain histories for this test provided an example of how the dynamic processes occurring in the panel would appear in terms of the radial and circumferential strains. The plastic bending wave that appeared was well documented in the postwar testing tests. The circumferential compressive strain, although mentioned in the historical results, appeared to be exacerbated by the chosen boundary conditions that allowed motion of the boundary in the radial direction.

It was anticipated that the composite air backed test panels would try to respond to an underwater shock in the same manner as the aluminum panel. Two properties of this composite material had the potential to disrupt or disguise the response of the air backed panels. The high tensile strength of the glass fabric and the brittle nature of the matrix material made it unlikely that the plastic bending would be as sharply defined as in the aluminum panel.

The transverse deflection measurements of the panels from T2A and T4A-1 indicated that both of the panels were tending to respond in the same manner as the aluminum air backed panel. The measured deflection of the composite panels was less than the deflection for the aluminum panel for two reasons. First, because the density of the composite

material is closer to that of water than is the density of the aluminum, less of the available energy of the shock wave was absorbed by the composite panels. Secondly, as the panel deflects out of the horizontal plane, tensile membrane stresses were generated in the radial direction that resisted the continued deflection of the panel. The composite material is very strong under tensile loading and resisted any permanent deformation in the radial direction. As anticipated the composite panels lacked the sharply defined shape of the aluminum panel due to the minimal plastic deformation allowed by the material. On the other hand, the brittle nature of the matrix material resulted in significant local matrix failure apparently under the action of the compressive circumferential strain. The strain histories for these panels clearly show the passage of a bending wave analogous to the plastic bending wave of the aluminum panel. The data obtained from the circumferential strain gages, which in the aluminum panels showed the time to peak transverse deflection quite clearly, were inconclusive for the composite panels. This was the probable result of the stress relief in the circumferential direction that accompanied the radially oriented local matrix failures experienced by the air backed composite panels.

A comparison of the predicted response with the actual response of the air backed test panels from T1A, T2A, and T4A-1 provides several interesting observations. The actual transverse deflection of the center of the panels was approximately twice the deflection predicted by the infinite plate model using equation (23), but was significantly less than the deflections predicted by the finite plate model in equation (25). The bending wave velocity predicted by equation (24) for the aluminum plate was within 12% of the velocity determined from the short time strain histories for T1A. The calculated bending wave

velocity for the composite panels was very high and not comparable to the measured velocities in T2A and T4A-1. Some quantity other than the first ply failure strength that is comparable to the yield strength for metals must be determined and used in the calculation of bending wave velocity before valid predictions can be made.

As expected the predominant failure mechanism of the aluminum panel of test T1A was plastic deformation of the material that resulted in a permanent transverse deflection of the panel. The observed failure mechanism of the composite panels from tests T2A and T4A-1 was primarily localized matrix failure induced by exceeding the compressive stress limit of the matrix material. It must be stressed that the boundary conditions under which these tests were conducted played a large role in determining the failure mode. In particular the allowed motion of the panels in the radial direction appeared to be a significant contributor to the observed failure mode of the composite panels. Different boundary conditions may result in significantly different failure modes.

### **C. RECOMMENDATIONS**

The following recommendations are presented as possible directions of future study:

1. The general trends and failure mechanisms identified by this report should be compared to the results predicted by several finite element models for composite materials. Modifications may be evident that could improve the predictive ability of these models.
2. Boundary conditions played such a central role in the response of the composite panels that additional tests should be conducted to determine the effects of other boundary conditions on the response of the panel. Of particular interest would be the effect that truly fixed boundaries or non-circular boundaries would have on the response of the composite material.

3. Propagation of the radially oriented matrix failures in the panels from tests T2A and T4A-1 appeared to have a significant effect on the measured strain values in the same vicinity. Stimulating this response on a more densely instrumented sample may shed light on this phenomena.
4. Fabricate composite test panels with strain gages imbedded in the panel. Similar tests could then be conducted to investigate the distribution of normal strain and interlaminar shear strain across the thickness of the composite panel.
5. Complete the ASTM tensile tests using samples from the other composite lay ups to provide a complete set of data for follow on testing.
6. Determine the dependence of sound velocity on fiber orientation for the composite material. Insight gained from determining the variation in sound velocity may prove useful in determining the bending wave speed in the composite.

## APPENDIX A: MATERIAL PROPERTIES

<u>PROPERTY</u>	<u>ALUMINUM</u>	<u>COMPOSITE</u>
Modulus of Elasticity (psi),		
$E_x$	$10.6 \times 10^6$ <sup>(1)</sup>	$2.87 \times 10^6$ <sup>(2)</sup>
$E_y$	$10.6 \times 10^6$ <sup>(1)</sup>	$7.10 \times 10^5$ <sup>(2)</sup>
Poisson's Ratio,		
$\nu_{yx}$	0.33 <sup>(1)</sup>	0.091 <sup>(2)</sup>
$\nu_{zx}$	0.33 <sup>(1)</sup>	0.250 <sup>(2)</sup>
$\nu_{zy}$	0.33 <sup>(1)</sup>	0.368 <sup>(2)</sup>
Fiber Tensile Strength (psi),		
$\sigma_{ut, fiber}$	N/A	$1.80 \times 10^5$ <sup>(2)</sup>
Tensile Strength (psi),		
$\sigma_{ut}$	$4.5 \times 10^5$ <sup>(1)</sup>	$7.20 \times 10^4$ <sup>(3)</sup>
Compressive Strength (psi),		
$\sigma_{uc}$	$4.5 \times 10^5$ <sup>(1)</sup>	$1.8 \times 10^4$ <sup>(3)</sup>
Yield Strength (psi),		
$\sigma_y$	$4.0 \times 10^5$ <sup>(1)</sup>	N/A
Density (lbf sec <sup>2</sup> in <sup>-4</sup> ),		
$\rho$	$2.54 \times 10^{-4}$ <sup>(1)</sup>	$1.80 \times 10^{-4}$ <sup>(2)</sup>
Resin Content (% by Weight)	N/A	$32 \pm 3$ <sup>(3)</sup>

<sup>(1)</sup> [Ref. 12: p. 6-10]

<sup>(2)</sup> [Ref. 13: p. 64]

<sup>(3)</sup> [Ref. 14: pp. 3,4]

## APPENDIX B: PHOTOGRAPHS OF PANEL DAMAGE

The following photographs detail the damage inflicted on the aluminum and composite panels from tests T1A, T2A, T3A, T4A-1, and T4A-2.

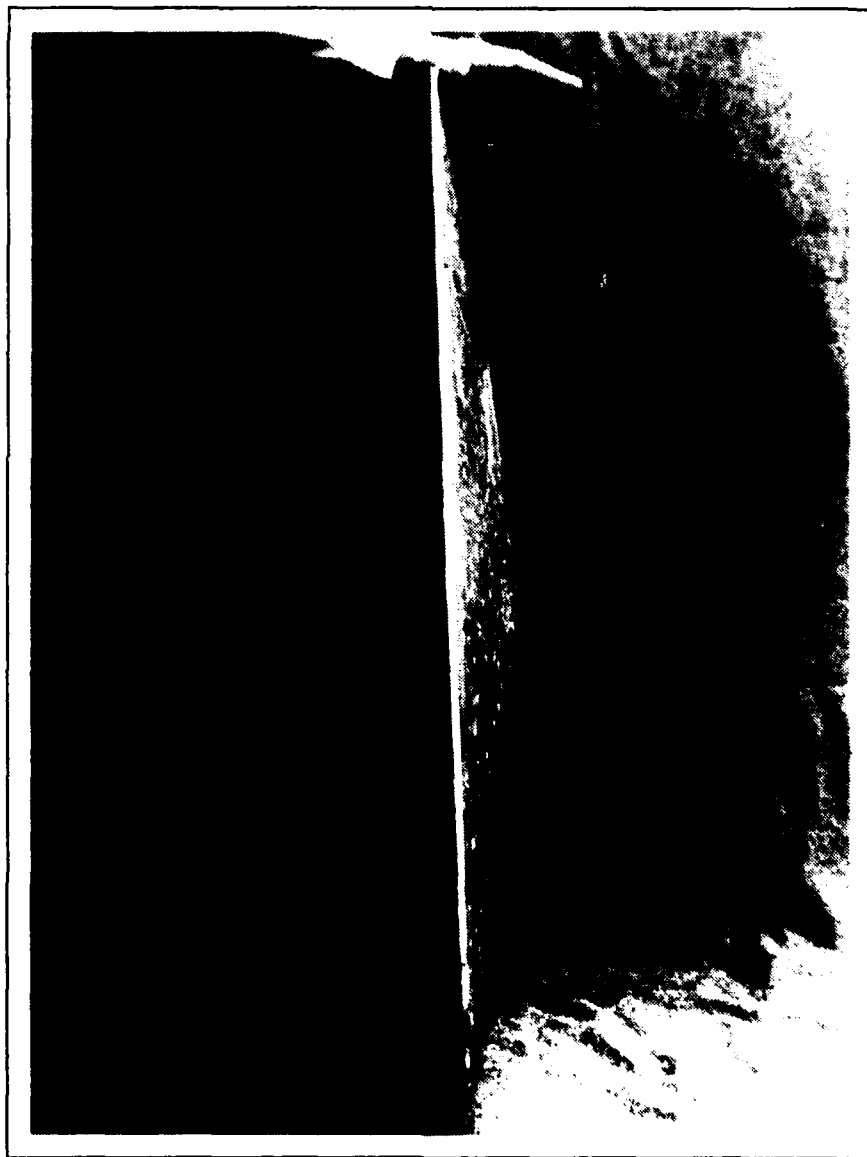
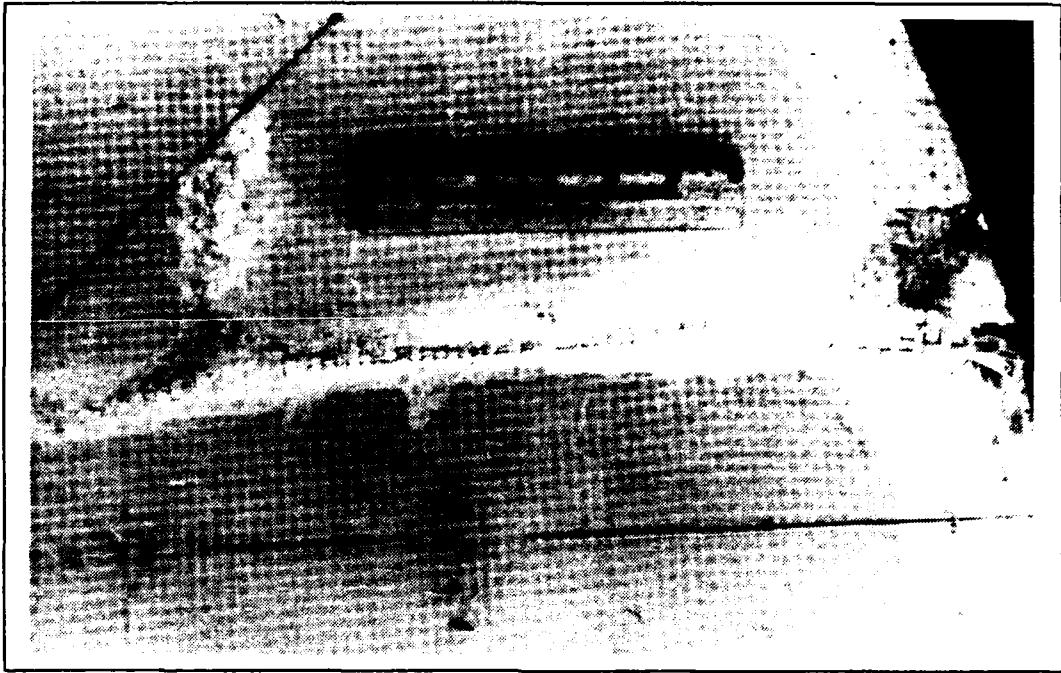
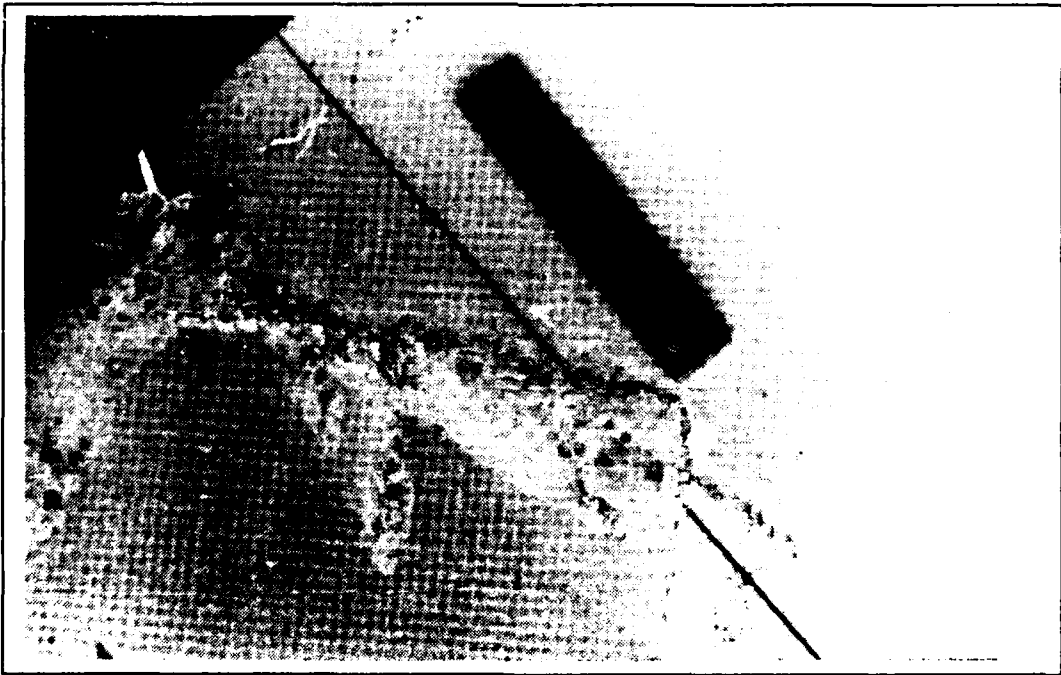


Figure 43. Side View of the Aluminum Panel From Test T1A.



**Figure 44. Detail From the Upper Quarter of the Panel From T2A.**



**Figure 45. Detail From the Lower Left Quarter of the Panel From T2A.**



**Figure 46. Detail of the Lower Right Quarter of the Panel From T2A.**



**Figure 47. Detail of the Right Quarter of the Panel From T2A.**

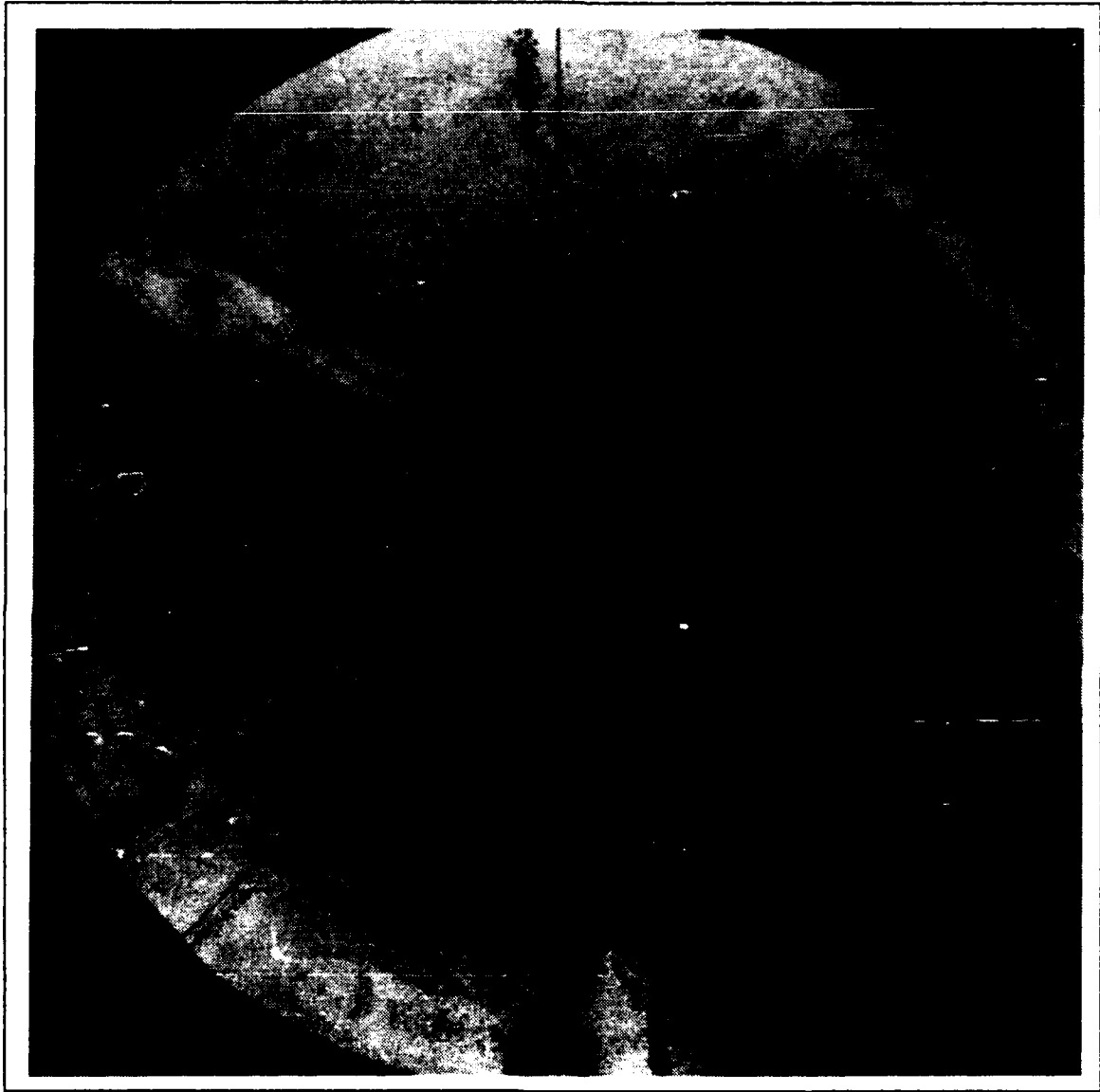


**Figure 48.** The Composite Panel From Test T3A.

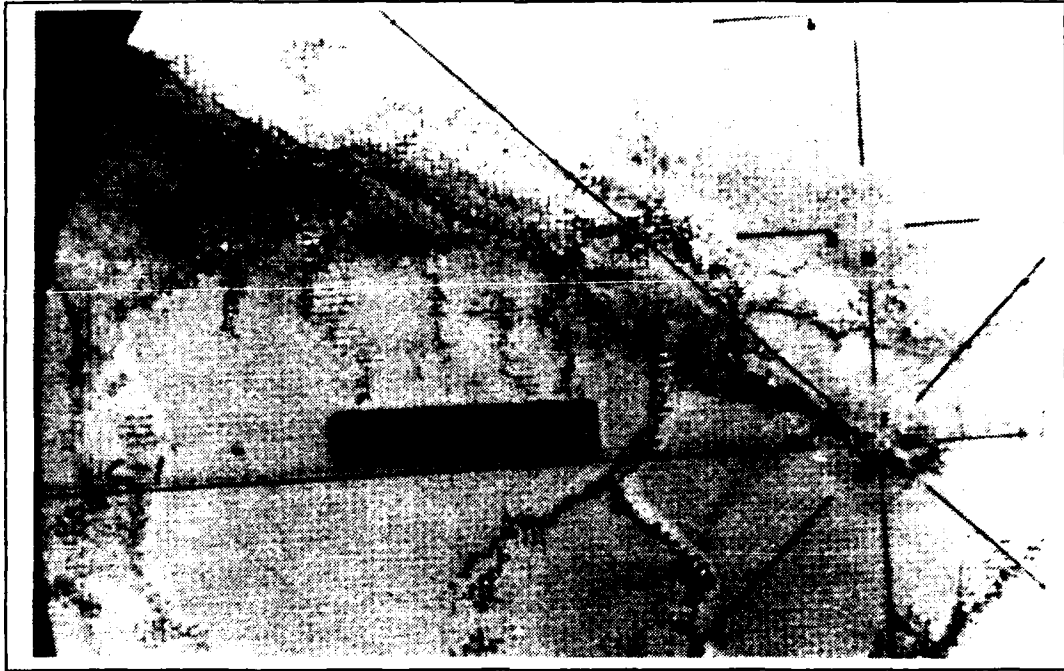


Figure 49. Detail of the Left Quarter of the Panel From T3A.

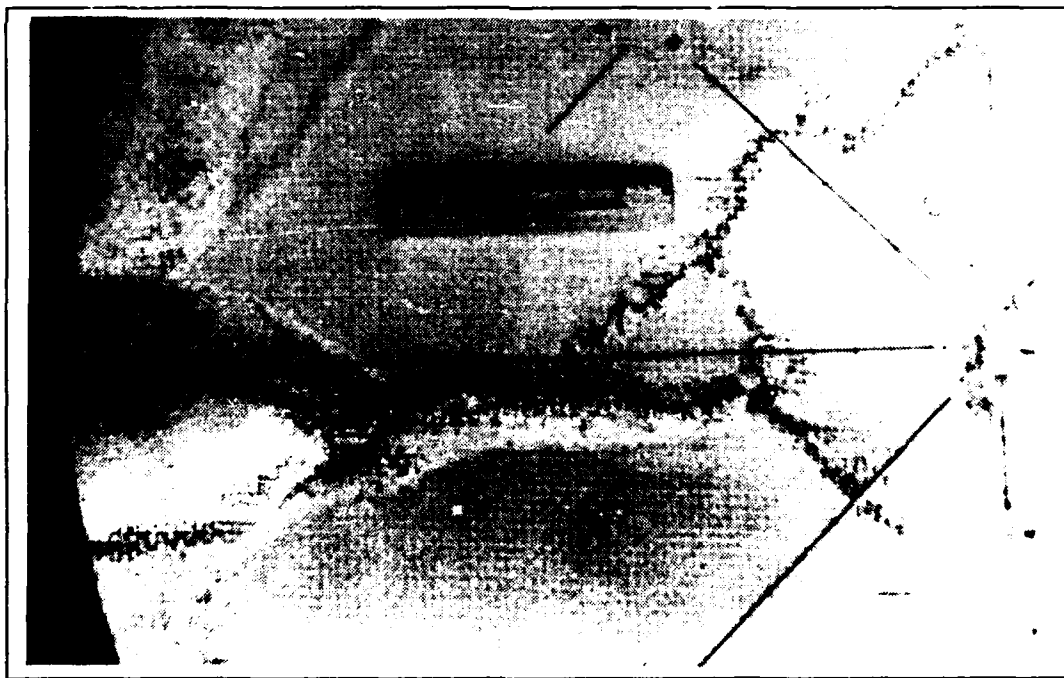


Figure 50. Detail of the Lower Quarter of the Panel From T3A.



Figure 51. Detail of the Right Quarter of the Panel From T3A.

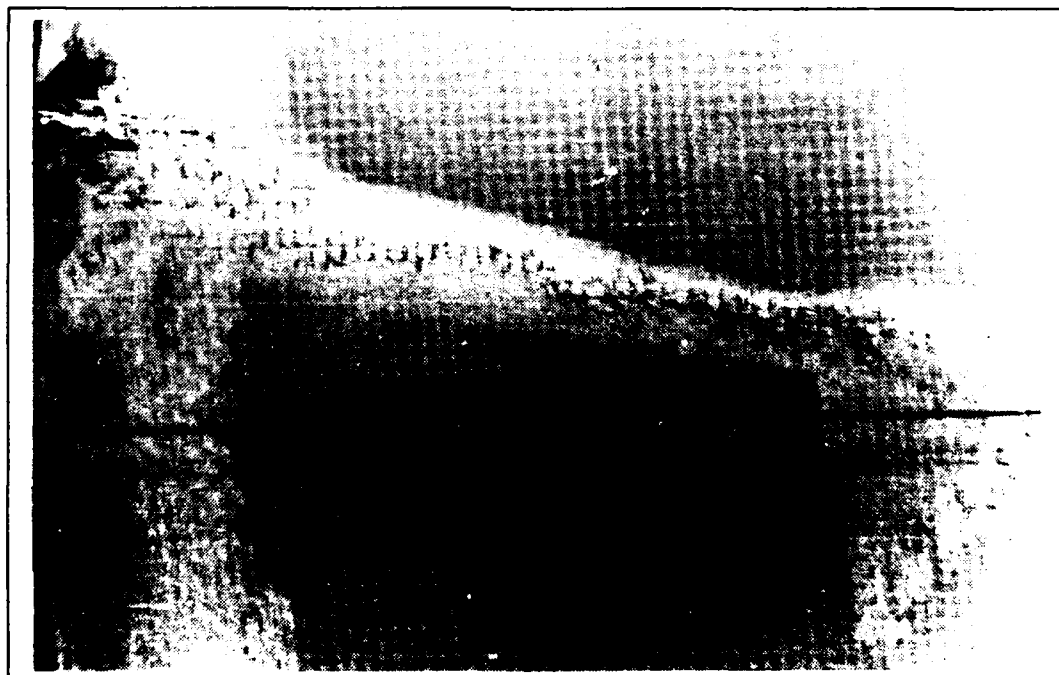
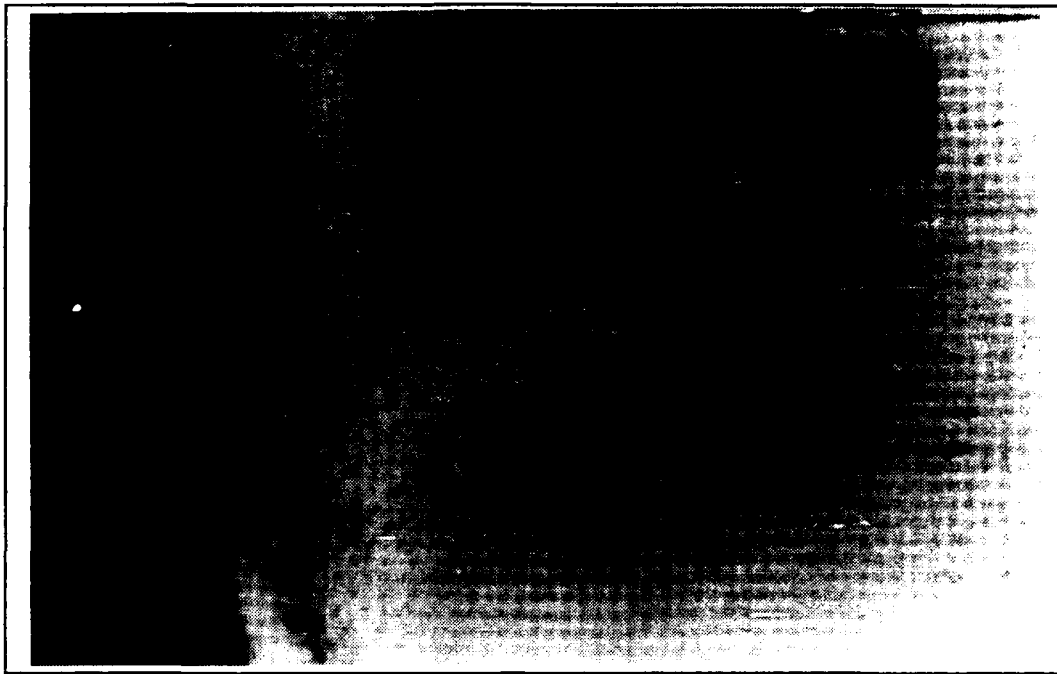
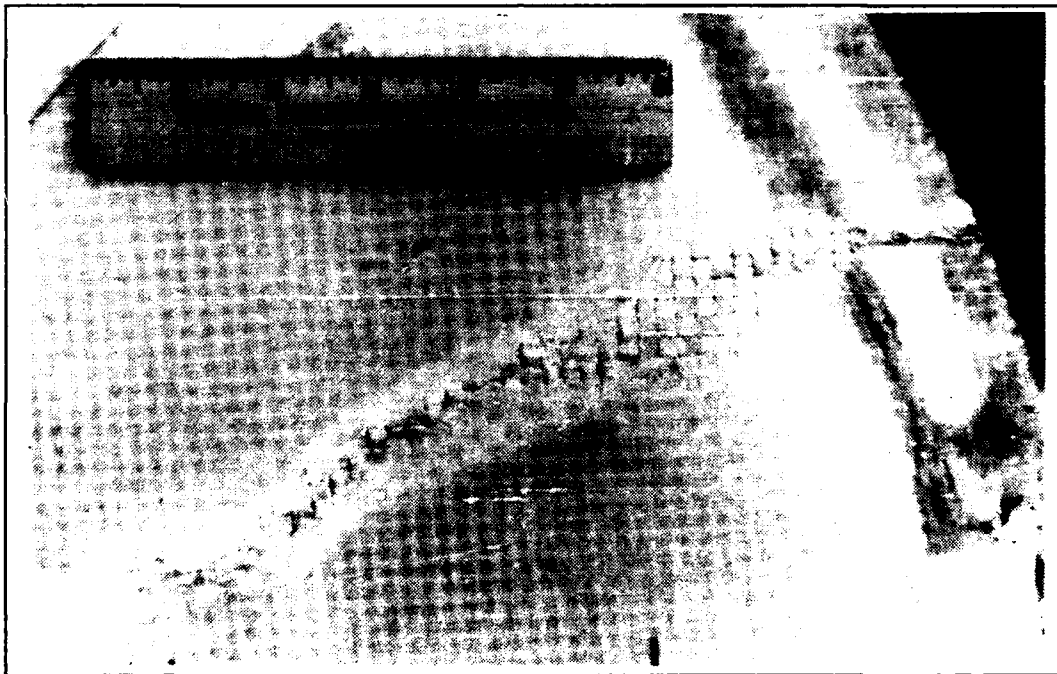


Figure 52. Detail of the Left Quarter of the Panel From T4A-1.



**Figure 53. Detail of the Lower Quarter of the Panel From T4A-1.**



**Figure 54. Detail of the Right Quarter of the Panel From T4A-1.**

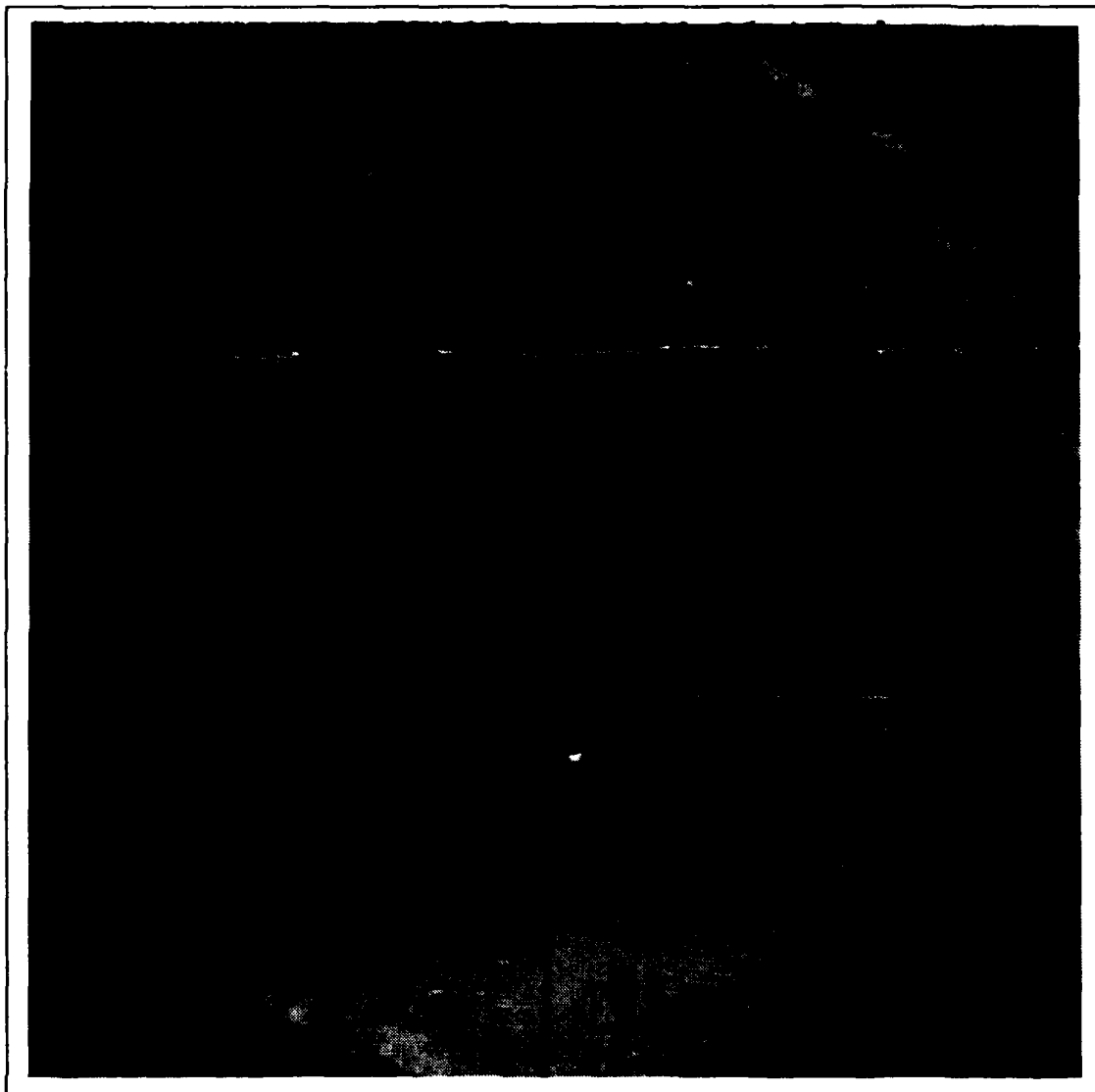


**Figure 55.** The Composite Panel From Test T4A-2.

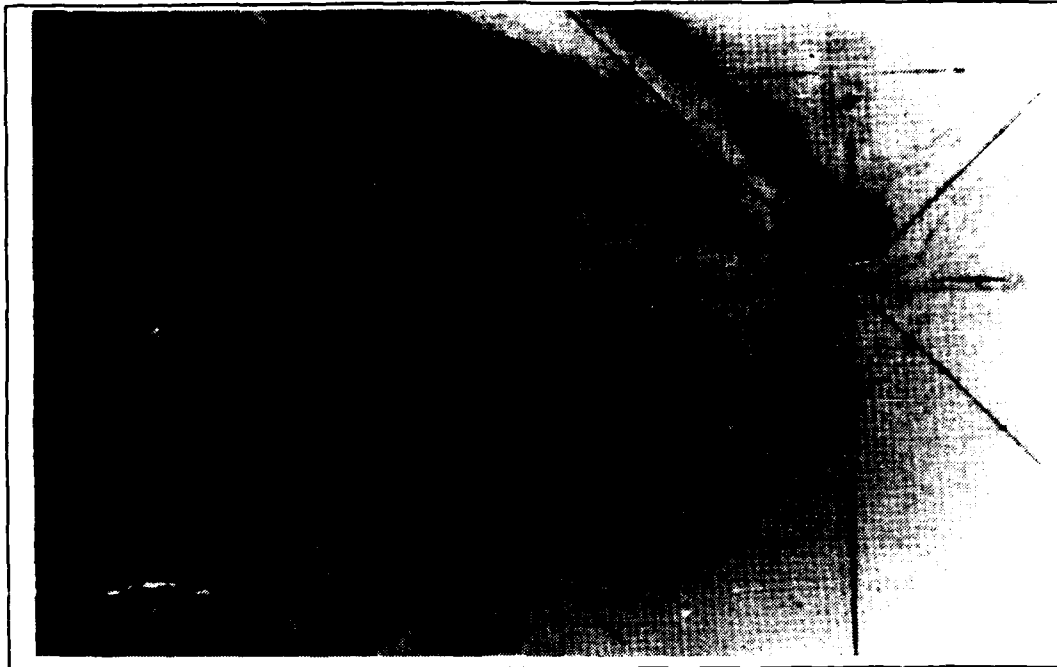


**Figure 56.** Detail of the Left Quarter of the Panel From T4A-2.

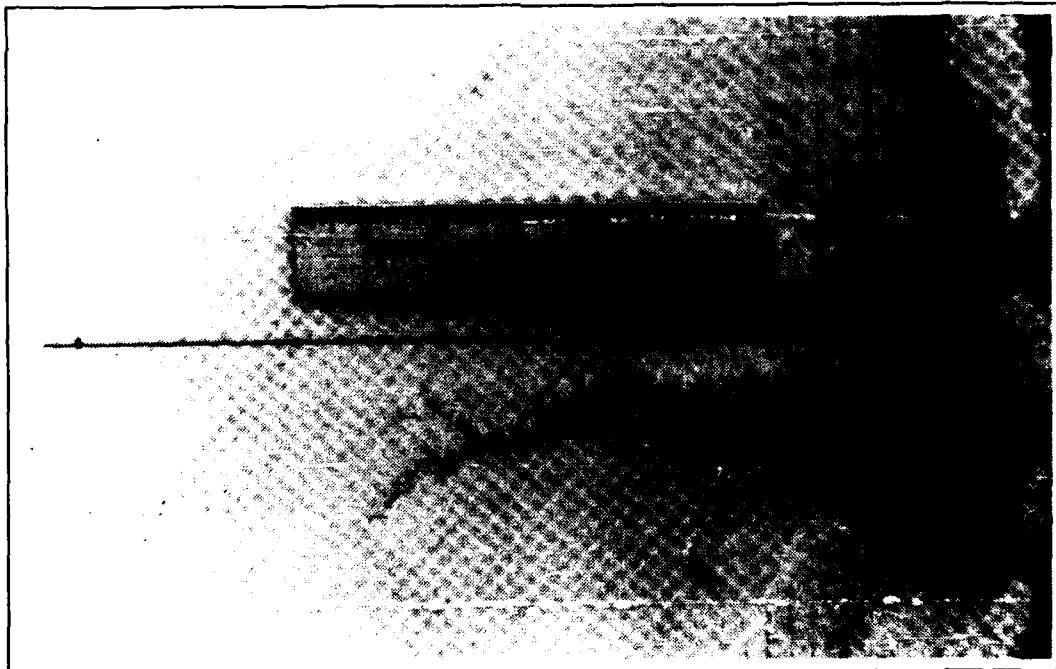


**Figure 57.** Detail of the Lower Right Quarter of the Panel From T4A-2.



Figure 58. Detail of the Upper Right Quarter of the Panel From T4A-2.

## LIST OF REFERENCES

1. Vinson, J. R., and Sierakowski, R. L., *The Behavior of Structures Composed of Composite Materials*, Martinus Nijhoff Publishers, 1986.
2. *Handbook of Composite Materials, Vol. III - Failure Mechanisms of Composites*, edited by G. C. Sih and A. M. Skudra, North-Holland Publishing Co., 1985.
3. Cole, R. H., *Underwater Explosions*, Princeton University Press, 1948.
4. Coles, J. S. and others, "Shock Wave Parameters from Spherical TNT Charges Detonated Underwater", *Underwater Explosion Research*, Vol I, Office of Naval Research, 1950.
5. Naval Weapons Center Report TR 80-299, (U) *Similitude Equations for Explosives Fired Underwater*, by R. S. Price, 16 November 1979. (Confidential)
6. Shin, Y. S. and Geers, T. L., *Response of Marine Structures to Underwater Explosions*, short course notes, 1989.
7. Taylor, G. I., "The Pressure and Impulse of Submarine Explosion Waves on Plates", *The Scientific Reports of Sir Geoffrey Ingram Taylor*, vol 3, edited by G. K. Batchelor, The University Press, Cambridge, U. K., 1963.
8. Hudson, G. E., "A Theory of the Dynamic Plastic Deformation of a Thin Diaphragm", *Underwater Explosion Research*, Vol III, Office of Naval Research, 1950.
9. Jones, R. M., *Mechanics of Composite Materials*, Hemisphere Publishing Corp., 1975.
10. American Society for Testing and Materials, Standard D 3039-74, *Standard Method of Test for Tensile Properties of Oriented Fiber Composites*, January 1975.
11. Naval Postgraduate School Technical Report 69-90-02, *The Response and Failure Mechanisms of Circular Metal and Composite Plates Subjected to Underwater Shock Loading*, by R. A. Jones and Y. S. Shin, February 1990.
12. *Standard Handbook for Mechanical Engineers*, 7th ed., McGraw-Hill Book Company, 1967.

13. Laulie, S. and Cheng, W., *Numerical Simulation of High Velocity Impact on Fiber-reinforced Composites*, Proceedings of the 1989 ASME Pressure Vessels and Piping Conference; Shock Wave Propagation, Fluid-Structure Interaction, and Structural Responses, PVP- Vol. 159, American Society of Mechanical Engineers, 1989.

14. FMC Corp., *Composite Infantry Fighting Vehicle Program Material Specification Number: CIFV-MS1*, rev. 3, 26 June 1987.

## INITIAL DISTRIBUTION LIST

	No. Copies
1. Defense Technical Information Center Cameron Station Alexandria, VA 22304-6145	2
2. Library, Code 0142 Naval Postgraduate School Monterey, CA 93943	2
3. Professor Y. S. Shin, Code 69Sg Department of Mechanical Engineering Naval Postgraduate School Monterey, CA 93943	5
4. Department Chairman, Code 69 Department of Mechanical Engineering Naval Postgraduate School Monterey, CA 93940	1
5. Dr. N. T. Tsai Defense Nuclear Agency SPSS Washington, D. C. 20305-1000	3
6. LCDR Charles Nofzinger, USN Defense Nuclear Agency SPSD 6801 Telegraph Road Alexandria, VA 22310-3398	1
7. Dr. Alfred Tucker Defense Advanced Research Projects Agency 1515 Wilson Blvd. Rosslyn, VA 22209	1

8. Mr. Robert Fuss, Director 1  
David Taylor Research Center  
Underwater Explosion Research Division  
Norfolk Naval Shipyard, Bldg 369  
Portsmouth, VA 23709
9. Mr. Frederick A. Costanzo 1  
David Taylor Research Center  
Underwater Explosion Research Division  
Norfolk Naval Shipyard, Bldg 369  
Portsmouth, VA 23709
10. Dr. B. Whang, Code 1750.2 1  
Hull Group Head, Submarine Protection Division  
David Taylor Naval Ship Research and  
Development Center  
Bethesda, MD 20084-5000
11. Dr. Milton O. Critchfield 1  
David Taylor Naval Ship Research and  
Development Center  
Bethesda, MD 20084-5000
12. Dr. Mel Baron 1  
Weidlinger Associates  
333 Seventh Avenue  
New York, NY 10001
13. Dr. Raymond Daddazio 1  
Weidlinger Associates  
333 Seventh Avenue  
New York, NY 10001
14. Professor Thomas L. Geers 1  
Department of Mechanical Engineering  
Campus Box 427  
University of Colorado  
Boulder, CO 80309
15. Mr. Weng Cheng 1  
Applied Mechanics Department  
FMC Corporate Technology Center  
1205 Coleman Avenue, Box 580  
Santa Clara, CA 95052

- |     |  |   |
|-----|--|---|
| 16. | <p><b>Dr. Philip Bogart</b><br/> <b>NKF Engineering, Inc.</b><br/> <b>4200 Wilson Blvd., Suite 1000</b><br/> <b>Arlington, VA 22203-1800</b></p> | 1 |
| 17. | <p><b>Dr. Kent Goering</b><br/> <b>Defense Nuclear Agency</b><br/> <b>6801 Telegraph Road</b><br/> <b>Alexandria, VA 22310</b></p>               | 1 |
| 18. | <p><b>LCDR Robert A Jones, USN</b><br/> <b>P.O. Box 615</b><br/> <b>Prattville, AL 36067</b></p>   | 1 |
| 19. | <p><b>Naval Engineering, Code 34</b><br/> <b>Naval Postgraduate School</b><br/> <b>Monterey, CA 93943</b></p>                                    | 1 |
| 20. | <p><b>Mr. Donald A. Jones</b><br/> <b>P.O. Box 615</b><br/> <b>Prattville, AL 36067</b></p>  | 1 |
| 21. | <p><b>Mr. Buel Hanners</b><br/> <b>1105 Rhodes St.</b><br/> <b>Hartselle, AL 35640</b></p>   | 1 |
| 22. | <p><b>Mr. Marty Walchek</b><br/> <b>Code H14</b><br/> <b>Naval Surface Warfare Center</b><br/> <b>Silver Spring, MD 20903-5000</b></p>           | 1 |
| 23. | <p><b>Mr. Ron Tussing</b><br/> <b>Code R15</b><br/> <b>Naval Surface Warfare Center</b><br/> <b>Silver Spring, MD 20903-5000</b></p>             | 1 |
| 24. | <p><b>Mr. Glenn N. Reid</b><br/> <b>Code U401</b><br/> <b>Naval Surface Warfare Center</b><br/> <b>Silver Spring, MD 20903-5000</b></p>          | 1 |